University of Bath

**UNIVERSITY OF BATH**

**PHD**

**Selective Catalytic Hydrogenation in a Structured Compact Multifunctional Reactor**

Fan, Xiaolei

*Award date:*
2010

*Awarding institution:*
University of Bath

[Link to publication](#)

# Selective Catalytic Hydrogenation in a Structured Compact Multifunctional Reactor

Xiaolei FAN

A thesis submitted for the degree of Doctor of Philosophy

University of Bath

Department of Chemical Engineering

February 2010

# Acknowledgements

At first, I would like to express my deep and sincere gratitude to my leading supervisor, Professor Alexei A Lapkin. His patience, his advice, his enthusiasm, his inspiration, and his great efforts led me to be a qualified PhD. I could never achieve this much without his help and guidance. I am so grateful.

I am also indebted to my supervisor Dr. Pawel K Plucinski. His wide knowledge on chemical engineering, his insightful discussion and wise advice on my results have been of great value for me.

I am grateful to the technical and administrative staff in the Department of Chemical Engineering at the University of Bath, for helping the project to run smoothly and for assisting me in so many different ways during my PhD. John Bishop, Fernando Acosta, Anne O'Reilly, Merv Newnes, Robert Brain, Elaine Odgers, Sally Barker, and Tatiana Vazhnova deserve special mention.

I wish to thank all my friends and student colleagues for providing a stimulating and fun environment in which I relaxed and enjoyed the life after daily work.

As the only child in my family, I am deeply feeling that I owe my loving thanks to my parents. They have lost a lot of family time with me due to my research abroad. I would never be me without their timeless encouragement, understanding, and blessing. I love you, my father Wei FAN and my mother Guoqin WU.

I would also like to thank a special lady in my life, my wife, Miss Aiting Jia. My life would never be so beautiful and full of joy without your company and sunshiny mirth. I love you, lil Jia.

# Abstract

Selective hydrogenation is an important class of chemical reactions for the production of speciality chemicals, pharmaceuticals and petrochemicals. The challenges in this type of reactions are to control selectivity in hydrogenation of poly-functional molecules, and avoid the possible risk of reaction runaway due to the high exothermisity. In this project the fundamentals of liquid-phase hydrogenation reactions in a structured compact multifunctional reactor were investigated. This technology represents an advance over the existing hydrogenation technologies because it exploits the effects of reduced characteristic paths of mass and heat transfer, attained in compact reactor architecture with mm-scale reaction channels and integrated static mixers and micro-heat exchangers. Catalysts based on mesoporous synthetic carbons were developed especially for preparing micro-packed beds in the compact reactor. The investigation resulted in fundamental information on reactor performance for selected model reactions, heat transfer efficiency of the integrated micro-heat exchangers, development of continuous tandem reaction, and evaluation of developed catalysts for hydrogenation and hydrodehalogenation reactions under the continuous flow conditions being used. The results demonstrate that the structured compact multifunctional reactor might be a promising technology to transfer conventional heterogeneous catalysis to flow regime.

# Table of Contents

# Chapter 1

# General introduction

A general introduction of the thesis is given, in which the research scope is defined. Multiphase catalytic reactors for pharmaceuticals and specialty chemicals are introduced and discussed in brief. Structured compact reactor is introduced and its fundamental and practical advantages are detailed. The structure of the thesis is described.

## 1.1    Introduction

Conventional technologies for synthesis of pharmaceuticals and fine chemicals were largely chemistry intensive with a focus on quality assurance and overall productivity.[1]    Due to the high value of these products, the processes are commercially feasible even with low yields[1] so that issues related to process efficiency and environmental impact were considered low priority.  In recent years, constraints imposed by the increasingly stringent environmental regulations and societal awareness of safety, coupled with increasing competition, have put great stress on traditional chemical industry.   Development and implementation of more sustainable chemistry and chemical technologies is one of the most essential requirements for the chemical industry to survive for the future.  These challenges drive innovations in both chemistry and chemical engineering.  Recently proposed solutions, for example Green Chemistry and Process Intensification, will make significant contribution to improved sustainability of the chemical industry in the next decades.

Introduction of concepts of Green Chemistry and Sustainable Chemistry encourages the design of products and chemical processes that reduce or eliminate the use and generation of hazardous substances such as non-renewable feedstocks, by-products, solvents and reagents.[2, 3] These new concepts have initiated a fundamental change in every aspect of the field of chemistry such as: (*i*) the application of alternative solvents, *e.g.* water,[4, 5] fluorous[6] and ionic liquids,[7, 8] supercritical media,[9, 10] and their combinations, (ii) the use of alternative feedstocks, such as biobased materials, *i.e.* sugars and starches, and waste products, *i.e.* carbon dioxide,[11] as basic chemical building blocks, and  (*iii*) maximisation of atom efficiency in the manufacture of fine, specialty, and pharmaceutical chemicals and materials by green catalysis.

Implementation of Process Intensification (PI), *i.e.* any chemical engineering development that leads to a substantially smaller, cleaner, and more energy-efficient technologies,[12] is probably the most popular strategy for developing new chemical

processes and equipment because of its nature of allowing technologies for 'sustainable manufacturing' using eco-efficiency (mass and energy); intrinsic safety (benign-by-design) with improved quality of the product; reduced environmental impact; rapid plant response and great possibilities for distributed manufacturing.[13, 14] There are a number of PI approaches and these include intensification of mass transfer in static mixers,[15, 16] micromixers[17, 18] and rotating packed bed;[19, 20] intensification of heat transfer using compact/micro heat exchangers[21, 22] and nanofluids,[23] integration of different processes in one multifunctional step to reduce plant size and increase process efficiency, *e.g.* reactive distillation[24] and membrane reactors;[25, 26] and adoption of new reactors *e.g.* compact/microreactors,[27, 28] heat exchange reactor (HEX),[29] spinning disk,[30] impinging jets reactors,[31] for realising smaller, cleaner, safer, efficient and flexible chemical processes. Engineering innovation alone will not suffice to ensure that sustainable technology is fully achieved, however, under the tangible framework established by the Green Chemistry principles,[3] which aim at reducing environmental impact of every aspects of chemistry, the ultimate goal of chemical engineers is to develop energy-efficient, process-intensified, and environment-friendly chemical processes for the future sustainable chemistry and chemical industries. The microreactor technology is one of the candidates with huge potential to achieve the goal due to their intrinsic advantages over traditional chemical processes, for instance, more efficient mixing, heat and mass transfer; lower hazard potential; higher selectivity and yield; reduced time-to-market; lower capital cost and easy scale-up.

In this thesis, experimental investigation will be carried out using a mm-scale structured compact reactor in order to evaluate its potential applications in fine chemical and pharmaceutical chemistry industries.

## 1.2    Multiphase catalytic reactors for pharmaceuticals and fine chemicals

### *1.2.1    Conventional multiphase catalytic systems*

Catalysis is pervasive in the chemical industry and estimates are that 90 % of all commercially produced chemical products involve catalysts at some stage in the process of their manufacture.[32] In comparison with homogeneous catalysis, heterogeneous catalysis offers the advantage that products are readily separated from the catalyst.  Processes based upon heterogeneous catalytic systems, *e.g.* multiphase reactors, occur in diverse application areas and form the basis for manufacture of various basic chemicals and intermediates.[33]    Some examples of employing multiphase reactors include:[33] (*i*) the upgrading and conversion of petroleum feed-stocks and intermediates; (*ii*) the manufacture of bulk commodity chemicals that serve as monomers and other basic building blocks for chemicals and polymers with bigger molecule; and (*iii*) the manufacture of pharmaceuticals or chemicals that are used in fine and specialty chemical markets as drugs or pharmaceuticals.

For the fine chemical and pharmaceutical industries, implementation of catalytic procedures eliminates drawbacks in the stoichiometric synthetic routes,[1] *i.e.* generation of waste products consisting of inorganic salts, and use of toxic and corrosive reagents or raw materials with significant safety issues.  An example is the establishment of cleaner catalytic direct oxidations with molecular oxygen to replace stoichiometric oxidants such as potassium dichromate and sulphuric acid, chromium oxides, permanganates, periodates, osmium oxide, or hazardous chlorine causing high salt freights and heavy metal-containing dump unable to be recycled, as well as relatively expensive hydroperoxides, alkylperoxides, and peroxycarbonic acids.[34] Besides, application of multiphase catalysis has also been driven by the discovery and development of either new or improved catalysts for either emerging or existing processes.[35] Two examples are (*i*) a new process with sulphonic acid resin catalysts for dehydration of *tert*-butanol to high purity isobutylene and (*ii*) improved low pressure trickle-bed reactor process with $Ni/Al_2O_3$ catalyst for synthesis of morpholine.

Various types of multiphase reactors used in chemical industry have been described and reviewed by Dudukovic *et al.*,[33, 35] Chaudhari and Mills,[1, 36] and Biardi and Baldi.[37] The slurry-type reactors, for example stirred tanks and slurry bubble columns, and trickle bed reactors are representatives of multiphase reactors, which have been being used most extensively in chemical industry.[1, 33, 35-37] Slurry-type reactors are frequently used as batch or semi-continuous reactors due to the simplicity of operation[37] and the use of particulate catalysts (micrometre scale, 5–50 μm) for better kinetic efficiency.[38] However, there are intrinsic disadvantages of the slurry-type reactors that seriously limit their application in certain processes. For instances, in the case of a stirred tank reactor, abrasion of catalysts results in difficult catalyst separation, especially for the very fine particles[37-39] and low conversion and selectivity in continuously-operated slurry bubble column reactors due to the back mixing.[39] A packed-bed reactor, such as the trickle-bed reactor, is more convenient in terms of product and catalyst separation. However, larger catalyst particles (millimetre scale, 1–3 mm) and the low gas-liquid velocities are required to avoid excessive pressure drop,[38] resulting in a mass-transfer limited regime. Furthermore, maldistribution of reactants in a catalyst bed, *i.e.* fluid channels and bypasses formed in the bed, may lead to poor performance, develop local hot spots, which may give rise to catalyst deactivation, decrease in selectivity, and reaction runaways.[37-39] Another major drawback of conventional reactors for multiphase reactions is the inconvenience and complexity of maintaining the heat and mass transfer level, which are achieved in laboratory scale operations, in pilot scale units or industrial size units.[38] All those drawbacks existing in conventional multiphase systems result in long development time, high operating costs and low productivity.

### 1.2.2 *Microreactors*

The limitations in conventional multiphase catalytic systems are unfavourable from the point of view of process economics.[39] This motivates a systematic search for alternative reactor types that would overcome as much as possible the limitations in the existing reactors. Microreactors (with cross-sectional channel dimension between about 10 μm and about few mm) are representatives of the new reactors

with potential to replace the conventional multiphase reactors. Several advantages distinguish them from other types of reactors and give them the potential to be the next generation of reactors for producing fine chemicals and pharmaceuticals.

One of the most important fundamental advantages is the decrease of the physical size of a reactor. For a given difference in a physical property, decrease of linear dimensions leads to an increase of the gradient of the processing parameters (such as temperature, concentration, density or pressure).[28] Accordingly, the mass transfer, heat transfer, and diffusional flux are enhanced. In these small devices, a high specific surface area in the range of 10,000–50,000 $m^2$ $m^{-3}$ is achieved, which enables an effective mass and heat transfer compared to traditional chemical reactors.[40] As reviewed in a recent monograph on microreactors,[28] heat transfer coefficients up to 200 kW $m^{-2}$ $K^{-1}$ was reached in micro heat exchangers, which exceeds that of conventional heat exchangers by at least one order of magnitude. This feature allows microreactors to avoid hot-spot formation, attain higher reaction temperatures and reduce reaction volumes, which in turn improves the energy efficiency and reduces the operational cost.[40]

Another fundamental advantage is the unique way of scaling up microreactors for potential practical applications. In a microreactor system, a mixing structure or a reaction microchannel is identical to the functional unit which can be duplicated to attain the required throughput. The fluidic devices, therefore, can be run in parallel with a separate feeding system for screening purposes, *e.g.* screening catalysts and processes, or a manifold for distributing single fluid flow into many channels. The former application has already been investigated and proved to be a promising screening method with cost-saving advantages.[41] When considering the throughput required for practical production, microreactors demonstrate us a unique approach, *i.e.* numbering-up, to achieve this purpose. In an ideal situation, once operating conditions are established in a basic functional unit, the increase of the total throughput of the reaction system can be simply obtained by numbering up the basic unit. The stacked-up reaction systems also result in a high flexibility of adapting production capacity to varying market demand (in principle, production ability can be modified by changing the number of the basic reaction units).[28] Moreover,

parallel operation of a microreaction system enables a reliable continuous run of the reaction since failed microreactor(s) can be easily isolated and replaced without shutting down the whole system.[42]  Relevant investigations, however, showed that the realisation of this goal is crucially based on the efficiency of flow distribution system for the whole reaction unit.[28]

The volume of microreactors is significantly decreased (in the range from a few µL to hundreds of µL) as compared with conventional chemical reactors.  The decreased reaction volume enhances process safety and, due to the shorter residence time, improves selectivity of certain reactions.[28]  The smaller devices provide easy transportation which enables a distributed point-of-use production of highly reactive toxic chemicals[42] and low cost of construction materials and energy used for chemical production.  In summary, based on various reports over the past decades,[28, 43-47] a consensus has emerged that the technical drivers for development of microreactors and micro-process systems can be attributed to five key factors (*i*) safety; (*ii*) improved heat and mass transfer characteristics; (*iii*) distributed production; (*iv*) easier scale-up and (*v*) utility for implementation of high throughput screening techniques.   These advantages might enable microreactors to be considered as prime candidates for future chemical processes, especially for fine chemical and pharmaceutical industries.

## 1.3    Structured compact reactor

In this study, a mm-scale compact reactor was employed as a demonstration of application of structured reactors in the field of synthetic chemistry.  The structured compact reactor shown in Fig. 1.1 was developed and described elsewhere.[27, 48, 49] This reactor provides many fundamental and practical advantages for synthetic chemistry, stemming from its compact multifunctional design, *i.e.* integrated functionalities of mixing, heat transfer and reaction in one single unit, and appropriate choice of reaction channel sizes as well as flow reactor chemical processes.

**Fig. 1.1** Structured compact reactor-micro heat exchanger used in this work.

This structured compact reactor features several advantages for performing organic syntheses:

- Integration of static mixers. Static mixers, which are embedded prior to reaction channels, enable presaturation of gas in a liquid phase (premixing and preheating) before introducing reactants into the reaction channels.

- Employment of mm-scale reaction channels. Five packed-bed channels (100 mm length) are imbedded in parallel between the two heat transfer sections. The reaction channels have square cross-section with three different sizes: 2 mm × 2 mm, 3 mm × 3 mm (three of) and 5 mm × 5 mm. Each channel is equipped with standard Swagelok® fittings for connecting liquid and gas feed lines. A mm-scale reaction channel offers: (*i*) high radial temperature gradient for intensifying the process, (*ii*) allows the use of heterogeneous catalysts prepared by conventional methods, unlike microreactors, which depend on the ability to deposit a catalyst onto reactor walls.

- Integration of microchannel heat exchangers. Microchannel heat exchangers are arranged in cross-flow with respect to the static mixers and the reaction channels. The micro heat exchangers consist of parallel micro channels (133 mm × 0.55 mm × 3 mm), with perforations in the channel walls for avoiding

channel blockage, and for distributing the flow and pressure evenly. The two heat transfer passages are located underneath and above all reaction channels. Subsequently, all reaction channels have an even temperature field. The integrated compact design ensures an intensified heat transfer for the reactor due to (*i*) the reduced conduction resistance between the process fluid and the heat transfer medium, with the distance between fluids *ca.* 100 μm, and (*ii*) the enhanced convective heat transfer coefficient by using microscale heat transfer fluid channels.

- Intrinsic safety. Integration of microchannel heat exchangers, continuous operation, and the small reaction volume provide the compact reactor with a lower operation risk for conducting highly exothermic and endothermic processes.

- Easy scale-up. Scale-up of the reaction system can be readily achieved with minimal or no process development work by running several reactors in parallel ('numbering up').

- Other advantages are (*i*) robust structure, *i.e.* upper operating pressure limit of 75 barg, and (*ii*) suitability for distributed production.

## 1.4    Research scope

The main aim of this thesis is to evaluate the ability of the structured compact reactor for performing continuous catalytic chemistry based on a laboratory scale catalytic system. Selective hydrogenations were used as model reactions to assess the continuous-flow process in the structured compact reactor. Performance of the compact reactor was compared with other types of processes. The effects of operating parameters on the reactor performance were assessed. The ability of the compact reactor for studying reaction kinetics was also evaluated.

Additionally, the ability of the multichannel compact reactor was further exploited for different application purposes, such as (*i*) further intensifying embedded microchannel heat exchangers and chemical reactions by integrating thermal 'nanofluids', (*ii*) performing continuous tandem reactions, and (*iii*) developing new catalysts based on mesoporous synthetic carbons for micro and compact reactors.

The project has been carried out in the Department of Chemical Engineering at the University of Bath, but I would like to acknowledge MAST Carbon Ltd. (UK) for supplying the synthetic carbons, and Professor Yulong Ding's group at the University of Leeds for supplying thermal 'nanofluids' and cooperating in the heat transfer experiments.

## 1.5    Thesis structure

Chapter 2 reviews the state-of-the-art of microreactors technology.  This chapter focuses on the commercialised microreactors and summarises the developing trends of the technology.

Chapter 3 describes the application of the compact reactor in a continuous hydrogenation process.  The catalytic liquid-phase hydrogenation of benzaldehyde to benzyl alcohol was chosen as the model reaction.  Performance of the structured compact reactor (in terms of product yield, selectivity, average reaction rate, and space-time yield) for continuous hydrogenation was evaluated and compared with other types of reactors.  The effects of reaction conditions, *i.e.* gas/liquid flow-rates, pressure, and temperature, on the reactor performance were studied in detail.  The use of sequential dosing of hydrogen for enhancing reactor performance was also investigated.

Chapter 4 considers the study of thermal 'nanofluids' in the integrated microchannel heat exchangers for further intensifying heat transfer in a compact reactor.  The

possibility of performing dynamic control of chemical reactions via enhanced heat transfer was also studied and presented in Chapter 4.

Chapter 5 reports a continuous tandem reaction performed in the compact multichannel reactor.

Chapter 6 demonstrates the development of Pd supported on mesoporous carbon catalysts for flow catalysis in the compact multichannel reactor. The preliminary characterisation of synthetic carbon and two developed Pd/C catalysts are described. In addition, flow hydrogenation and hydrodehalogenation reactions were used to assess performance of the Pd/C catalysts in the structured compact reactor.

Chapter 7 is a summary of all experimental results and includes suggested future work needed for continuing this project.

## References

1.   Chaudhari, R. V.; Mills, P. L., Multiphase catalysis and reaction engineering for emerging pharmaceutical processes. *Chem. Eng. Sci.* **2004,** 59, (22–23), 5337–5344.

2.   Anastas, P. T.; Farris, C. A., *Benign by Design: Alternative Synthetic Design for Pollution Prevention*. American Chemical Society: Washington, DC, 1994.

3.   Anastas, P. T.; Warner, J. C., *Green Chemistry: Theory and Practice*. Oxford University Press: Oxford, 1998.

4.   Li, C. J., Organic-reactions in aqueous-media – With a focus on carbon-carbon bond formation. *Chem. Rev.* **1993,** 93, (6), 2023–2035.

5.   Li, C. J., Organic reactions in aqueous-media – With a focus on carbon-carbon bond formations: A decade update. *Chem. Rev.* **2005,** 105, (8), 3095–3165.

6.   Horvath, I. T., Fluorous biphase chemistry. *Acc. Chem. Res.* **1998,** 31, (10), 641–650.

7.   Binnemans, K., Lanthanides and actinides in ionic liquids. *Chem. Rev.* **2001,** 107, (6), 2592–2614.

8.    Pârvulescu, V. I.; Hardacre, C., Catalysis in ionic liquids. *Chem. Rev.* **2007,** 107, (6), 2615–2665.

9.    Jessop, P. G.; Leitner, A., *Chemical Synthesis Using Supercritical Fluids*. Wiley–VCH: Weinheim, 1999.

10.   Jessop, P. G., Homogeneous catalysis using supercritical fluids: Recent trends and systems studied. *J. Supercrit. Fluids* **2006,** 38, (2), 211–231.

11.   Park, S.-E.; Lee, K.-W.; Chang, J.-S., *Carbon Dioxide Utilisation for Global Sustainability*. Elsevier: Amsterdam, 2004.

12.   Stankiewicz, A. I.; Moulijn, J. A., Process Intensification: Transforming chemical engineering. *Chem. Eng. Prog.* **2000,** 96, 22–34.

13.   Jenck, J. F.; Agterberg, F.; Droescher, M. J., Products and processes for a sustainable chemical industry: A review of achievements and prospects. *Green Chem.* **2004,** 6, (11), 544–556.

14.   Perkins, J. D. In *Process intensification in practice: Applications and opportunities*, 2nd International Conference on Process Intensification in Practice, Antwerp, Belgium, 1997; Semel, J., Ed. Mechanical Engineering Publications Limited: Antwerp, Belgium, 1997; pp 17-22.

15.   Bourne, J. R.; Lenzner, J.; Petrozzi, S., Micromixing in static mixers: An experimental study. *Ind. Eng. Chem. Res.* **1992,** 31, (4), 1216–1222.

16.   Thakur, R. K.; Vial, C.; Nigam, K. D. P.; Nauman, E. B.; Djelveh, G., Static mixers in the process industries – A review. *Chem. Eng. Res. Des.* **2003,** 81, (A7), 787–826.

17.   Bökenkamp, D.; Desai, A.; Yang, X.; Tai, Y.; Marzluff, E. M.; Mayo, S. L., Microfabricated silicon mixers for submillisecond quench–Flow Analysis. *Anal. Chem.* **1998,** 70, (2), 232 –236.

18.   Ehrfeld, W.; Golbig, K.; Volker Hessel, V.; Löwe, H.; Richter, T., Characterisation of mixing in micromixers by a test reaction: Single mixing units and mixer arrays. *Ind. Eng. Chem. Res.* **1999,** 38, (3), 1075–1082.

19.   Peel, J.; Howarth, C. R.; Ramshaw, C., Process intensification: HIGEE seawater deaeration. *Chem. Eng. Res. Des.* **1998,** 76, (A5), 585–593.

20.   Ramshaw, C., HIGEE distillation – An example of process intensification. *Chem. Eng. (London)* 1983, pp 13–14.

21.   Tuckerman, D. B.; Pease, R. F. W., High-performance heat sinking for VLSI. *IEEE Electron Device Lett.* **1981,** EDL-2, (5), 126–129.

22.   Mundinger, D.; Beach, R.; Benett, W.; Solarz, R.; Krupke, W.; Staver, R.; Tuckerman, D. B., Demonstration of high-performance silicon microchannel heat-exchangers for laser diode-array cooling. *Appl. Phys. Lett.* **1988,** 53, (12), 1030–1032.

23.    Fan, X. L.; Chen, H. S.; Ding, Y. L.; Plucinski, P. K.; Lapkin, A. A., Potential of 'nanofluids' to further intensify microreactors. *Green Chem.* **2008,** 10, (6), 670–677.

24.    Harmsen, G. J., Reactive distillation: The front-runner of industrial process intensification. A full review of commercial applications, research, scale-up, design and operation. *Chem. Eng. Proc.* **2007,** 46, (9), 774–780.

25.    Adris, A. M.; Elnashaie, S.; Hughes, R., A fluidized-bed membrane reactor for the steam reforming of methane. *Can. J. Chem. Eng.* **1991,** 69, (5), 1061–1070.

26.    Tsotsis, T. T.; Champagnie, A. M.; Vasileiadis, S. P.; Ziaka, Z. D.; Minet, R. G., Packed-bed catalytic membrane reactors. *Chem. Eng. Sci.* **1992,** 47, (9–11), 2903–2908.

27.    Bavykin, D. V.; Lapkin, A. A.; Kolaczkowski, S. T.; Plucinski, P. K., Selective oxidation of alcohols in a continuous multifunctional reactor: Ruthenium oxide catalysed oxidation of benzyl alcohol. *Appl. Catal. A: Gen.* **2005,** 288, (1–2), 175–184.

28.    Ehrfeld, W.; Hessel, V.; Löwe, H., *Microreactors*. WILEY–VCH: Weinheim, 2000; p 288.

29.    Phillips, C. H.; Lauschke, G.; Peerhossaini, H., Intensification of batch chemical processes by using integrated chemical reactor-heat exchangers. *Appl. Therm. Eng.* **1997,** 17, (8-10), 809-824.

30.    Boodhoo, K. V. K.; Jachuck, R. J., Process intensification: Spinning disk reactor for styrene polymerisation. *Appl. Thermal Eng.* **2000,** 20, (12), 1127–1146.

31.    Mahajan, A. J.; Kirwan, D. J., Micromixing effects in a two-impinging-jets precipitator. *AIChE J.* **1996,** 42, (7), 1801–1814.

32.    Recognizing the best in innovation: Breakthrough catalyst. *R&D Magazine* September, 2005, p 20.

33.    Dudukovic, M. P.; Larachi, F.; Mills, P. L., Multiphase reactor – revisited. *Chem. Eng. Sci.* **1999,** 54, (13–14), 1975–1995.

34.    Hoelderich, W. F.; Kollmer, F., Oxidation reactions in the synthesis of fine and intermediate chemicals using environmentally benign oxidants and the right reactor system. *Pure Appl. Chem.* **2000,** 72, (7), 1273–1287.

35.    Dudukovic, M. P.; Larachi, F.; Mills, P. L., Multiphase catalytic reactors: A perspective on current knowledge and future trends. *Catal. Rev.* **2002,** 44, (1), 123–246.

36.    Mills, P. L.; Chaudhari, R. V., Multiphase catalytic reactor engineering and design for pharmaceuticals and fine chemicals. *Catal. Today* **1997,** 37, (4), 367–404.

37.     Biardi, G.; Baldi, G., Three-phase catalytic reactors. *Catal. Today* **1999,** 52, (2–3), 223–234.

38.     Roy, S.; Bauer, T.; Al-Dahhan, M.; Lehner, P.; Turek, T., Monoliths as multiphase reactors: A review. *AIChE J.* **2004,** 50, (11), 2918–2938.

39.     Pangarkar, K.; Schildhauer, T. J.; van Ommen, J. R.; Nijenhuis, J.; Kapteijn, F.; Moulijn, J. A., Structured packings for multiphase catalytic reactors. *Ind. Eng. Chem. Res.* **2008,** 47, (10), 3720–3751.

40.     Renken, A.; Hessel, V.; Lob, P.; Miszczuk, R.; Uerdinggen, M.; Kiwi-Minsker, L., Ionic liquid synthesis in a microstructured reactor for process intensification. *Chem. Eng. Proc.* **2007,** 46, (9), 840–845.

41.     Abdallah, R.; Meille, V.; Shaw, J.; D., W.; de Bellefon, C., Gas-liquid and gas-liquid-solid catalysis in a mesh microreactor. *Chem. Commun.* **2004,** 4, 372–373.

42.     Charpentier, J. C., Process intensification by miniaturisation. *Chem. Eng. Technol.* **2005,** 28, (3), 255–258.

43.     Mills, P. L.; Quiram, D. J.; Ryley, J. F., Microreactor technology and process miniaturisation for catalytic reactions – A perspective on recent developments and emerging technologies. *Chem. Eng. Sci.* **2007,** 62, (24), 6992–7010.

44.     Worz, O.; Jackel, K. P.; Richter, T.; Wolf, A., Microreactors, a new efficient tool for optimum reactor design. *Chem. Eng. Sci.* **2001,** 56, (3), 1029–1033.

45.     Hessel, V.; Lowe, H., Microchemical engineering: Components, plant concepts user acceptance – Part I. *Chem. Eng. Technol.* **2003,** 26, (1), 13–24.

46.     Hessel, V.; Lowe, H., Microchemical engineering: Components, plant concepts, user acceptance – Part II. *Chem. Eng. Technol.* **2003,** 26, (4), 391–408.

47.     Hessel, V.; Lowe, H., Microchemical engineering: Components, plant concepts, user acceptance – Part III. *Chem. Eng. Technol.* **2003,** 26, (5), 531–544.

48.     Plucinski, P. K.; Bavykin, D. V.; Kolaczkowski, S. T.; Lapkin, A. A., Application of a structured multifunctional reactor for the oxidation of a liquid organic feedstock. *Catal. Today* **2005,** 105, (3–4), 479–483.

49.     Plucinski, P. K.; Bavykin, D. V.; Kolaczkowski, S. T.; Lapkin, A. A., Liquid-phase oxidation of organic feedstock in a compact multichannel reactor. *Ind. Eng. Chem. Res.* **2005,** 44, (25), 9683–9690.

# Chapter 2

# A review of microreactor technology

Microreactors open a new window for process intensification and for developing new reaction routes due to their unique advantages such as intensive heat and mass transfers, continuous operation, environmentally benign features, and a numbering-up concept of scaling throughput.  Successful applications of microreaction systems in a wide range of areas speedup their appearance in chemical processes.

## 2.1 Introduction

Microreactors, inspired by high heat-transfer performance of microchannel heat sinks, have been in development since the early 1980s.[1] For the following thirty years, intensive research has been carried out to investigate the design and applications of microreactors due to their exciting features. The emergence of microreactors on the market and their industrial uptake occurred very quickly. In this chapter, a brief review will be given, reviewing the primary advantages of microreactors and the laboratory-scale applications of microreaction technology in synthetic chemistry. Furthermore, commercialised microreactors are also discussed in this review.

The characteristic dimensions of the internal structures of microreactors, for instance, fluid channels, typically range from the submicrometre to the sub-millimetre range.[2] Other terms, for example 'nanoreactors', 'milli-/minireactors', 'meso-scale reactors' or 'compact reactors', are also used for devices with the characteristic dimensions at the lower or the upper boundary of this dimensional range.[2] In author's opinion, compared with the sizes of conventional industrial reactors, all the reactors with the characteristic dimensions in the range from nanometres to millimetres exploit the benefits of miniaturisation of the structures where chemical reactions occur. Therefore, only one term, *i.e.* 'microreactor', will be used in this review.

## 2.2 Primary advantages of microreactors

### *2.2.1 Enhanced transport phenomena*

The small dimensions and the integrated compact design provide microreactors with the ability to effect excellent reaction control. For a given difference in a physical property, a decrease in linear dimensions leads to an increase in the gradient of the process parameters such as temperature, concentration, or pressure.[2] Accordingly, heat transfer, mass transfer, or diffusional flux are enhanced (Fig. 2.1).

**Fourier's Law:**

$$q_{heat}[J \cdot m^{-2} \cdot s^{-1}] \propto \frac{dT}{dy}$$

**Fick's Law:**

$$J_{diffusion}[mol \cdot m^{-2} \cdot s^{-1}] \propto \frac{dC}{dy}$$

Flux (q or J)

← Linear dimentions of reactors (y) ——
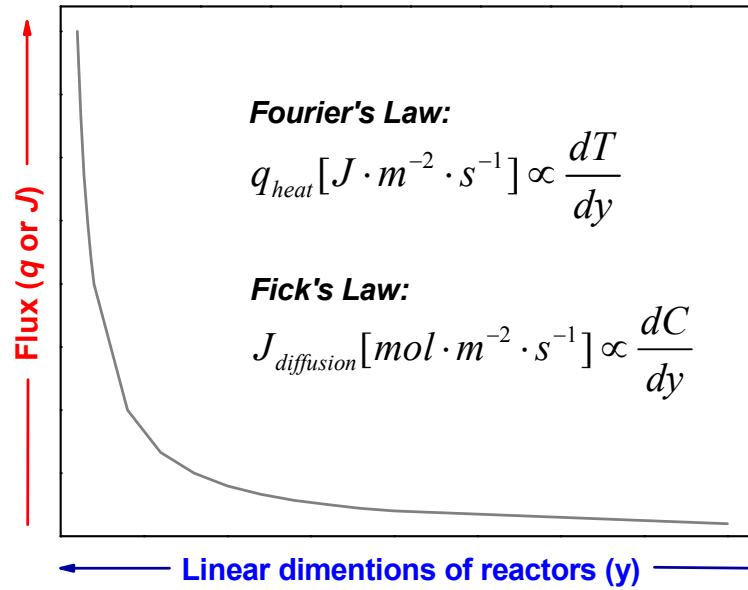
**Fig. 2.1** Schematic diagram of enhancement in transport phenomena by miniaturisation of characteristic diameter of reactors.

Most of micro devices employ multiple parallel channels with diameters between 10 and several 100s micrometres, where low Reynolds number laminar flows dominate. Therefore, the Nusselt number ($Nu$) is expected to be close to unity.[3] According to the single phase internal flow correlation for convective heat transfer (Eq. 2.1),[4, 5] in which heat transfer coefficient ($h$) scales inversely with channel width, $h$ can be enhanced theoretically as the channel diameter decreases.

$$h = Nu \cdot \frac{k}{D_h} \tag{2.1}$$

where $k$ is the thermal conductivity of the fluid and $D_h$ is the hydraulic diameter of the channel, $D_h$ is defined as:

$$D_h = \frac{4 \cdot A_{cross-section}}{U} \tag{2.2}$$

where $A_{cross-section}$ is the cross sectional area of the channel and $U$ is the perimetre of the channel.

Based on the aforementioned equation (2.1), heat transfer in microchannels was first studied by Tukerman and Pease in 1981.[1] Experimental results showed good improvement of heat transfer in microchannels, *i.e.* a forty-fold enhancement in reducing thermal resistance compared to conventional devices. These simple theoretical predictions were also evidenced by a number of studies concerning heat transfer in micro devices. As summarised in a recent monograph:[2] the majority of current microreactor/heat exchanger devices contain microchannels with typical widths of 50 μm to 500 μm; the separating wall material between reaction and heat transfer channels can kept down to 20 to 50 μm, if necessary. As a result, heat transfer coefficients up to 200 kW m$^{-2}$K$^{-1}$ measured in micro devices exceed those of conventional heat exchangers by at least one order of magnitude.

Good heat transfer properties in microreactors offer a precise temperature control of reactions, which is especially advantageous in the case of running heat-transfer-limited reactions. Subsequently, reactions of highly exothermic nature, *e.g.* hydrogenation of nitrobenzene[6] and nitration,[7, 8] can be performed under almost isothermal conditions in microreactors. For instance, nitration reactions, which are deemed to be particularly dangerous in industrial processes due to their very high reaction enthalpy and rates and the possibility to generate explosive byproducts.[7] A comparison was made using the autocatalytic nitration of phenol (Scheme 2.1) between a batch reactor (1 L capacity) and a microreactor (500 μm width, 2.0 mL internal volume).[7] An adiabatic temperature increase of 55 K was measured in a batch reactor, in contrast the temperature of the microreactor increased by less than 5 K under the same conditions. Consequently, a better selectivity to mononitro isomers (78 % in microreactor *vs.* 56 % in batch reactor) and higher yields of them (75 % in microreactor *vs.* 55 % in batch reactor) were achieved in the microreactor.
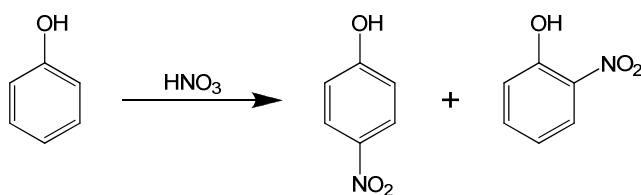
**Scheme 2.1** Nitration of phenol to the mononitro isomers.

Furthermore, it is also possible to change the temperature of microstructured reactors very rapidly to intentionally achieve a non-isothermal behaviour, *e.g.* rapid dynamic switch of chemical reactions[9] or reaction quenching.

Molecular diffusion is the predominant mixing pattern in microreactors since a laminar flow regime exists in almost all microreactors due to the small channel dimensions. Diffusional transport obeys Fick's law (refer to Fig. 2.1) which correlates to the change of concentration with time, and hence to the product of the diffusion coefficient and concentration gradient.[2] By rearrangement of this relationship, the dependence of the mixing time ($t_{mixing}$) on the width of the lamellae ($d_l$) is revealed by Eq. 2.3,[10] where it can be seen the positive effect of miniaturisation of characteristic structures on mixing. Consequently, a rather rapid diffusion mixing is promoted in microreactors compared with the turbulence and chaotic mixing in conventional reactors, *i.e.* mixing time scale in microseconds in microreactors[11] *vs.* seconds or longer in classical reactors.[12]

$$t_{mixing} \propto \frac{d_l^2}{D} \qquad\qquad (2.3)$$

where $D$ is the diffusion coefficient, which depends on temperature and properties of fluids, $d_l$ is the lamella width, which can be linearly related with the width of typical microstructures, *e.g.* channels.[2, 10]

Diffusion is already quite efficient on a microscale as the dominant mixing mechanism, it is still a rather slow process for many applications where mixing in extremely short intervals is usually required, for example mass-transfer-limited liquid-liquid[13] and liquid-gas reactions.[14] Subsequently, apart from streaming mixing,

various mixing principles were developed, such as splitting and recombination, bending, drilling, *etc.* (as summarised in ref. 2 and Fig. 2.2), to further enhance mixing processes in microreactors by reducing diffusional paths and increasing contact areas.
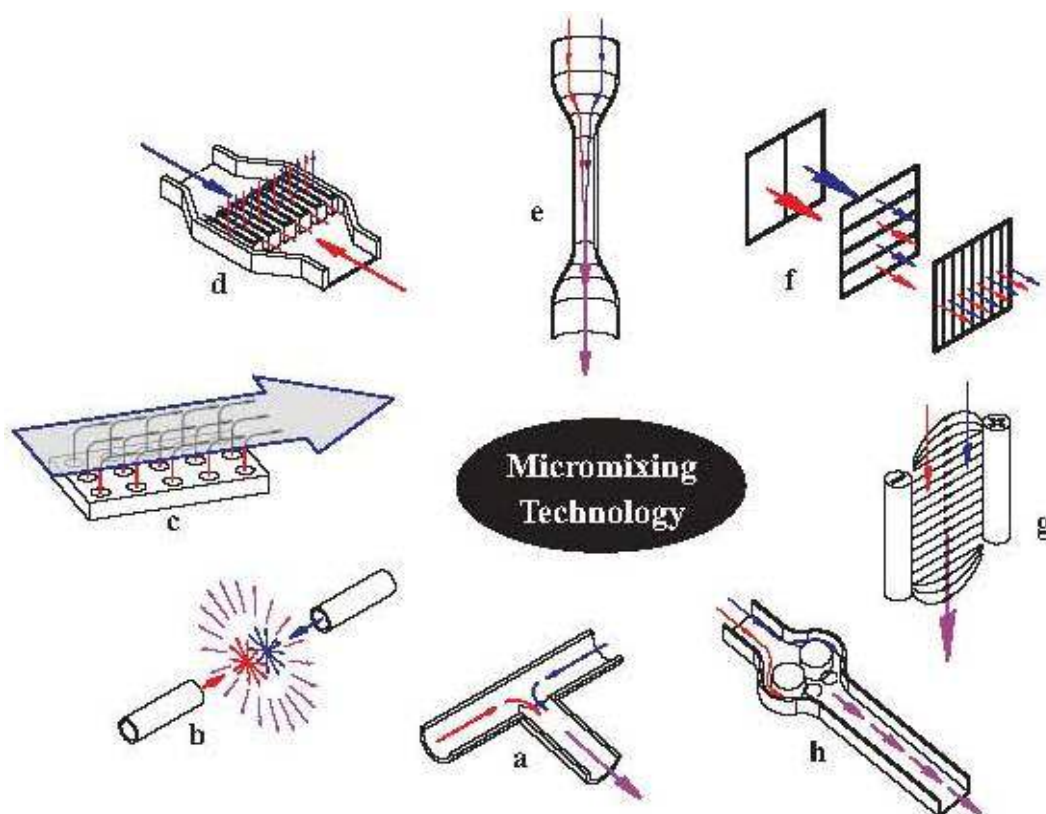
**Fig. 2.2** Generic design bases (derived from different mixing principles) for micro-mixing technology.[2] **a**: Contacting of two substreams, **b**: Collision of two high energy substreams, **c**: Injection of many small substreams of one component in a main stream of another component, **d**: Injection of many substreams of two components, **e**: Decrease of diffusion path perpendicular to the flow direction by increase of flow velocity, **f**: Manifold splitting and recombination, **g**: Externally forced mass transport, *e.g.* by stirring, ultrasonic wave, or electrical energy, **h**: Periodic injection of small fluid segments.

### 2.2.2  *Intrinsically safe and environmentally friendly processes*

Microreactors are inherently safe due to the effective reaction management, *i.e.* control of mixing, heat and mass transfer enhancement, and the inherently small processing volume. The substantial reduction of the active volume in microreactors allows the safe use of highly toxic reactants by reducing the risk of exposure to the personnel and the environment (even in case of accidents). Chambers and Spink

successfully demonstrated the use of a microreactor (100 mm × 500 μm × 500 μm) for efficient and safe fluorination and perfluorination reactions (Scheme 2.2) involving using fluorine gas, and generating HF as a byproduct.[15]
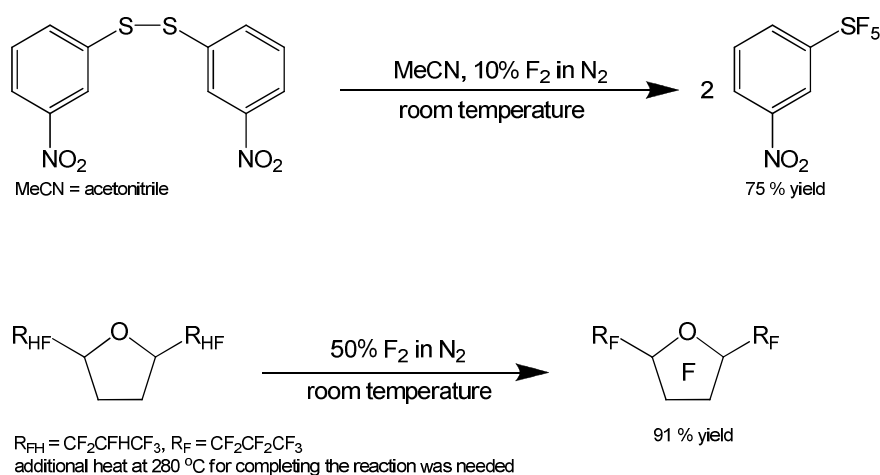


**Scheme 2.2** Fluorination and perfluorination reactions requiring $F_2$ addition.

The potentially explosive reactions also benefit from employing microreactors because explosions could be suppressed by simply using the small channels with a hydraulic diameter below the radical quenching distance.[16] Gas phase Pt-catalysed $H_2 + O_2$ reaction (a typical radical chain reaction of the sufficiently exothermic nature) was performed using a quartz tubular microreactor (600 μm diameter) and showed the possibility of conducting this highly explosive reaction without the occurrence of flame or explosions at temperatures in excess of 1273 K (at ambient pressure).[16] Even working with pure oxygen at elevated pressure might be possible in a laboratory-scale setting. An attempt to study the hazardous oxidation reaction (Scheme 2.3) at up to 24 atm undiluted oxygen pressure was examined with a mm-scale compact reactor (100 mm × 3 mm × 3 mm) by Bavykin *et al.*[17] The capital and operating cost, from a practical point of view, could be significantly decreased due to miniaturisation of the reactor sizes, the close reaction control and the increased reaction intensity and throughput.
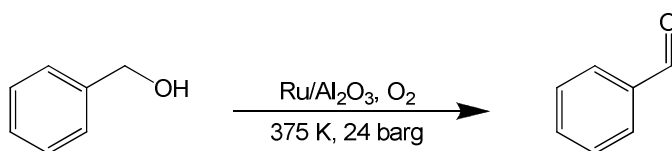
**Scheme 2.3** Oxidation of benzyl alcohol with molecular oxygen.

### 2.2.3 Time- and cost-saving scale-up

The many unique properties and advantages of microreactors originated from miniaturisation, conventional scale-up procedure therefore is not suitable for microreactors to increase their throughput to the industrially relevant level. The strategy known as 'numbering-up' provides microreactors with an alternative approach to implement in practice high-throughput production. In the microreactor systems once the reactor functions and operation conditions are established for a single basic functional unit, the increase in the total throughput of the system can be simply obtained by numbering up the basic unit, *i.e.* using multiple reactors as needed in parallel, and the identical quality achieved in a single unit can be sustained in the pilot-plant or production-scale quantities.[11, 18]

The feasibility of this concept was demonstrated with a microreactor system (micromixer-based system) for performing Grignard reaction (Scheme 2.4).[19] And an identical level of product yield was achieved for the transfer of synthesis from lab-scale to a pilot reactor. A laboratory-scale set-up resulted in a yield of 83 % desired product (phenyl boronic acid), whereas a 'numbering-up' system achieved a yield of 89 % with even higher selectivity.



PhMgCl = Phenyl Magnesium Chloride
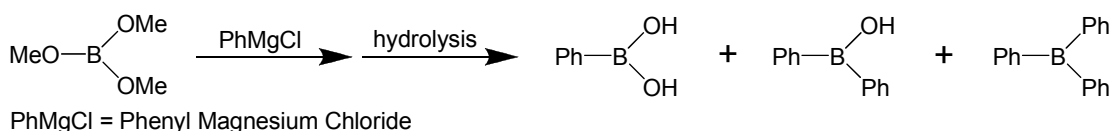
**Scheme 2.4** Grignard addition to trimethylborate.

This concept was also successfully demonstrated in several industrial projects by using integrated microreaction systems developed by Cellular Process Chemistry

Systems (known as CPC-Systems).[18]  One example is a microreaction system which was tailored to the specific demands of a precipitation process with a capacity of 30 t/a.[18]

Stacked-up microreaction systems also provide good flexibility in adapting production capacity to varying market demands (in principle, production ability can be modified by changing the number of basic reaction units).[2]  Relevant investigations, however, showed that the realisation of this goal is crucially based on the efficiency of flow distribution system for the whole reaction unit.[2]  Moreover, parallel operation microreaction systems enable a reliable continuous run of the reaction (*i.e.* failed unit(s) can be easily isolated and replaced without shutting down the whole system).[20]  This might be of importance for industrial operations when considering saving the operational time and cost.

## 2.3    Laboratory-scale application of microreactors

Applications of microreactors in organic synthesis has burgeoned into a widely studied field in industrial and academic environments since mid-1990s.[12]  Several recent reviews have summarised the application examples carried out in microreactors for the organic transformations.[11, 19, 21-29]  The majority of studies are conducted as laboratory-scale applications of microreactors and in the following sections a brief review is given of these applications.  The first part focuses on the homogeneous reactions (in synthetic chemistry), which include stoichiometric reactions and catalysis with soluble catalysts in flow, and the second section details the heterogeneous catalytic reactions in microreactors.

### *2.3.1    Liquid phase synthetic chemistry in microreactors*

Microreactors are interesting for liquid-liquid reactions, either stoichiometric synthetic routes or reactions powered by soluble catalysts, because of the ease of manipulation of the reactions in comparison with conventional reactors.  The

application of microreactors for reaction optimisation is demonstrated by using a glycosylation reaction (Scheme 2.5). Glycosylations are very challenging in conventional processes due to the dependence of the stereochemical outcome on multiple reaction variables, such as the nature of the coupling partners, *i.e.* their conformation, sterics, and electronics, concentration, temperature, residence time, and stoichiometry, which gives rise to great complexity in searching for optimal reaction conditions for a desired transformation.[30] A silicon microreactor system (Fig. 2.3) was used to obtain the comprehensive information of the model reaction (Scheme 2.5) in a short time (44 reactions at different conditions in one day) for determining the optimum conditions (temperature and residence time) for producing the desired product **3**. Moreover, only small amount of valuable glycosylating agent (2 mg) was required for each run, which significantly saved the operational cost in comparison with the traditional batch processes.



TMSOTf = Trimethylsilyl trifluoromethanesulfonate
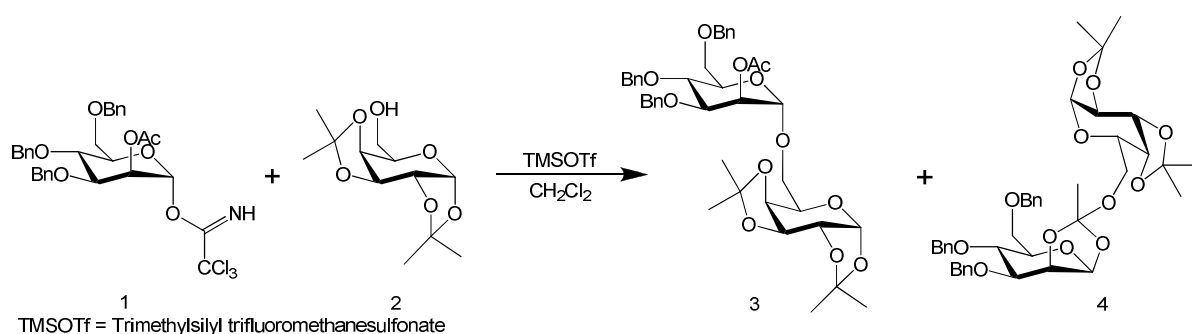
**Scheme 2.5** Glycosylation of glycosyl donor **1** and nucleophile (glycosyl acceptor) **2** to fashion disaccharide (desired product) **3** with byproduct orthoester **4**.
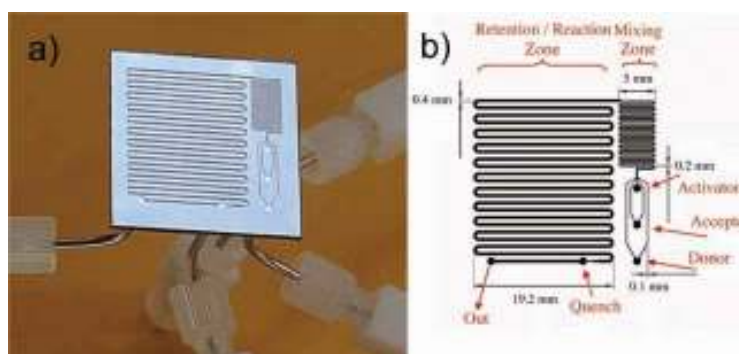


**Fig. 2.3** The silicon microreactor used in Ratner *et al.*[30] a) the microreactor, b) schematic diagram of the microreactor system.

When using conventional batch reactors inefficient temperature control is common, especially in running fast and highly exothermic reactions, where complex control strategies are required for maintaining the product quality and avoiding thermal runaways. Microreactors' good ability on the reaction thermal control (section 2.2.1) makes them efficient to run these reactions. For instance, a fast and exothermic Girgnard exchange reaction (Scheme 2.6) was conducted in a reaction system consisting of micromixers and shell and tube micro heat exchangers (micro tube with 500 μm i.d.).[31] Effective control of the reaction was achieved by virtue of fast mixing and efficient heat transfer in the microsystem. The microreaction system therefore is able to run the reaction at higher temperatures with better yields (*e.g.* at 353 K with a yield of *ca.* 98 %, at 5 second residence time),
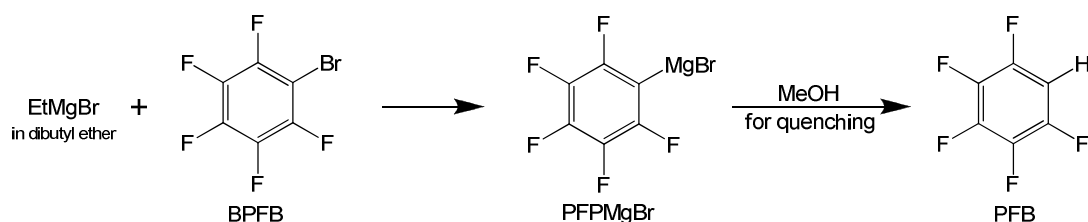


**Scheme 2.6** Grignard exchange reaction. Ethylmagnesium bromide (EtMgBr) reacts with bromopentafluorobenzene (BPFB) to form pentafluorophenylmagnesium bromide (PFPMgBr). Methanol is added after the reaction to quench the reaction and form pentafluorobenzene (PFB) for GC analysis.

Similar to Grignard reactions, nitration reactions were successfully performed in microreactors.[7, 8, 32-35] Dummann *et al.*[34] presented the use of a capillary-microreactor (i.d. = 0.5–1.0 mm) for nitration of single ring aromatics. Due to the high specific surface area of the small diameter capillaries and the resulting high heat transfer rates, isothermal operation could be maintained for the highly exothermic process. In addition, for this homogeneously catalysed reaction (liquid-liquid two phase, sulphuric acid in the aqueous phase as catalyst), the two-phase plug-flow with a well-defined flow pattern of alternating plugs of the two phases formed in the capillary gives a constant specific interfacial area between the two immiscible phases, and results in a fast mass transfer between the phases. The enhanced mass transfer at the boundaries between phases is very important for enhancing the product yield and selectivity of the mass transfer limited reactions. This was further confirmed by Antes *et al.*[8] in the nitration of toluene using a silicon microreactor. The high

mononitrotoluene yields of 89–92 % were obtained and the selectivity for the para-substituted product was increased considerably compared to the selectivity in the industrial process (43.5 % *vs.* 33 %).[8]

The multi-liquid-phase reaction systems, which in batch reactors usually demand the extra agitation for intensifying phase transfer, also benefit from the large specific interfacial areas offered by microreactors. A phase-transfer alkylation reaction was promoted successfully by using a glass microreactor (45 cm × 200 μm × 100 μm).[36]
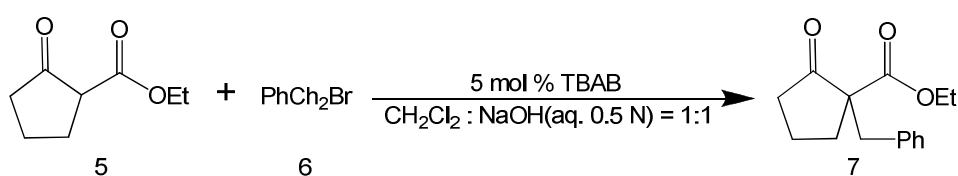


**Scheme 2.7** Phase-transfer benzylation reaction. Organic phase: dichloromethane solution containing the substrate (ethyl 2-oxocyclopentanecarboxylate **5**) and the alkylating agent (benzyl bromide **6**); aqueous phase: aqueous solution containing the phase-transfer catalyst (tetrabutylammonium bromide, TBAB) and the sodium hydroxide.

A 57 % yield of product 7 was obtained in the microreactor at 60 seconds residence time, whereas, only 37 % yield was achieved in a batch reactor (round-bottomed flask) after vigorous stirring (1350 rpm) for 60 seconds. By optical microscope study, it was found that the organic phase formed small droplets (segments) inside the aqueous tube, which resulted in a more extended interfacial area for accelerating the reaction.

The promising results obtained in the laboratory studies for microreactors in homogeneous synthesis accelerate the pace of their acceptance in the commercialisation market. A recent commercialised demonstration is the structured compact reactors known as the ART® plate reactors (see Fig. 2.4), from Alfa Laval.[37] The compact reaction system contains flow-directing reactor plates (mm-scale channel), heat transfer plates, and pressure plates, which allows easy numbering-up for increasing productivity and quick disassembly, reassembly for cleaning. Due to the advantages, *i.e.* (*i*) continuous operation, (*ii*) effective heat transfer by the integrated plate heat exchangers, and (*iii*) flexible reactant addition and sampling

along the reaction channels, the ART® plate reactors were demonstrated as efficient tools for performing several homogeneous liquid reactions (Scheme 2.8) such as solvent-free Red-Al reduction and Grignard reactions, and tandem BuLi reaction (halogen-lithium exchange with sequential carbonyl addition).
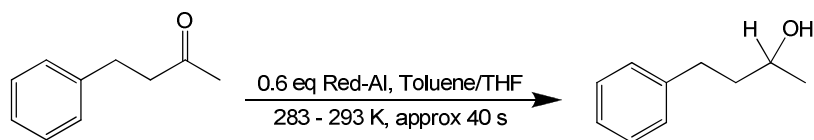


benzyl acetone — 0.6 eq Red-Al, Toluene/THF; 283 - 293 K, approx 40 s → 4-phenyl-2-butanol

THF = Tetrahydrofuran, Red-Al = Sodium bis(2-methoxyethoxy)aluminumhydride
(a) solvent-free Red-Al reduction, 99 % yield.
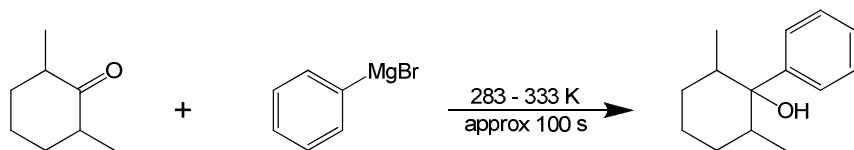
2,6-dimethylcyclohexanone + PhMgBr — 283 - 333 K, approx 100 s → 1-(1-phenyl-2,6-dimethyl) cyclohexanol

PhMgBr = phenylmagnesium bromide
(b) solvent-free Grignard reaction, 98 % yield.
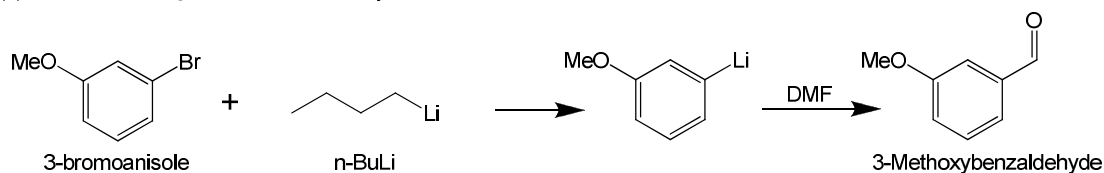
3-bromoanisole + n-BuLi → [MeO-phenyl-Li] — DMF → 3-Methoxybenzaldehyde

(c) tandem BuLi reaction, max yield of 98 % at 264 K, total residence time 40 - 90 s.

**Scheme 2.8** Homogeneous liquid reactions performed in ART® plate reactors from Alfa Laval.
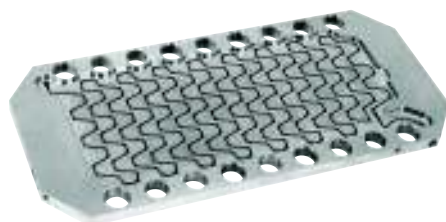


(a)                                          (b)

**Fig. 2.4** The ART® plate reactor from Alfa Laval:[37] (a) the reactor plate, (b) the reactor assembly.

Apart from the application examples introduced here, a wide variety of liquid-phase reactions have been successfully performed in microreactors, *e.g.* soluble metal catalysts promoted cross coupling and ring-closing metathesis reactions, stoichiometric nucleophilic aromatic substitution and Wittig reactions demonstrated by Comer and Organ,[38] glycosylations, olefinations and epoxidations by Snyder *et al.*,[39] peptide couplings by Watts *et al.*,[40, 41] aldol reactions by Wiles *et al.*[42] and Mikami *et al.*[43] There are minimal application limits for performing liquid-phase reactions in microreactors except the processes with the potential for generating precipitating products or byproducts that might clog up reaction channels.[23]

### 2.3.2 *Heterogeneous catalysis in microreactors*

Catalysis often provides cleaner and more efficient routes for synthetic chemistry in comparison with stoichiometric synthesis. In conventional processes, the use of heterogeneous catalysts facilitates the catalyst recycling and reuse. The negative effects on the selectivity and yield though, caused by the limited heat and mass transfers in heterogeneous systems are hard to avoid,[29] furthermore high operating pressure is often needed for increase of reaction rates. In industry, however, reactions at high pressures using batch reactors should be avoided for safety and economical reasons.[44]

If fine catalyst particles are used for a more kinetically efficient process,[45] as used by stirred tank reactors and slurry bubble columns,[46-48] the problem of catalysts separation rises and demands extra operations and costs. In microreactors, large gradients in concentration and temperature and high specific surfaces achieved by shrinking the characteristic dimensions give rise to exceptional fast transfer phenomena which are especially advantageous for the highly exothermal reactions and for the heat- and mass-transfer-limited reactions. Furthermore, the intensified mass transfer in microreactors normally avoids the necessity of using higher pressures.

Catalytic solid-liquid reactions[49-53] benefit from the excellent thermal management and the continuous diffusional mixing in flow in the microreactor systems.    In conventional processes such reactions, especially for those with strong exothermicity, are usually operated in stirred tank reactors with slowly dosing of on a reactant (portion by portion) for maintaining the isothermal conditions due to the limited heat removal capacity.   Consequently, the process time is no longer dependent on the kinetics but instead on the time constant of heat removal.[54]   For the stirred-tank reactors, the characteristic time of heat transfer ($t_{tr}$) increases proportional to the diameter (Eq. 2.4), whereas it decreases with the square of the diameter for the microreactors (Eq. 2.5).[54]

$$t_{tr} = \frac{\rho \cdot V \cdot c_p}{U \cdot A} \tag{2.4}$$

$$t_{tr} = \frac{\rho \cdot c_p \cdot D^2}{4 \cdot \lambda \cdot Nu} \tag{2.5}$$

where $\rho$ is density (kg m$^{-3}$),  $V$ is the reactor volume (m$^3$), $c_p$ is the specific heat capacity (J kg$^{-1}$ K$^{-1}$), $U$ is the overall heat transfer coefficient (W m$^{-2}$ K$^{-1}$), $A$ is the heat exchange surface area of the reactor (m$^2$), $D$ is the reactor diameter (m, for microreactors, the diameter of the channel), $\lambda$ is the thermal conductivity (W m$^{-1}$ K$^{-1}$), $Nu$ is the Nusselt number.

In a stirred-tank reactor with an inventory of several thousand litres this leads to a process time of several hours, whereas the same or even higher yields can be obtained in microstructured reactors within a few seconds.[54]   Moreover, separation steps become unnecessary due to the strategies of introducing heterogeneous catalysts in micro reactors such as immobilisation of catalysts[49, 50] on the channel surface and use of packed-bed.[51-53]   For example, Knoevenagel condensation (Scheme 2.9) was promoted by a zeolite catalyst coated microreactor with yields up to 80 %.[50]   This reaction, typically catalysed by organic bases, was shown to be cleaner since solid-phase catalysts precluded catalyst mixing with the product. Metal-catalysed  Heck  coupling  reactions  were  successfully  transferred  to

microreactor systems[51, 55, 56] and demonstrated in a continuous Pd/C catalysed (10 % palladium on charcoal loaded in a cartridge) microreaction system (Scheme 2.10).[51] In a 30 minute of residence time at 403 K, a 99 % substrate conversion and 100 % selectivity to the desired product were achieved in the flow system. Suzuki–Miyaura coupling reaction (Scheme 2.11) in a microreactor was shown by Greenway *et al.*[53] In this T-shaped microchannel reactor, a THF/water solvent mixture was used to facilitate the electroosmotic flow. Unlike conventional Suzuki reactions, the base addition was found unnecessary in this microreaction system. This phenomenon was explained by the presence of high electrical field needed for the electro-osmotic flow water can form hydroxide ions on the large silica surface, which has the potential to be sufficient to perform the function of the conventional organic or inorganic base.
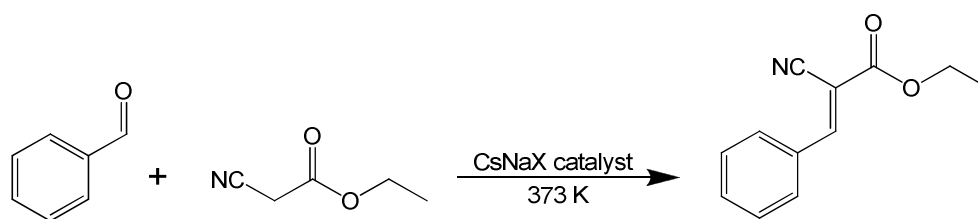


**Scheme 2.9** Knoevenagel condensation between benzaldehyde and ethyl cyanoacetate catalysed by catalyst-functionalised zeolite coatings on microchannel.
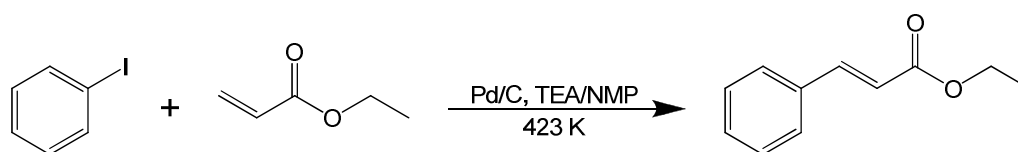


TEA = triethanolamine, NMP = *N*-Methyl-2-pyrrolidone

**Scheme 2.10** Heck reaction forming ethyl cinnamate by reacting iodobenzene with ethyl acrylate.
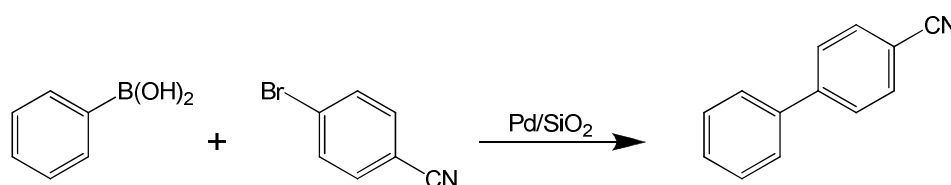


**Scheme 2.11** Suzuki-Miyaura coupling of 4-bromobenzonitrile and phenylboronic acid.

In comparison with the batch reactor, an acylation reaction (Scheme 2.12) was proved to be more productive in a flow packed-bed microreactor (capillary packed with immobilised 4-dimethylaminopyridine catalyst on the methacrylate-based amberzyme oxirane resin, AO-DMAP),[52] *i.e.* 3.2 *vs.* 1.0 in mmol product $mL^{-1} min^{-1}$ mmol catalyst$^{-1}$.
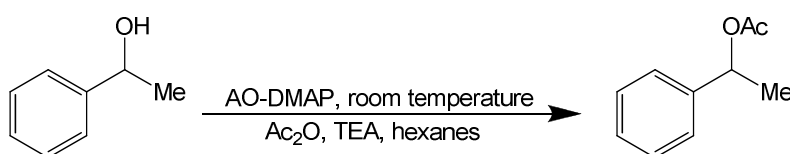


**Scheme 2.12** The acylation of *sec*-phenethyl alcohol.

Multiphase catalytic reactions, such as catalytic hydrogenation and oxidation reactions, are important in chemical industry.[23] Molecular oxygen and hydrogen are deemed the ultimate green reactants for these chemical processes; however, the limited mass transfer between phases, difficulty to activate $O_2$ and $H_2$, and the high-level safety requirements restrict their applications in conventional chemical processes. In microreactors, these reactions can be promoted more efficient due to the abovementioned advantages. Jensen's group studied catalytic partial oxidation of $NH_3$ (molecular oxygen, thin-film Pt-catalyst) with a microreactor and demonstrated feasibility of conducting catalytic gas phase reactions in microfabricated systems.[57] The group of Kobayashi conducted intensive studies with Pd-immobilised microreactors for hydrogenation reactions.[49, 58, 59] The system was proved to be very efficient for reducing various of substrates, such as mono-, bi-, and trisubstituted alkenes and alkynes, deprotected benzyl ether and carbamate protecting groups. High efficiency and yields were attributed to the small dimensions of the microreactor. Narrow channels enabled greater interaction between the solid, liquid, and gaseous phases than in a batch, increasing the reaction rates.[11]

Commercialised examples of catalysts-immobilised microreactors are the falling film microreactors (Fig. 2.5) from the Institut für Mikrotechnik Mainz GmbH (known as IMM, Germany).[60] The microchannel falling film reactors (typical dimension: 78

mm × 300 μm × 100 μm , 64 channels, separated by 100 μm wide walls) are able to generate stable films less than 100 μm thick, which is an extraordinary enhancement compared to the films with thickness on the order of 0.5–3 mm in the conventional falling-film systems.[61]  Hence, these reactors offer good heat and mass transfer characteristics which were proven with the Pd-catalysed hydrogenation of nitrobenzene,[6] and hydrogenation of cyclohexene.[62]  In both cases alumina was deposited on the wall by washcoating with subsequent Pd deposition by different methods, such as wet impregnation, incipient wetness, sputtering, and UV-decomposition of precursors.[6, 62]
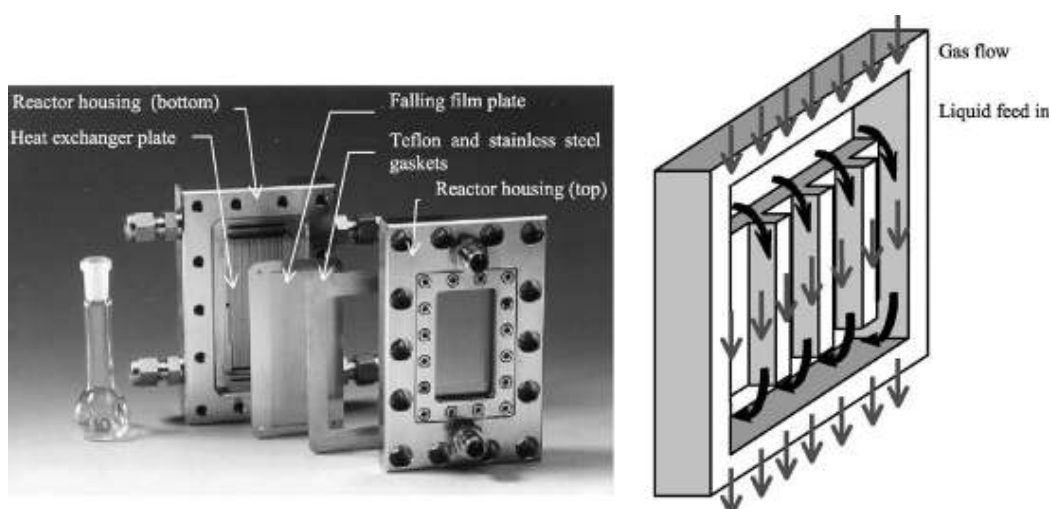


**Fig. 2.5** Components and schematic of the microstructured falling film reactor.  Adopted from ref. 6.

In the author's opinion, compared with wall-immobilised heterogeneous catalytic microreactors, packed-bed microreactors are more attractive in the field of liquid-gas-solid reactions from a practical point of view.  Packed-bed microreactors allow to use heterogeneous catalysts prepared by conventional methods, such as carbon supported metal catalysts, which are more economical and practicable, compared with the complex wall-coating methods.  A series of laboratory-scale investigations were conducted with packed-bed microreactors, such as packed-capillary reactor for hydrogenation reactions,[44] packed-bed microchannel reactor for phosgene synthesis,[63] sunflower oil hydrogenation,[64] and a packed-bed enzymatic microreactor.[65]

A series of commercialised microreactor systems, known as H-Cube® and X-Cube® systems, from ThalesNano Inc. (Hungary)[66] received much attention for their contribution to heterogeneous gas-liquid catalysis. Several applications, such as catalytic nitro/nitrile reduction,[67] catalytic double-bond/heterocycle saturation,[67] selective hydrogenation of cinnamaldehyde to cinnamyl alcohol,[67] diastereoselective hydrogenation of dihydropyrimidones,[67] enantioselective hydrogenation of activated ketones,[68] catalytic hydrogenation of imines to amines,[69] and aminocarbonylation,[70] were demonstrated for verifying their efficiency in the field of heterogeneous catalysis, especially for hydrogenation reactions.

Another approach is to use mm-scale reaction channels packed with well-structured catalyst particles. An example is the compact reactor developed at Bath, see Fig. 2.6. Selective oxidation by molecular oxygen,[17, 71, 72] selective hydrogenation by molecular hydrogen,[73] and continuous tandem synthesis[74] were all successfully transferred to this compact reactor flow system. Scale-up was also conducted for studying the feasibility of using the compact reactor system for high-throughput production.

**Fig. 2.6** (a) Structured compact reactor with mm-scale reaction channels, (b) the pilot-scale compact reactor (192 of 500 mm length, 3 mm i.d. channels, up to 150 t/a liquid throughput).

## 2.4 Commercialisation of microreactors

Driven by the distinct advantages of microreactors, a number of microreactors or microreactor-based reaction systems have emerged in the commercial market. Ehrfeld Mikrotechnik BTS GmbH (a wholly-owned subsidary of Bayer Technology Services GmbH, Germany)[75] and Institut für Mikrotechnik Mainz GmbH (IMM, Germany)[60] are leading companies for providing technical solutions with metal-based miniaturised reactors. Ehrfeld is well-known for the modular microreaction system[75] which provides a wide variety of micro structured modules, such as mixers, heat exchangers, reactors, sensors and actuators. A microreaction plant for a given process can be quickly and simply constructed by combining the required modules and embedding them on a base plate (clamping modules and sealing plates are needed for ensuring stability and safety). This design offers the highest flexibility for different applications in different areas and several reactions were performed in the modular microreaction system, such as Wittig reaction, Grignard reaction, Suzuki coupling and heterogeneous catalysis. Another product from Ehrfeld is the Miprowa® Technology,[75] which can be adapted as either heat exchangers or reactors. Rapid temperature equalisation and intensive cross-mixing can be achieved by the forced flow even at low laminar flow velocities due to the use of micro structured flow channels (channel sizes: $12 \times 1.5$ mm for lab scale devices, $18 \times 3$ mm for pilot and production scale apparatuses) equipped with the changeable comb-type inserts. This design allows good adaptability to regulate the pressure drop, area/volume ratio, mixing intensity and flow velocity for optimising the service performance of channels, and easy cleaning and maintenance. Standardised Miprowa® apparatuses can be tailored either for laboratory and R&D areas (3-200 L h$^{-1}$ throughput) or for large application ranges (up to 50,000 L h$^{-1}$ throughput).

IMM is also a pioneer in the field of implementing process intensification by miniaturisation.[60] The slit interdigital microstructured mixers, caterpillar mixers, and falling film microreactors have been successfully applied in laboratory-scale investigations, for example phenyl boronic acid synthesis,[76] high-efficient extraction processes[77] and direct fluorination of toluene with elemental fluorine.[78] Modular microreactor based systems for production plants are also realised based on these

standard microstrcutured devices. Another commercially available metal-based microreactor systems are the ART® plate reactors (see above) from Alfa Laval.[37]

A wide range of glass-based microreactors is also available on the market. Companies such as Chemtrix BV (Netherlands & UK),[79] Mikroglas Chemtech GmbH (Germany),[79] Micronit Microfluidics BV (Netherlands),[80] Bartels Mikrotechnik GmbH (Germany),[81] Fraunhofer ICT (Germany)[82] and Corning (USA)[83] are manufacturing glass chips with different microchannel configurations. The Corning's Advanced-flow™ glass reactors[83] can be scaled up for potential manufacturing purposes through the modular design.

Automation and standardisation of the microreaction system is a significant challenge, which must be overcome for their successful commercialisation. Process automation in microreactor system is of importance for rapid and highly flexible development of processes and products, especially for the R&D stage. 'FAMOS*flexible*' (a fully automated microreaction system) from Fraunhofer ICT[82] makes possible systematic screening of parameters and generation of sample databases for subsequent investigations. In addition, the integrated safety features and optional remote control and observation system enable the investigation of potentially hazardous reactions.

The innovative microreactor systems should be standardised and easily integrated with the existing chemical processing infrastructure, such that time and cost generated by the system migration or mergence can be significantly reduced.

Integration of on-time process analysis with the microreactor systems is another significant development and commercial opportunities. This might be important to gain the detailed information of the physical-chemical processes for improving the processes, such as target and optimise specific reaction steps, to achieve consistent product quality and reduce process costs. Conducting online analysis on a microscale is simpler than in conventional processes; some pioneered works have been reported by Fraunhofer ICT.[82] For example, adoption of optical spectroscopic analysis methods (IR, Raman and UV/Vis/NIR) for process analysis as inline, online

or atline measurement technologies for the design and optimisation of chemical processes. High-speed microscopy and fibre optics can be used for visual monitoring and imaging of processes in microchannels. Integration of reaction calorimetres allows to study thermodynamics and kinetics in microchannels. Through these analyses, a direct insight about product composition, kinetic and mechanistic data about the processes could be obtained, which is valuable when designing process components and selecting suitable process conditions.

## 2.5    Conclusions

The numerous investigations of microreactors at different application scales have shown the promise. In comparison with conventional chemical processes, their advantages demonstrated, *i.e.* enhanced reaction control in terms of heat and mass transfer, inherent safety, continuous operation, increased atom efficiency (decreased raw inputs and wastes), simple scale-up, easy optimisation, and potential for distributed manufacturing business model, ensure that this technology will have a substantial impact on the future chemistry and chemical industries. The problems that persist, such as lack of experience in production-scale operation and high cost of manufacturing of complex microreactors, however, still remain as barriers for rapid adoption of microreactors into widespread use.

## References

1.    Tuckerman, D. B.; Pease, R. F. W., High-performance heat sinking for VLSI. *IEEE Electron Device Lett.* **1981,** EDL-2, (5), 126–129.

2.    Ehrfeld, W.; Hessel, V.; Löwe, H., *Microreactors*. WILEY–VCH: Weinheim, 2000; p 288.

3.    Incropera, F. P.; DeWitt, D. P., *Fundamentals of Heat and Mass Transfer*. 4th ed.; Wiley: New York, 1996.

4.  Brandner, J. J.; Benzinger, W.; Schygulla, U.; Zimmermann, S.; Schubert, K., Metallic micro heat exchangers: Properties, applications and long term stability. In *ECI Heat Exchanger Fouling and Cleaning–VII*, Portugal, 2007.

5.  Brandner, J. J.; Bohn, L.; Henning, T.; Schygulla, U.; Schubert, K., Microsructure heat exchanger applications in laboratory and industry. *Heat Transfer Eng.* **2007,** 28, (8–9), 761–771.

6.  Yeong, K. K.; Gavriilidis, A.; Zapf, R.; Hessel, V., Catalyst preparation and deactivation issues for nitrobenzene hydrogenation in a microstructured falling film reactor *Catal. Today* **2003,** 81, (4), 641–651.

7.  Ducry, L.; Roberge, D. M., Controlled autocatalytic nitration of phenol in a microreactor. *Angew. Chem. Int. Ed.* **2005,** 44, (48), 7972–7975.

8.  Antes, J.; Boskovic, D.; Krause, H.; Loebbecke, S.; Lutz, N.; Tuercke, T.; Schweikert, W., Analysis and improvement of strong exothermic nitrations in microreactors. *Chem. Eng. Res. Des.* **2003,** 81, (A7), 760–765.

9.  Fan, X. L.; Chen, H. S.; Ding, Y. L.; Plucinski, P. K.; Lapkin, A. A., Potential of 'nanofluids' to further intensify microreactors. *Green Chem.* **2008,** 10, (6), 670–677.

10. Branebjerg, J.; Gravesen, P.; Krog, J. P.; Nielsen, C. R. In IEEE 9th Annual International Workshop on Micro Electro Mechanical Systems – An Investigation of Micro Structures, Sensors, Actuators, Machines and Systems, San Diego, CA, USA, Feb. 11-15, 1996, IEEE: San Diego, CA, USA, pp 441–446.

11. Mason, B. P.; Price, K. E.; Steinbacher, J. L.; Bogdan, A. R.; CMcQuade, D. T., Greener approaches to organic synthesis using microreactor technology. *Chem. Rev.* **2007,** 107, (6), 2300–2318.

12. Jahnisch, K.; Hessel, V.; Lowe, H.; Baerns, M., Chemistry in microstructured reactors. *Angew. Chem. Int. Ed.* **2004,** 43, (4), 406–446.

13. Waterkamp, D. A.; Engelbert, M.; Thöming, J., On the effect of enhanced mass transfer on side reactions in capillary microreactors during high-temperature synthesis of an ionic liquid. *Chem. Eng. Technol.* **2009,** 32, (11), 1717–1723.

14. Walter, S.; Malmberg, S.; Schmidt, B.; Liauw, M. A., Mass transfer limitations in microchannel reactors. *Catal. Today* **2005,** 110, (1–2), 12–25.

15. Chambers, R. D.; Spink, R. C. H., Microreactors for elemental fluorine. *Chem. Commun.* **1999**, (10), 883–884.

16. Veser, G., Experimental and theoretical investigation of $H_2$ oxidation in a high-temperature catalytic microreactor. *Chem. Eng. Sci.* **2001,** 56, (4), 1256–1273.

17. Bavykin, D. V.; Lapkin, A. A.; Kolaczkowski, S. T.; Plucinski, P. K., Selective oxidation of alcohols in a continuous multifunctional reactor:

Ruthenium oxide catalysed oxidation of benzyl alcohol. *Appl. Catal. A: Gen.* **2005,** 288, (1–2), 175–184.

18. Taghavi-Moghadam, S.; Kleemann, A.; Golbig, K. G., Microreaction technology as a novel approach to drug design, process development and reliability. *Org. Proc. Res. Dev.* **2001,** 5, (6), 652–658.

19. Pennemann, H.; Hessel, V.; Lowe, H., Chemical microprocess technology – from laboratory-scale to production. *Chem. Eng. Sci.* **2004,** 59, (22-23), 4789–4794.

20. Charpentier, J. C., Process intensification by miniaturisation. *Chem. Eng. Technol.* **2005,** 28, (3), 255–258.

21. Ahmed-Omer, B.; Brandt, J. C.; Wirth, T., Advanced organic synthesis using microreactor technology. *Org. Biomol. Chem.* **2007,** 5, (5), 733–740.

22. Seeberger, P. H.; Geyer, K.; Codée, J. D. C., Microreactors as Tools in the Hands of Synthetic Chemists. In *Ernst Schering Foundation Symposium Proceedings*, Seeberger, P. H.; Blume, T., Eds. Heidelberg: Springer–Verlag Berlin, 2006; Vol. 3, pp 1–19.

23. Geyer, K.; Codée, J. D. C.; Seeberger, P. H., Microreactors as tools for synthetic chemists – The chemists' round-bottomed flask of the 21st century? *Chem. Eur. J.* **2006,** 12, (33), 8434–8442.

24. Hessel, V.; Lowe, H., Organic synthesis with microstructured reactors. *Chem. Eng. Technol.* **2005,** 28, (3), 267–284.

25. Mills, P. L.; Quiram, D. J.; Ryley, J. F., Microreactor technology and process miniaturisation for catalytic reactions – A perspective on recent developments and emerging technologies. *Chem. Eng. Sci.* **2007,** 62, (24), 6992–7010.

26. Klemm, E.; Doring, H.; Geisselmann, A.; Schirrmeister, S., Microstructured reactors in heterogeneous catalysis. *Chem. Eng. Technol.* **2007,** 30, (12), 1615–1621.

27. Watts, P.; Haswell, S. J., The application of micro reactors for organic synthesis. *Chem. Soc. Rev.* **2005,** 34, (3), 235–246.

28. Kobayashi, J.; Mori, Y.; Kobayashi, S., Multiphase organic synthesis in microchannel reactors. *Chem. Asian. J.* **2006,** 1, (1–2), 22–35.

29. Kiwi-Minsker, L.; Renken, A., Microstructured reactors for catalytic reactions. *Catal. Today* **2005,** 110, (1–2), 2–14.

30. Ratner, D. M.; Murphy, E. R.; Jhunjhunwala, M.; Snyder, D. A.; Jensen, K. F.; Seeberger, P. H., Microreactor-based reaction optimisation in organic chemistry glycosylation as a challenge. *Chem. Commun.* **2005**, (5), 578–580.

31. Wakami, H.; Yoshida, J., Grignard exchange reaction using a microflow system: From bench to pilot plant. *Org. Proc. Res. Dev.* **2005,** 9, (6), 787–791.

32. Panke, G.; Schwalbe, T.; Stirner, W.; Taghavi-Moghadam, S.; Wille, G., A practical approach of continuous processing to high energetic nitration reactions in microreactors. *Synthesis* **2003,** 18, 2827–2830.

33. Burns, J. R.; Ramshaw, C., A microreactor for the nitration of benzene and toluene. *Chem. Eng. Commun.* **2002,** 189, (12), 1611–1628.

34. Dummann, G.; Quittmann, U.; Groschel, L.; Agar, D. W.; Worz, O.; Morgenschweis, K., The capillary-microreactor: A new reactor concept for the intensification of heat and mass transfer in liquid-liquid reactions. *Catal. Today* **2003,** 79, (1–4), 433–439.

35. Burns, J. R.; Ramshaw, C., Development of a microreactor for chemical production. *Chem. Eng. Res. Des.* **1999,** 77, (A3), 206–211.

36. Ueno, M.; Hisamoto, H.; Kitamori, T.; Kobayashi, S., Phase-transfer alkylation reactions using microreactors. *Chem. Commun.* **2003**, (8), 936–937.

37. http://www.alfalaval.com (15 May 2009).

38. Comer, E.; Prgan, M. G., A microreactor for microwave-assisted capillary (continuous flow) organic synthesis. *J. Am. Chem. Soc.* **2005,** 127, (22), 8160–8167.

39. Snyder, D. A.; Noti, C.; Seeberger, P. H.; Schael, F.; Bieber, T.; Rimmel, G.; Ehrfeld, W., Modular microreaction systems for homogeneously and heterogeneously catalysed chemical synthesis. *Helv. Chim. Acta.* **2005,** 88, (1), 1-9.

40. Watts, P.; Wiles, C.; Haswell, S. J.; Pombo-Villar, E., Investigation of racemisation in peptide synthesis within a micro reactor. *Lab Chip* **2002,** 2, (3), 141–144.

41. Watts, P.; Wiles, C.; Haswell, S. J.; Pombo-Villar, E., Solution phase synthesis of beta-peptides using micro reactors. *Tetrahedron* **2002,** 58, (27), 5427–5439.

42. Wiles, C.; Watts, P.; Haswell, S. J.; Pombo-Villar, E., The aldol reaction of silyl enol ethers within a micro reactor. *Lab Chip* **2001,** 1, (2), 100–101.

43. Mikami, K.; Yamanaka, M.; Islam, M. N.; Kudo, K.; Seino, N.; Shinoda, M., 'Fluorous nanoflow' system for the Mukaiyama aldol reaction catalysed by the lowest concentration of the lanthanide complex with bis(perfluorooctanesulfonyl)amide ponytail. *Tetrahedron* **2003,** 59, (52), 10593–1–597.

44. Yoswathananont, N.; Nitta, K.; Nishiuchi, Y.; Sato, M., Continuous hydrogenation reactions in a tube reactor packed with Pd/C. *Chem. Commun.* **2005**, (1), 40–42.

45. Roy, S.; Bauer, T.; Al-Dahhan, M.; Lehner, P.; Turek, T., Monoliths as multiphase reactors: A review. *AIChE J.* **2004,** 50, (11), 2918–2938.

46.  Biardi, G.; Baldi, G., Three-phase catalytic reactors. *Catal. Today* **1999,** 52, (2–3), 223–234.

47.  Dudukovic, M. P.; Larachi, F.; Mills, P. L., Multiphase reactor – revisited. *Chem. Eng. Sci.* **1999,** 54, (13–14), 1975–1995.

48.  Dudukovic, M. P.; Larachi, F.; Mills, P. L., Multiphase catalytic reactors: A perspective on current knowledge and future trends. *Catal. Rev.* **2002,** 44, (1), 123–246.

49.  Kobayashi, J.; Mori, Y.; Kobayashi, S., Hydrogenation reactions using $scCO_2$ as a solvent in microchannel reactors. *Chem. Commun.* **2005**, (20), 2567–2568.

50.  Zhang, X. F.; Lai, E. S. M.; Martin-Aranda, R.; Yeung, K. L., An investigation of Knoevenagel condensation reaction in microreactors using a new zeolite catalyst. *Appl. Catal. A: Gen.* **2004,** 261, (1), 109–118.

51.  Snyder, D. A.; Noti, C.; Seeberger, P. H.; Schael, F.; Bieber, T.; Rimmel, G.; Ehrfeld, W., Modular microreaction systems for homogeneously and heterogeneously catalysed chemical synthesis. *Helv. Chim. Acta* **2005,** 88, (1), 1–9.

52.  Bogdan, A. R.; Mason, B. P.; Sylvester, K. T.; McQuade, D. T., Improving solid-supported catalyst productivity by using simplified packed-bed microreactors. *Angew. Chem. Int. Ed.* **2007,** 46, (10), 1689–1701.

53.  Greenway, G. M.; Haswell, S. J.; Morgan, D. O.; Skelton, V.; Styring, P., The use of a novel microreactor for high throughput continuous flow organic synthesis. *Sens. Actuator B: Chem.* **2000,** 63, (3), 153–158.

54.  Lomel, S.; Falk, L.; Commenge, J. M.; Houzelot, J. L.; Ramdani, K., The microreactor: A systematic and efficient tool for the transition from batch to continuous process? *Chem. Eng. Res. Des.* **2006,** 84, (A5), 363–369.

55.  Schwalbe, T.; Autze, V.; Homann, M.; Stirner, W., Novel innovation systems for a cellular approach to continuous process chemistry from discovery to market. *Org. Proc. Res. Dev.* **2004,** 8, (3), 440–454.

56.  Liu, S. F.; Fukuyama, T.; Sato, M.; Ryu, I., Continuous microflow synthesis of butyl cinnamate by a Mizoroki-Heck reaction using a low-viscosity ionic liquid as the recycling reaction medium. *Org. Proc. Res. Dev.* **2004,** 8, (3), 477–481.

57.  Srinivasan, R.; Hsing, I. M.; Berger, P. E.; Jensen, K. F.; Firebaugh, S. L.; Schmidt, M. A.; Harold, M. P.; Lerou, J. J.; Ryley, J. F., Micromachined reactors for catalytic partial oxidation reactions. *AIChE J.* **1997,** 43, (11), 3059–3069.

58.  Kobayashi, J.; Mori, Y.; Kobayashi, S., Triphase hydrogenation reactions utilizing palladium-immobilised capillary column reactors and a

demonstration of suitability for large scale synthesis. *Adv. Synth. Catal.* **2005,** 347, (15), 1889–1892.

59. Kobayashi, J.; Mori, Y.; Okamoto, K.; Akiyama, R.; Ueno, M.; Kitamori, T.; Kobayashi, S., A microfluidic device for conducting gas-liquid-solid hydrogenation reactions. *Science* **2004,** 304, (5675), 1305–1308.

60. http://www.imm-mainz.de/ (10 May 2009).

61. Hessel, V.; Angeli, P.; Gavriilidis, A.; Lowe, H., Gas-liquid and gas-liquid-solid microstructured reactors: Contacting principles and applications. *Ind. Eng. Chem. Res.* **2005,** 44, (25), 9750–9769.

62. Lee, J. W.; Yeong, K. K.; Gavriilidis, A.; Zapf, R.; Hessel, V. In the International Conference on Microreaction Technology (IMRET 8), Allanta, USA, 2005; Allanta, USA, 2005.

63. Ajmera, S. K.; Losey, M. W.; Jensen, K. F.; Schmidt, M. A., Microfabricated packed-bed reactor for phosgene synthesis. *AIChE J.* **2001,** 47, (7), 1639–1647.

64. Ramirez, E.; Recasens, F.; Fernandez, M.; Larrayoz, M. A., Sunflower oil hydrogenation on Pd/C in SC propane in a continuous recycle reactor. *AIChE J.* **2004,** 50, (7), 1545–1555.

65. Li, Y.; Yan, B.; Deng, C. H.; Yu, W. J.; Xu, X. Q.; Yang, P. Y., Efficient on-chip proteolysis system based on functionalized magnetic silica microspheres. *Proteomics* **2007,** 7, (14), 2330–2339.

66. http://www.thalesnano.com/ (19 May 2009).

67. http://www.thalesnano.com/products/h-cube (19, May 2009).

68. Szöllősi, G.; Hermán, B.; Fülöpb, F.; Bartóka, M., Continuous enantioselective hydrogenation of activated ketones on a Pt-CD chiral catalyst: Use of H-Cube reactor system *React. Kinet. Catal. Lett.* **2006,** 88, (2), 391–398.

69. Saaby, S.; Knudsen, K. R.; Ladlow, M.; Ley, S. V., The use of a continuous flow-reactor employing a mixed hydrogen-liquid flow stream for the efficient reduction of imines to amines *Chem. Commun.* **2005**, (23), 2909–2911.

70. Csajági, C.; Borcsek, B.; Niesz, K.; Kovács, I.; Székelyhidi, Z.; Bajkó, Z.; Urge, L.; Darvas, F., High-efficiency aminocarbonylation by introducing CO to a pressurized continuous flow reactor. *Org. Lett.* **2008,** 10, (8), 1589–1592.

71. Plucinski, P. K.; Bavykin, D. V.; Kolaczkowski, S. T.; Lapkin, A. A., Liquid-phase oxidation of organic feedstock in a compact multichannel reactor *Ind. Eng. Chem. Res.* **2005,** 44, (25), 9683–9690.

72. Plucinski, P. K.; Bavykin, D. V.; Kolaczkowski, S. T.; Lapkin, A. A., Application of a structured multifunctional reactor for the oxidation of a liquid organic feedstock *Catal. Today* **2005,** 105, (3–4), 479–483.

73.     Fan, X. L.; Lapkin, A. A.; Plucinski, P. K., Liquid phase hydrogenation in a structured multichannel reactor. *Catal. Today* **2009,** 147S, S313–S318.

74.     Fan, X. L.; Manchon Gonzalez, M.; Karen, W.; Tennison, S. R.; Kozynchenko, A.; Plucinski, P. K.; Lapkin, A. A., Coupling of Heck and hydrogenation reactions in a continuous compact reactor. *J. Catal.* **2009,** 267, 114–120.

75.     http://www.ehrfeld.com/english/ (12 June 2009).

76.     Hessel, V.; Hofmann, C.; Lowe, H.; Meudt, A.; Scherer, S.; Schonfeld, F.; Werner, B., Selectivity gains and energy savings for the industrial phenyl boronic acid process using micromixer/tubular reactors. *Org. Proc. Res. Dev.* **2004,** 8, (3), 511–523.

77.     Benz, K.; Jackel, K. P.; Regenauer, K. J.; Schiewe, J.; Drese, K.; Ehrfeld, W.; Hessel, V.; Lowe, H., Utilisation of micromixers for extraction processes. *Chem. Eng. Technol.* **2001,** 24, (1), 11–17.

78.     Jahnisch, K.; Baerns, M.; Hessel, V.; Ehrfeld, W.; Haverkamp, V.; Lowe, H.; Wille, G.; Guber, A., Direct fluorination of toluene using elemental fluorine in gas/liquid microreactors. *J. Fluorine Chem.* **2000,** 105, (1), 117–128.

79.     http://www.mikroglas.com (25 May 2009).

80.     http://www.micronit.com/ (10 April 2008).

81.     http://www.bartels-mikrotechnik.de (29 May 2009).

82.     http://www.mikroreaktionstechnik.info/english/ (20 May 2009).

83.     http://www.corning.com/reactors (15 May 2009).

# Chapter 3

# Continuous Selective Hydrogenation of Benzaldehyde in the Structured Compact Reactor

A structured multifunctional compact reactor was studied in the processes of continuous catalytic hydrogenation reactions. A 41 % calculated product yield (1 mol $L^{-1}$ initial substrate concentration which is close to industrial conditions), corresponding to a space-time yield of product of 34 mol $L_{reactor}^{-1}$ $h^{-1}$, in a single pass (10 cm length) at a liquid phase residence time of *ca*. 40 second was attained. High process efficiency was attributed to good control of temperature and a short residence time achieved due to a more intensive reaction regime in the micro-packed bed reactor. The kinetics of the three-phase hydrogenation was evaluated showing: (*i*) reaction limitation for applied reaction conditions, (*ii*) Langmuir-Hinshelwood mechanism of hydrogenation, and (*iii*) the dominating role of adsorption of reactant and the solubility of hydrogen in the mechanism of hydrogenation at higher temperatures. Staged injection of hydrogen into the reactor was found beneficial to the flow process. This chapter is based on the paper: X. Fan, P. Plucinski, A. Lapkin, *Catal. Today*, 2009 (147S), S313–S318.

## 3. 1 Introduction

Hydrogenation reactions are widely used in both petrochemical, speciality chemicals and pharmaceuticals production, using both gas-solid and three phase gas-liquid-solid processes.[1] Due to their high reaction enthalpy, *e.g.* hydrogenation of nitrobenzene with a reaction enthalpy of 443 kJ mol$^{-1}$ and a corresponding adiabatic temperature rise of *ca.* 2,673 K,[2] practical large-scale applications require the use of diluted reactants and slow addition of hydrogen for better reaction control. Furthermore, in the gas-liquid-solid multiphase systems the hydrogenation reactions are frequently limited by the supply of hydrogen. In order to improve mass transfer, elevated pressure is always necessary for increasing the concentration of dissolved hydrogen; in turn this leads to high reaction rates and the potential for thermal runaway.

A number of new developments in reactor technology are aiming to improve the efficiency of hydrogenation reactions.[3] Thus, membrane contactors allow to establish high gas-liquid interface within the structure of porous membranes and, therefore, a faster addition of hydrogen directly to the region of catalytic reaction.[4, 5] Integrated catalytic reactors heat-exchangers provide efficient heat transfer for strongly exothermic reactions to avoid temperature runaways.[6] Microreactors may eliminate many of the problems of conventional hydrogenation processes due to (*i*) effective control over reaction conditions and (*ii*) scale-up by numbering of identical small reactors.[7, 8] A number of representative studies of hydrogenation reactions in microreactors are summarised in Table 3.1.

**Table 3.1** Representative studies of catalytic hydrogenation reactions in microreactors.

| Microreactor | Conditions | Catalyst and substrate | Space-time yield / mol $L_{reactor}^{-1}$ $h^{-1}$ |
|---|---|---|---|
| Packed-bed microreactor[9]  1 mm i.d., 25 cm length | $T = 363$ K $P = 25$ bar $F_{Liquid} = 0.038$ mL min$^{-1}$ in methanol | 5 wt.% Pd/C  cyano/carbonyl group | *ca.* 2 |
| Pd-immobilised capillary microreactor[10]  200 μm i.d., 40 cm length | $T$ = ambient $P$ = ambient $F_{Liquid} = 0.015$ mL min$^{-1}$ in THF | microencapsulated Pd catalyst  alkene group | *ca.* 25 |
| Pd-immobilised glass microreactor[11, 12]  200 μm width, 100 μm depth, 45 cm length | $T = ca.$ 323 K $P$ = ambient $F_{Liquid} = 0.015$ mL min$^{-1}$ in scCO$_2$ or THF | microencapsulated Pd catalyst  alkene/alkyne group | *ca.* 11 |
| Microstructured falling film reactor[13]  300 μm width, 100 μm depth, 7.8 cm length. | $T = 333$ K $P$ = ambient $F_{Liquid} = 0.5$ mL min$^{-1}$ in ethanol | immobilised Pd catalysts  nitro group | *ca.* 16 |

Microreactors with characteristic dimensions in the range from micrometres to millimetres typically have high heat transfer coefficients, up to 200 kW m$^{-2}$ K$^{-1}$, in comparison with conventional batch reactors, *e.g.* ~10 kW m$^{-2}$ K$^{-1}$ in a 1 L flask.[7] High heat transfer enables higher hydrogenation reaction rates to be attained safely, as was demonstrated in the studies cited in Table 3.1. However, these studies were performed in microreactors with relatively low product throughputs and limited integration of functionalities. In order to attain maximum efficiency of catalytic hydrogenation it is essential to resolve not only the problem of heat transfer, but also enhance hydrogen supply and establish effective mixing in a three-phase system.

Furthermore, microreactors are normally operating in the laminar flow regime, therefore mixing is slow and requires introduction of specific mixing elements.

Earlier studies have shown that efficient heat- and mass-transfer, and a plug-flow hydrodynamic regime could be established in the mm-scale catalytic micro-packed bed reactor integrated with micro heat-exchanger and a simple baffle static mixer.[14-16] Staged injection of a gaseous reactant produced stable and uniform hydrodynamic regime along the catalyst bed. In such a reactor reasonably high product throughputs could be attained. The mm-scale multifunctional reactor concept offers a lower-cost and easier to scale-up alternative to microreactors.

In this chapter, hydrogenation reactions are investigated in the micro-packed-bed integrated reactors. The gas-liquid-solid hydrogenation of benzaldehyde to benzyl alcohol (Scheme 3.1) was chosen as a model reaction. Performance of the structured compact reactor (in terms of calculated product yield, selectivity, and average reaction rate) for continuous hydrogenation was evaluated and compared with other types of continuous reactors. The effects of reaction conditions, *i.e.* gas/liquid flow-rates, pressure, and temperature, on the reactor performance were studied in detail. Staged injection of hydrogen was also investigated.



$\Delta H_r^0 = -67 \text{ kJ mol}^{-1}$
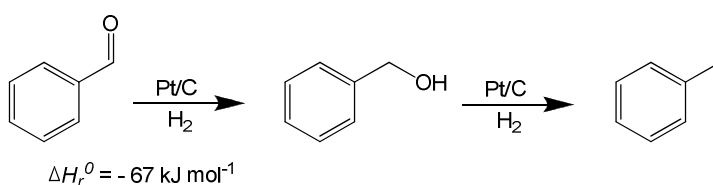
**Scheme 3.1** Hydrogenation of benzaldehyde to benzyl alcohol with (unwanted) consecutive reaction to toluene.

## 3. 2    Experimental

### 3.2.1    *Pt/C catalyst and reagents*

The Pt/C catalyst (Pt 3 % by weight) was prepared by impregnating the microspherical (110–150 μm) mesoporous synthetic carbon support (Mast Carbon Ltd., Guildford, UK) using $H_2PtCl_6$ as Pt precursor as described by van Dam and van

Bekkum.[17]   The loading capacity of compact reactor is *ca.* 0.5 g of catalyst per channel.  For kinetic study the catalyst was diluted (total amount = 0.1 g) with acid-washed glass beads (150–212 μm, Sigma-Aldrich).  All chemicals used in this study, *i.e.* benzaldehyde, benzyl alcohol, toluene, dodecane, (all in *ReagentPlus®* grade) and propan-2-ol (HPLC grade) were obtained from Sigma-Aldrich and used without further purification.

### 3.2.2   *Structured compact reactor*

The structured multichannel reactor was a bonded assembly of thin shims (316 stainless steel) that incorporate channels created within it.  A schematic diagram of the reactor assembly is shown in Fig. 3.1.  The diffusion bonding produces a robust structure with the capability of operating at high pressures (up to 75 barg).  Static mixers are embedded prior to the reaction channels (above the reaction channels) for premixing and preheating the liquid and gas reactants before introducing the mixture into the reaction channels.  Five packed-bed channels (100 mm length) are imbedded in parallel between the two micro-heat exchangers.  The reaction channels have a square cross-section with three different sizes: 2 mm × 2 mm, 3 mm × 3 mm (three of) and 5 mm × 5 mm.  The pressure-driven laminar flows with the liquid Reynolds number < 10 can be established in the channels under the conditions used in this study (refer to section 3.3 for the conditions).  The two micro-heat exchangers are located underneath and above all the reaction channels (arranged in cross-flow with respect to reaction channels).  All reaction channels, therefore, have an even temperature field during operation.  Details about the design concepts and hydrodynamic characteristics of the compact reactor are specified elsewhere.[14-16]
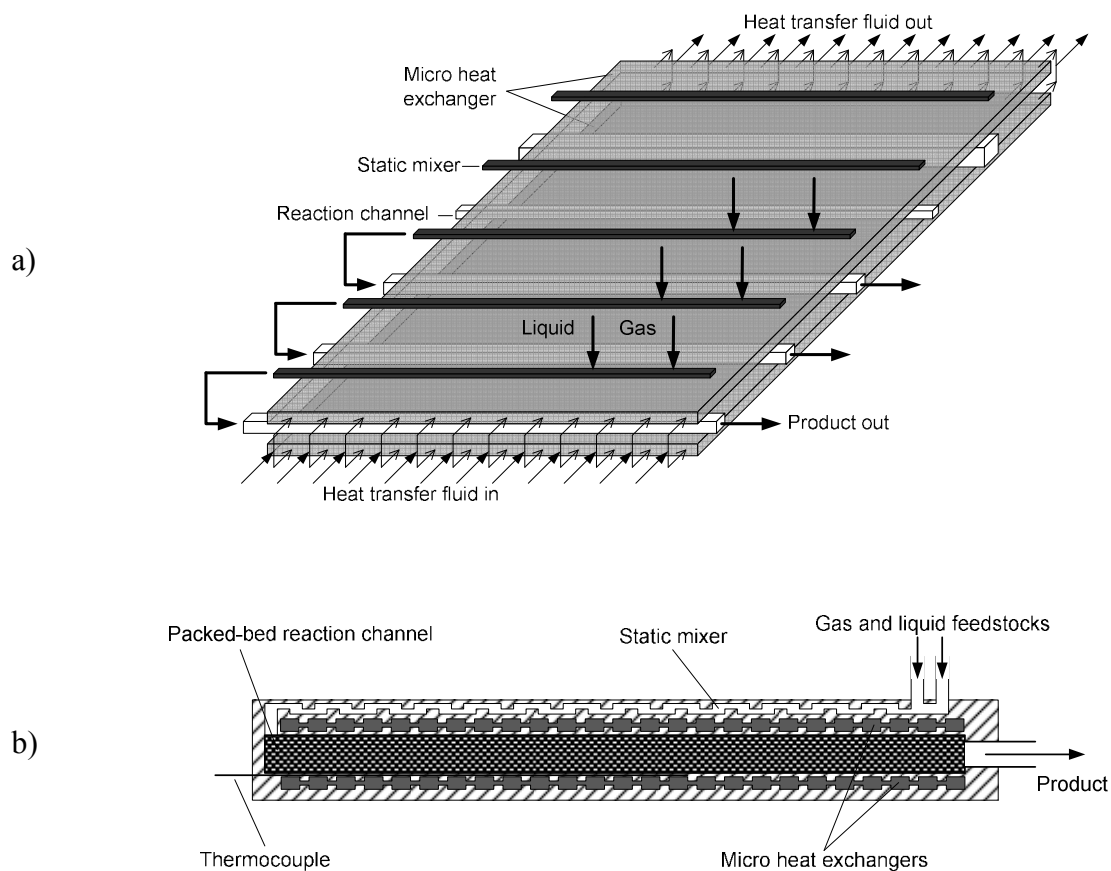
**Fig. 3.1** Schematic diagram of the structured compact reactor–microchannel heat exchanger: (a) channel arrangements and (b) cross-sectional view.

### 3.2.3 Continuous catalytic rig and procedure for continuous experiments

The continuous catalytic rig was set up as shown schematically in Fig. 3.2. Liquid reagents were premixed and placed in the feed vessel. A HPLC pump (Kontron) was used to pump liquid feed through packed-bed reaction channels; the product was collected in another vessel via a low dead-volume six-way valve (Valco) equipped with a 250 μL sample loop. Temperature was controlled by using a re-circulating bath (Haake) to circulate heat transfer fluid through the micro-heat exchangers. The operating pressure was controlled by a back pressure regulator (Brooks) and the pressure drop across the reactor was monitored using a differential pressure transducer (Bronkhorst).
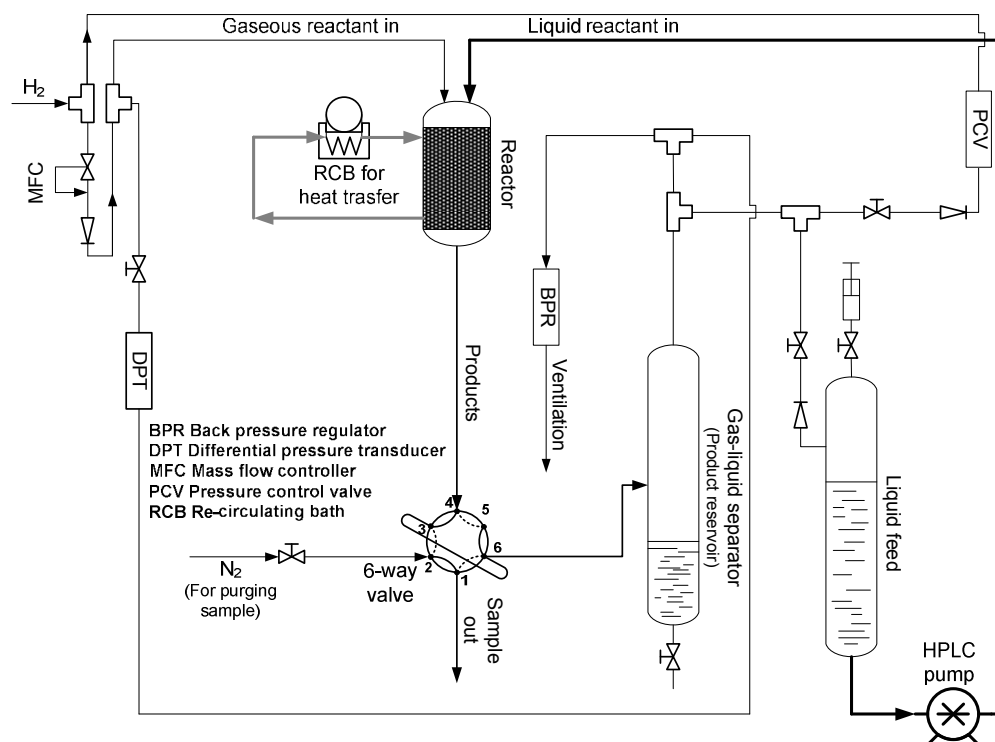
**Fig. 3.2** Schematic diagram of the catalytic rig for continuous experiments.

### 3.2.4    *Analysis techniques*

Reaction products were analysed by gas chromatography (GC, Varian CP-3800) equipped with a non-polar capillary column (CP Sil 5 CB).  Samples taken from the experiments were analysed without further preparation.

MS analysis (microTOF, Bruker) and ^{1}H NMR analysis (NMR) spectrometre (300 MHz, Bruker) were employed for the determination of the chemical structures of byproducts.  Low temperature nitrogen adsorption (ASAP 2010, Micrometrics) was measured to characterise specific surface area and pore size distribution of the catalysts.

## 3. 3    Results and discussion

### *3.3.1    Performance of the compact flow reactor*

For the substrate concentration used in this study (0.2 mol L$^{-1}$), a 100 % conversion of the benzaldehyde (corresponds to a space-time yield of *ca.* 13 mol h$^{-1}$ L$^{-1}$) was achieved in a single pass under mild operating conditions, *i.e.* 320 K, 8 barg, and 20 s liquid phase residence time, and using one fully loaded reaction channel (3 mm × 3 mm × 10 cm) with catalyst mass of 0.45 g.

In order to highlight the effectiveness of the developed multiphase compact flow reactor, a set of activity data from other hydrogenation processes were summarised in Table 3.2. The average reaction rate for flow reactors was calculated as:

$$(r) = \frac{\dot{V}_L \cdot C_P}{m_{metal}}$$

(3.1)

where $\dot{V}_L$ is the volumetric flow rate of liquid phase; $C_P$ is the exit concentration of product, $m_{metal}$ is the mass of metal on catalyst in an individual channel.

In comparison with other studies for hydrogenating the same substrate in batch reactor, the structured compact reactor demonstrated a better performance in terms of the specific activity per kilogram of metal (observed reaction rate, *r*). The measured average reaction rate in the compact reactor is about one order of magnitude larger than ones calculated from batch applications[18, 19] (for Pt/C catalysts in ref. 19, the average reaction rate must be much smaller than the presented value of the initial reaction rate, *i.e.* 0.13 mol kg$_{metal}^{-1}$ s$^{-1}$). Apart from better activity of the continuous-flow system, a higher throughput was also presented by the compact reactor compared with the continuous monolith reactor, *i.e.* space-time yield of product: 13 mol L$_{reactor}^{-1}$ h$^{-1}$ *vs.* 7.9 mol L$_{reactor}^{-1}$ h$^{-1}$. The throughput of the structured compact reactor can be increased by running reactions with undiluted catalyst bed and concentrated feed solutions. Thus, under similar flow conditions, *e.g.* 1 mol L$^{-1}$

initial concentration, 0.73 kg m$^{-2}$ s$^{-1}$ liquid flow rate (*ca.* 40 second residence time), a 41 % product yield was achieved, which corresponds to *ca.* 34 mol L$_{reactor}^{-1}$ h$^{-1}$ of space-time yield, or three times higher than the one obtained with the diluted reactant solutions.

**Table 3.2.** Activities for different reactors for selective hydrogenation of benzaldehyde to benzyl alcohol over supported metal catalysts.

| Reactors | Catalyst | Conditions | | $r$ |
|---|---|---|---|---|
| | | $T$ / K | $P$ / barg | / mol kg$_{metal}^{-1}$ s$^{-1}$ |
| This study | Pt/C catalyst[a] | 317 | 8 | 0.49[a] |
| Batch reactor[18] | Pt/C[b] | 323 | 1[b] | 0.13[b] |
| Batch reactor[19] | Pd/C[c] | 481 | 1 | 0.034[c] |
| Batch reactor[19] | Pd/C[d] | 481 | –[d] | 0.06[d] |
| Monolith reactor[20] | Ni monolithic catalyst[e] | 373 | 10 | 0.35[e] |

[a] continuous three phase catalysis, 3 wt.% Pt/C, 0.2 mol L$^{-1}$ initial concentration, average reaction rate.

[b] batch three phase catalysis, 5 wt.% Pt/C (commercial catalyst), 0.2 mol L$^{-1}$ initial concentration, continuous H$_2$ bubbling through the liquid phase, initial reaction rate.

[c] batch three phase catalysis, 5 wt.% Pd/C, *ca.* 0.6 mol L$^{-1}$ initial concentration, average reaction rate.

[d] batch two phase catalysis, with liquid borrowing hydrogen (potassium formate as the hydrogen donor), 5 wt.% Pd/C, ca. 0.6 mol L$^{-1}$ initial concentration, average reaction rate.

[e] continuous three phase catalysis, 1 wt.% Ni (egg-shell), 0.18 mol L$^{-1}$ initial concentration, average reaction rate.

In order to study the kinetics of the reaction, a diluted catalysts bed (with glass beads) was employed in the consecutive experiments. Fig. 3.3 shows benzyl alcohol concentration (as product yield) in the outlet solution as a function of time-on-stream. For the two liquid flow-rates used, the reaction profiles over a given time were identical, *i.e.* the product yield initially decreased with time followed by a plateau after *ca.* 8 minutes time-on-stream. This indicates that the steady state was achieved in the reaction system 8 minutes after introducing the reagents. A lower product yield was measured for the higher liquid flow-rate. This was due to the reduction in the liquid phase residence time in the reaction channel. An increase of liquid flow-rate promotes the transition of rate-limiting step from mass transfer regime to kinetic regime. Therefore, a low yield can be expected due to the short contact time between reactants and active sites on catalysts. Further, the higher liquid flow-rate also

affected the hydrodynamic regime of the mixed gas-liquid flow through the solid packed bed.
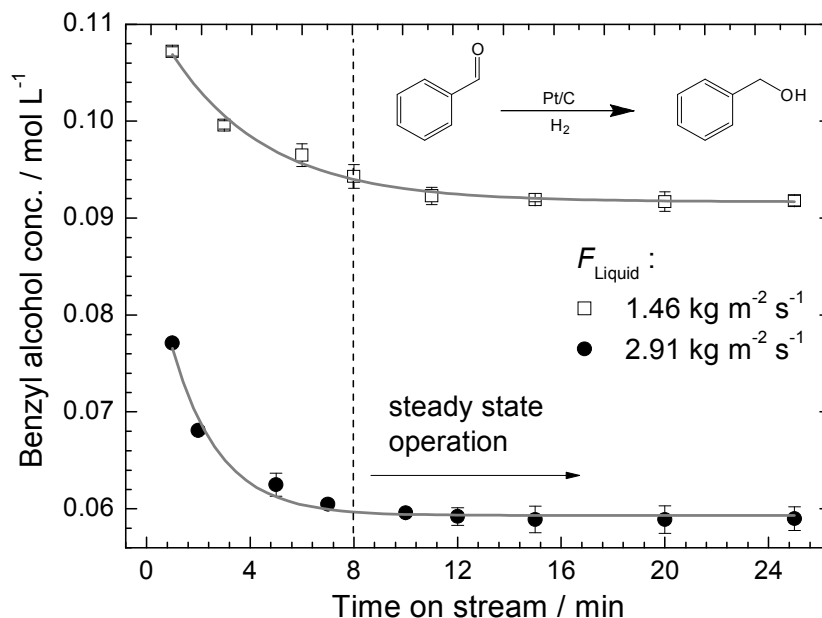


**Fig. 3.3** Product concentration in the outlet of the reactor as a function of time-on-stream. $P = 8$ barg, $T = 327$ K, $F_{Gas} = 2.66 \times 10^{-3}$ kg m$^{-2}$ s$^{-1}$, $C_{Substrate, 0}$ (by GC) $= 0.2$ mol L$^{-1}$.

Fig. 3.4 shows the product yield, reaction rate (steady state reaction rate), and selectivity in a single pass channel as a function of the hydrogen flow-rate at 317 K and 8 barg. At low gas flow-rates, the outlet concentration of benzyl alcohol depends linearly on the hydrogen flow-rate. The product yield correlates well with the maximum stoichiometric yield based on the hydrogen amount supplied to the reactor, similarly as it was observed for the oxidation reaction under conditions of the gaseous reactant limitation.[14-16] This indicates that for the low range of the hydrogen flow-rates (up to $1.00 \times 10^{-3}$ kg m$^{-2}$ s$^{-1}$), the reaction was limited by the supply of hydrogen. The product yield was found to be almost independent of the gas flow-rate for the higher range of flow-rates ($> 1.00 \times 10^{-3}$ kg m$^{-2}$ s$^{-1}$).

**Fig. 3.4** (a) Product yield/average reaction rate, and (b) selectivity to product as a function of hydrogen flow-rate. $T = 317$ K, $P = 8$ barg, $F_{Liquid} = 1.46$ kg m$^{-2}$ s$^{-1}$, $C_{Substrate, 0} = 0.2$ mol L$^{-1}$. Solid lines are drawn for the convenience of viewing.

The increase in the gas flow-rate decreases the liquid phase volumetric fraction ($\beta_L$, defined as in Eq. (3.2)) and increases the superficial velocity of the liquid phase.[21]

$$\beta_L = \frac{\dot{V}_L}{\dot{V}_L + \dot{V}_G} \tag{3.2}$$

where $\dot{V}_L$ and $\dot{V}_G$ are volumetric flow-rates of liquid and gas phases in the reactor.

The independence of the exit concentration of the hydrogenation product (benzyl alcohol) on the flow-rate of the gas phase excludes the possibility of the influence of the external mass transfer on the overall observed reaction kinetics. Therefore, hydrogenation in a compact reactor could be limited either by the chemical reaction itself, or by internal diffusion. The calculations of Weisz-Prater criterion, *i.e.* $C_{WP} = 0.308$, (Eq. (3.3))[22, 23] and measured Langmuir-Hinshelwood-type kinetics (see further discussion of Fig. 3.7) excluded the possibility of the internal diffusion to be

a rate limiting step. Thus, it could be confirmed unequivocally, that the hydrogenation reaction in a compact reactor was limited by the catalytic reaction itself.

$$C_{WP} = \frac{r_{obs} \cdot R_p^{\ 2}}{D_{eff} C_s}$$

(3.3)

where $r_{obs}$ is the observed reaction rate (per volume of catalyst, mol s$^{-1}$ m$^{-3}$), $R_p$ is the catalyst particle radius (m), $C_s$ is the reactant concentration at the particle surface (mol m$^{-3}$), and $D_{eff}$ is the effective diffusivity. In small pores (< 100 nm) where Knudsen diffusion dominates, $D_{eff} \approx D_{Kn}$ ($D_{Kn}$ is Knudsen diffusivity and defined as in Eq. (3.4)).[23]

$$D_{Kn} = \bar{v} \frac{d_p}{3}$$

(3.4)

where $\bar{v}$ is the mean velocity of gas (m s$^{-1}$), $d_p$ is the average pore diameter (m).

### 3.3.2 *Effect of operating pressure and concentration*

The product yield was found to be strongly dependent on the operating pressure, which is shown in Fig. 3.5. An increase in the yield of benzyl alcohol was observed with the increase in the pressure of hydrogen over the pressure range used in this study (1–8 barg). The elevated hydrogen pressure results in the enhanced solubility of hydrogen in propan-2-ol.[9, 24] Therefore, an acceleration in the rate of reaction was expected at elevated hydrogen pressures. Based on the data provided in ref. 24 (Fig. 3.6), a *ca.* 4.8-fold increase in hydrogen solubility in propan-2-ol was estimated when the pressure changed from 1 to 8 barg. This increment showed a satisfactory agreement with the experimental results, *i.e.* the measured product yield at 8 barg is *ca.* 4.3 times higher than that at 1 barg.

The lack of the influence of the gas flow-rate on the overall reactor performance (see analysis in Section 3.1), *i.e.* the lack of the influence of hydrogen mass transfer on

global kinetics, proves the reaction limitation of the process. This can also be seen by analysing the data shown in Fig. 3.7, the asymptotic approach of the reaction rate as a function of the initial aldehyde concentration. This is in good agreement with other kinetic studies of the liquid phase hydrogenations.[25]
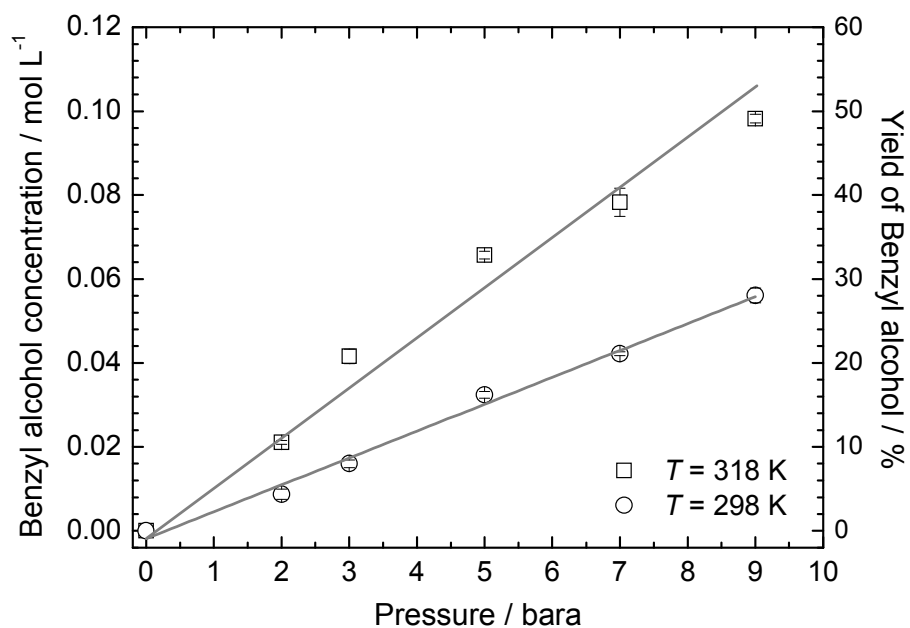


**Fig. 3.5** Effect of the absolute pressure on the production of benzyl alcohol.
$F_{Liquid} = 1.46$ kg m$^{-2}$ s$^{-1}$, $F_{Gas} = 2.66 \times 10^{-3}$ kg m$^{-2}$ s$^{-1}$, $C_{Substrate, 0} = 0.2$ mol L$^{-1}$.
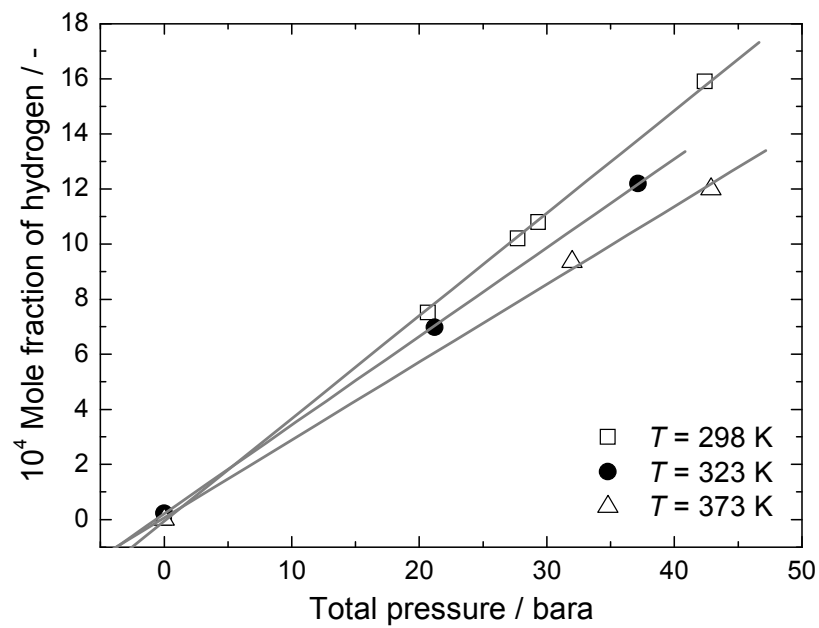
**Fig. 3.6** Hydrogen solubility in propan-2-ol at different temperatures and total hydrogen pressures. Data are adopted from ref. 24.



**Fig. 3.7** Product concentration in the outlet of the reactor as a function of initial substrate concentration. $P = 8$ barg, $F_{Gas} = 2.66 \times 10^3$ kg m$^{-2}$ s$^{-1}$.

### 3.3.3 Effect of the reaction temperature

The temperature dependencies of benzaldehyde conversion and the yield of benzyl alcohol are shown in Fig. 3.8. Isothermal conditions were kept at all conversion levels, which was proven by temperature measurements in close proximit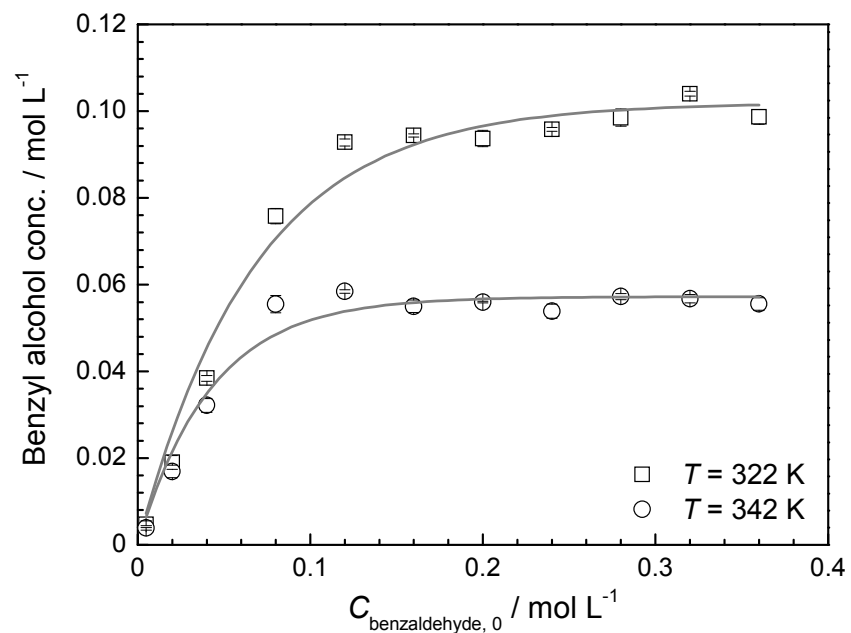y to the reaction channel (distance from thermocouple to reaction fluid *ca.* 100 μm). Hydrogenation of benzaldehyde is a mildly exothermic reaction with the standard reaction enthalpy of $-67$ kJ mol$^{-1}$ (thermodynamic properties of compounds involved in the reaction were obtained from ref. 26 and 27). However, very effective heat transfer characteristics of the compact reactor ensured the isothermal mode of operation.

The observed bell-shaped dependencies of conversion and yield on temperature may result from the following factors: (*i*) the effect of the reaction species adsorption equilibrium, (*ii*) change of rate constants with temperature (Arrhenius' law), and (*iii*) change of hydrogen solubility in propan-2-ol with temperature (Henry's law). Adsorption of benzaldehyde and dissolved hydrogen on the metal surface decreases with the increase in temperature, thus decreasing the rate of reaction. The sorption capacity of the carbon support was measured at the operating temperatures (benzaldehyde as adsorbate) and summarised in Table 3.3. Clearly, the drops for both $Q_{Sat.}$ and $K_A$ (calculated equilibria parameters, $Q_{Sat.}$ = saturated sorption capacity, $K_A$ = equilibrium constant) were found with the increase of temperature, which implies a reduction in adsorbed molecules at the higher temperatures. Similarly, hydrogen solubility in propan-2-ol decreases with the increase in temperature,[24] decreasing the concentration of dissolved hydrogen at the surface of a catalyst and therefore decreasing the rate of hydrogenation. The only positive effect of temperature on the reaction rate (dominating in the temperature region 303 K < T < 318 K) is related to Arrhenius law. Thus, it follows that at temperatures higher than *ca.* 325 K the negative effects of absorption and adsorption prevailed in the overall hydrogenation mechanism.
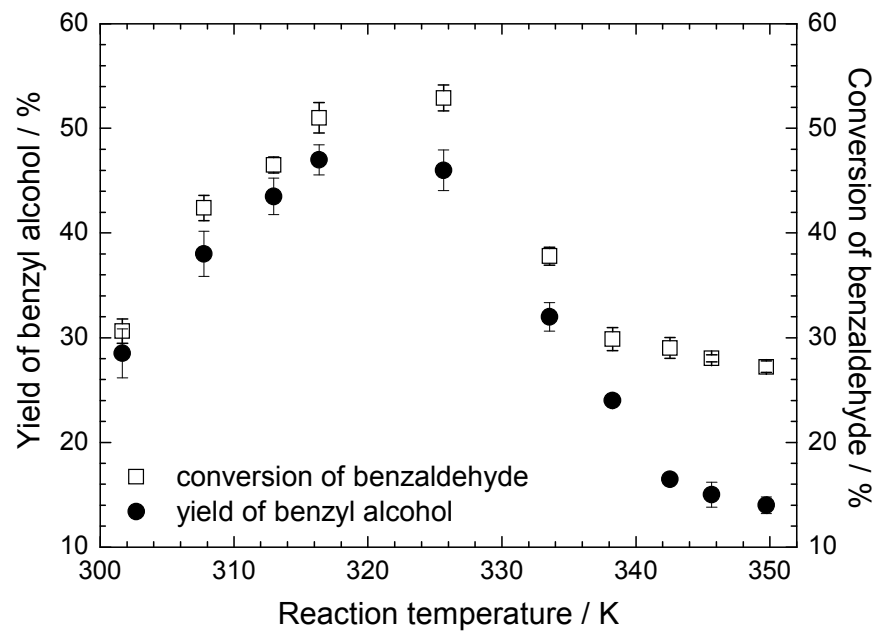
**Fig. 3.8** Yield of benzyl alcohol and benzaldehyde conversion in the compact reactor as a function of reaction temperature. $P = 8$ barg, $F_{\text{Liquid}} = 1.46$ kg m$^{-2}$ s$^{-1}$, $F_{\text{Gas}} = 2.66 \times 10^{-3}$ kg m$^{-2}$ s$^{-1}$, $C_{\text{Substrate, 0}} = 0.2$ mol L$^{-1}$.

**Table 3.3** Langmuir parameters for benzaldehyde adsorption onto activated carbons.

| Temperature / K | $Q_{Sat}$ / mol$_A$ kg$_{\text{carbon}}^{-1}$ | $K_A$ / 10$^{-3}$ m$^3$ mol$_A^{-1}$ |
|---|---|---|
| 298 | 2.63 | 2.68 |
| 323 | 1.45 | 2.55 |
| 353 | 0.43 | 1.25 |

Based on the data obtained, reaction kinetics was studied for the liquid-phase hydrogenation carried out in compact flow reactor. Taking into account the kinetic data presented in Fig. 3.5 and 3.7, the following Langmuir-Hinshelwood type rate equation might be suggested:

$$\left(-r_A\right) = \frac{k\,K_A\,K_H\,C_A C_H}{\left(1 + K_A C_A\right)} \tag{3.5}$$

which assumes the dual site mechanism (the adsorption of benzaldehyde and hydrogen at the same adsorption sites would demand denominator term in the

equation in power 2 with maximum at the curve $(-r_A)$ as a function of benzaldehyde concentration, $C_A$) and weak adsorption of hydrogen on platinum (see Fig. 3.5). In Eq. (3.5), $k$ is the overall rate constant, $K_A$ and $K_H$ is the adsorption constant of aldehyde and hydrogen, $C_A$ and $C_H$ is the surface concentration of aldehyde and hydrogen.

For the saturation region of aldehyde concentration of L–H kinetics (Fig. 3.7) the Eq. (3.5) could be simplified to Eq. (3.6).

$$\left(-r_A\right) = k \ K_H \ C_H \tag{3.6}$$

*i.e.* the rate of hydrogenation is independent on the concentration of benzylaldehyde and its adsorption constant. Assuming, that the mass transfer of hydrogen is fast, and taking into account Henry's law, one can rewrite Eq. (3.6).

$$\left(-r_A\right) H_H = k \ K_H \ p_H \tag{3.7}$$

Then, the right term of the Eq. (3.7) depends on temperature *via* a temperature-dependent rate constant (Arrhenius law), a temperature-dependent hydrogen constant (van't Hoff law), as well as on a temperature-dependent maximum adsorption capacities of benzaldehyde and hydrogen. The corresponding experimental data of the temperature influence on the overall reaction rate multiplied by Henry's constant is shown in Fig. 3.9.
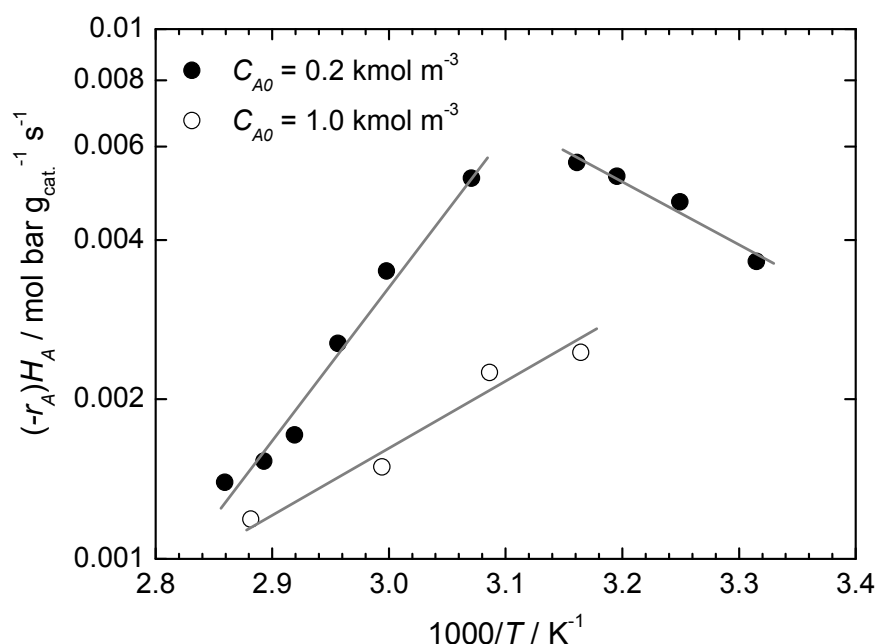
**Fig. 3.9** The overall reaction rate (multiplied by Henry's constant) as a function of temperature (in Arrhenius coordinates) for two temperature regimes in the compact reactor. $P = 8$ barg, $F_{Gas} = 2.66 \times 10^{-3}$ kg m$^{-2}$ s$^{-1}$.

For the lower temperature range (K < 325 K), the effective activation energy $\Delta E_A = 23.1$ kJ mol$^{-1}$ can be evaluated, slightly lower that that observed in the liquid phase hydrogenation of citral ($\Delta E_A = 29.4$ kJ mol$^{-1}$).[25] In the high temperature region (K > 325 K), the temperature-dependent adsorption effects prevail (positive slopes observed in Fig. 3.9). Unfortunately, due to the lack of literature data on adsorption of hydrogen on platinum in liquid phase, further interpretation of the data is impossible.

### 3.3.4 Selectivity and catalyst deactivation

For the model reaction studied, a good selectivity to the target alcohol product was achieved, *i.e.* selectivity above 96 % was observed at temperatures below 330 K. No over-hydrogenated products (toluene and methylcyclohexane) were detected (by GC) for all the conditions used. The observed high selectivity can be attributed to (*i*) a better mixing providing, most likely, a plug flow regime, (*ii*) a better control of

temperature, and (*iii*) a shorter residence time. However, a deterioration of selectivity with the increase in temperature was found as shown in Fig. 3.10, and a byproduct with a high molecular weight was detected by GC. The structure of the byproduct was elucidated with $^1$H-NMR and MS-spectroscopy analysis and identified as benzaldehyde dipropyl acetal ($^1$H-NMR analysis refer to section III in Appendix.). It is suggested that the byproduct is formed by acetalisation of carbonyl with alcohol, which can be easily initiated in the presence of an acid H$^+$:
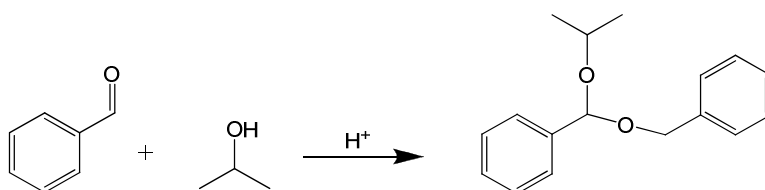


**Scheme 3.2** Acetalisation of benzaldehyde with propan-2-ol.

Two possible reasons were considered for the acid-induced side reaction, *i.e.* the formation of benzoic acid in the reactant solution due to benzaldehyde oxidation, and the residual acidity of catalysts due to the method of depositing metal on the support and the adsorption of acidic gases on the carbon support. High temperatures were found to favour the side reaction, which was also confirmed by GC analysis.
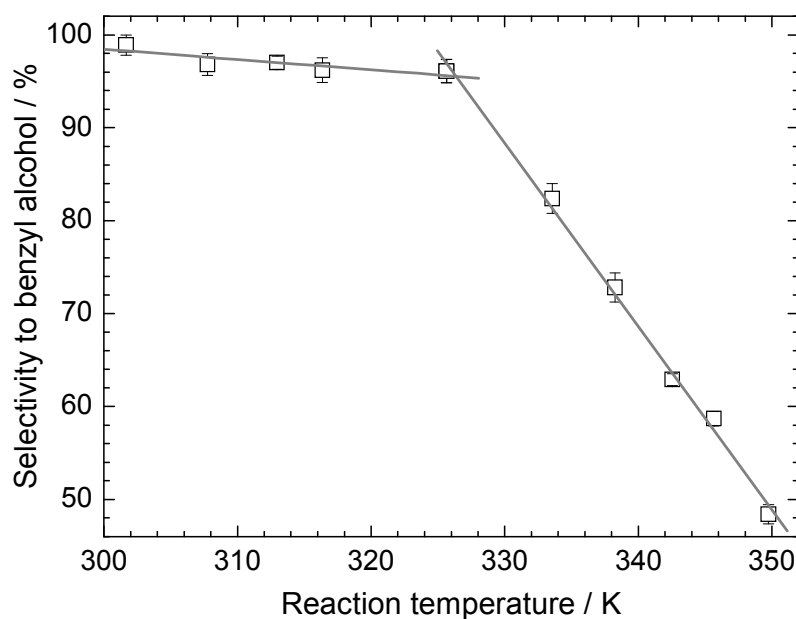
**Fig. 3.10** Selectivity to benzyl alcohol as a function of the reaction temperature. $P = 8$ barg, $F_{\text{Liquid}} = 1.46$ kg m$^{-2}$ s$^{-1}$, $F_{\text{Gas}} = 2.66 \times 10^{-3}$ kg m$^{-}$ s$^{-1}$, $C_{\text{Substrate, 0}} = 0.2$ mol L$^{-1}$.

The formation of the byproduct slowly deactivates the catalysts during continuous operation. The deactivation was likely to be linked with blocking of active sites, which was caused by adsorption of the byproduct onto catalysts. In comparison with the fresh catalyst, the spent catalyst had a lower specific surface area ($S_{BET}$, 1,108 *vs.* 1,491 m$^2$ g$^{-1}$), confirming loss of accessibility of the highly developed surface area of the catalyst (refer to Appendix II for the details of $N_2$ adsorption analysis).

Catalyst regeneration by solvent washing and reactants purification was studied. A series of experiments was carried out with an ascending temperature sequence and a sequential descending temperature with or without catalyst washing between each run. The results are shown in Fig. 3.11. As one can see, the catalyst regained almost all of its initial activity after washing and the bell-shaped dependence of the benzyl alcohol remained unaffected. The identified byproduct was observed in the outlet of the reactor during the washing of the catalyst bed.

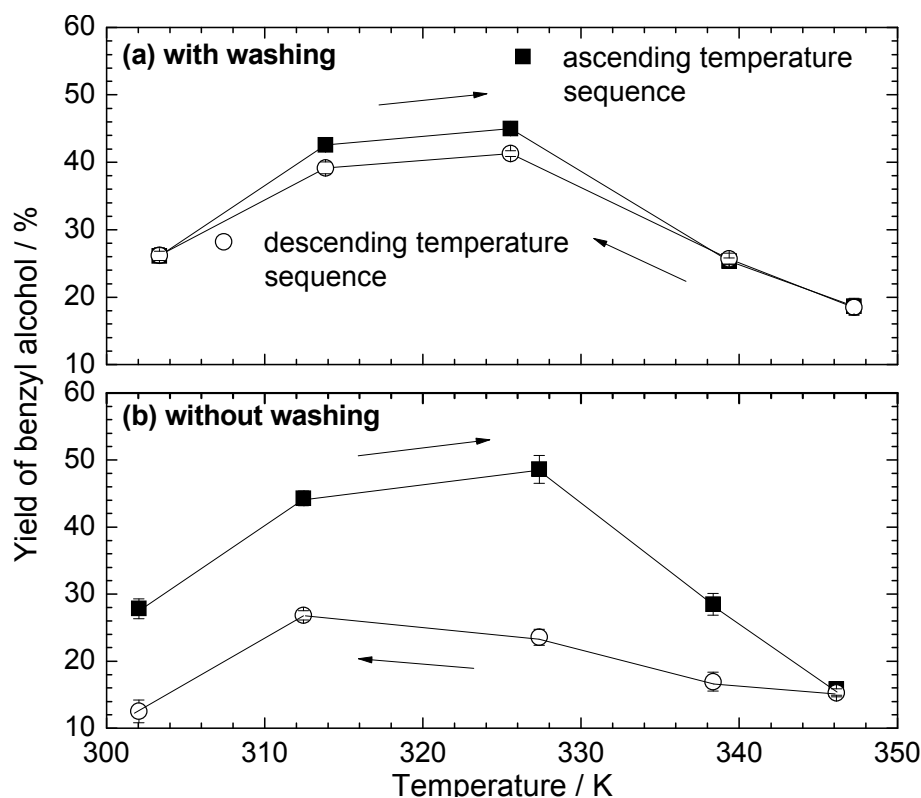**Fig. 3.11** Test of catalyst deactivation and regeneration.  Benzyl alcohol yield as a function of reaction temperature. (a) Washing catalyst bed with solvent in descending temperature run. (b) Benzyl alcohol concentration variation with the reaction temperature, without washing catalyst bed using solvent. $P$ = 8 barg, $F_{Liquid}$ = 1.46 kg m$^{-2}$ s$^{-1}$, $F_{Gas}$ = 2.66 × 10$^{-3}$ kg m$^{-2}$ s$^{-1}$, $C_{Substrate, 0}$ = 0.2 mol L$^{-1}$. Solid lines are for the convenience of viewing.

### 3.3.5    *Enhanced reactor efficiency with staged injection of hydrogen*

The possibility of using staged injection of hydrogen to increase the reactor efficiency was also investigated.  The reaction channel arrangements, *i.e.* different gas injection options, are illustrated in Fig. 3.12.  For all configurations, the amount of hydrogen supplied relative to the catalyst amount used remained the same. Compared with the arrangement A, a double amount of hydrogen was used due to the two-fold increase of the catalyst amount in the arrangements B and C.  Therefore, the two-phase flow pattern along the channels, as well as the residence time of the liquid phase in the reactor, may have changed, and both are likely to affect conversion. Exemplary, a *ca.* 12 % increase in the product yield (up to 55 %) was measured with the arrangement B in comparison with the arrangement A (Fig. 3.13).   For the arrangement C, an identical total amount of hydrogen as in the case B was split and injected at the entrance of the two consecutive channels.   Therefore, the

hydrodynamic regime in the two channels was believed to be identical to that in the case A. As anticipated, the maximum product yield was increased by 52 % (calculated yield, up to 73 %) due to the doubling of the total residence time. In all three cases selectivity to benzyl alcohol remained the same *ca.* 96 % (by GC).
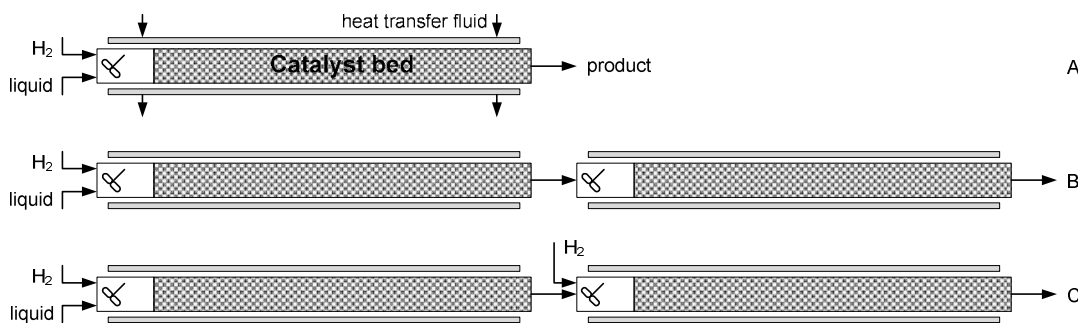


**Fig. 3.12** Channel arrangement for split hydrogen injection experiments. (a) Single channel, injection of hydrogen at length $L = 0$ cm, (b) double channel, injection of hydrogen at length $L = 0$ cm, and (c) double channel, injection of hydrogen at lengths $L = 0$ cm and $L = 10$ cm.
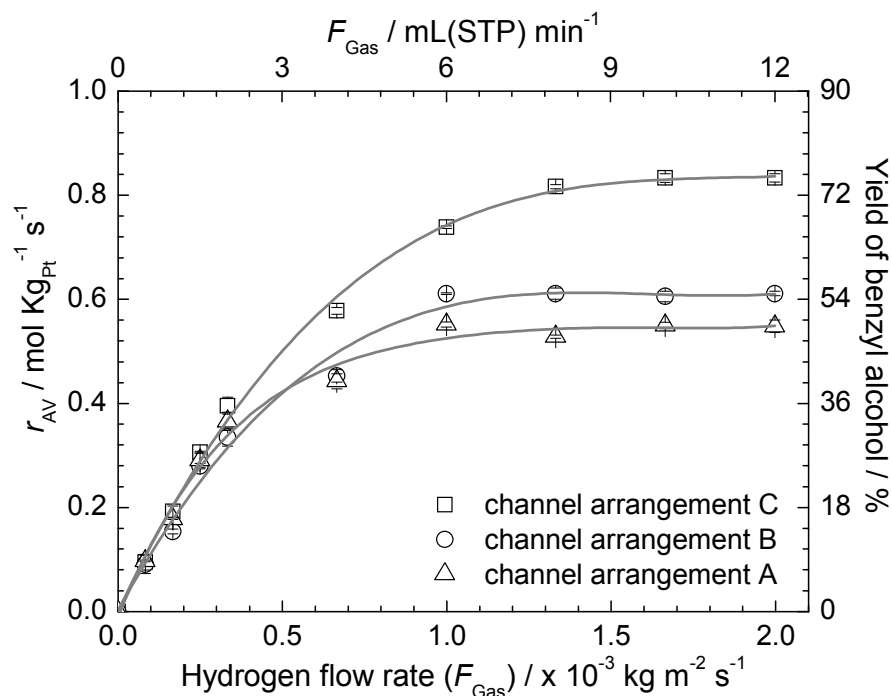


**Fig. 3.13** Benzyl alcohol yield against gas flow-rate for different hydrogen injection strategies. $P = 8$ barg, $T = 318$ K, $F_{Liquid} = 1.46$ kg m$^{-2}$ s$^{-1}$, $C_{Substrate, 0} = 0.2$ mol L$^{-1}$.

With regard to this simple model reaction investigated in this work, the split gas distribution along the length of the reaction channel resulted in a higher yield of the desired product. However, the concept of dosing the required amount of gaseous reactant at different positions along the catalyst bed (at different levels of conversion) might have been a flexible method of performing more complex reactions continuously, such as consecutive oxidation/hydrogenation[14] and tandem reactions.[28]

## 3. 4    Conclusions

The effectiveness of a compact multichannel reactor for performing continuous catalytic hydrogenation was demonstrated. Due to the integration of heat transfer, mixing and reaction functionalities into a single reactor, a more intensified process for the model hydrogenation reaction was attained in comparison to other reported continuous or batch applications. Thus, a 41 % calculated yield, corresponding to a space-time yield of product of *ca.* 34 mol $L_{reactor}^{-1} h^{-1}$, was achieved at 317 K for the single pass through the reaction channel with undiluted catalyst bed at *ca.* 40 second residence time. Results also showed that, owing to the enhanced transport phenomena, the compact reactor is a suitable tool for studying kinetics of mass- and heat-transfer-limited reactions. A byproduct formed through an acid-induced side reaction was found in the reaction system and caused reversible catalyst deactivation. Catalyst was effectively regenerated by solvent washing. The staged injection of hydrogen was shown to be beneficial for this model reaction, which was attributed to a better hydrodynamic regime.

## Acknowledgements

## References

1. Blaser, H. U.; Malan, C.; Pugun, B.; Spindler, F.; Steiner, H.; Studer, M., Selective hydrogenation for fine chemicals: Recent trends and new developments. *Adv. Synth. Catal.* **2003,** 345, (1–2), 103–151.

2. Klemm, E.; Amon, B.; Redlingshofer, H.; Dieterich, E.; Emig, G., Deactivation kinetics in the hydrogenation of nitrobenzene to aniline on the basis of a coke formation kinetics – investigations in an isothermal catalytic wall reactor. *Chem. Eng. Sci.* **2001,** 56, (4), 1347–1353.

3. Lapkin, A. A.; Plucinski, P. K., Engineering factors for efficient flow processes in chemical industries. In *Chemical Reactions and Processes under Flow Conditions*. Luis, S. V.; Garcia-Verdugo, E., Eds. The Royal Society of Chemistry: Cambridge, 2010.

4. Vospernik, M.; Pintar, A.; Bercic, G.; Levec, J.; Walmsley, J.; Raeder, H.; E., I. E.; Miachon, S.; Dalmon, J. A., Performance of catalytic membrane reactor in multiphase reactions. *Chem. Eng. Sci.* **2004,** 59, (22–23), 5363–5372.

5. Peureux, J.; Torres, M.; Mozzanega, H.; Giroir-Fendler, A.; Dalmon, J.-A., Nitrobenzene liquid-phase hydrogenation in a membrane reactor. *Catal. Today* **1995,** 25, (3–4), 409–415.

6. Kirillov, V. A.; Kuzin, N. A.; Mescheryakov, V. D.; Droboshevich, V. I., Catalytic heat-exchanger reactor for strongly exothermic reactions. *Chem. Eng. Sci.* **2001,** 56, (2), 381–386.

7. Ehrfeld, W.; Hessel, V.; Löwe, H., *Microreactors*. WILEY–VCH: Weinheim, 2000; p 288.

8.    Renken, A.; Hessel, V.; Lob, P.; Miszczuk, R.; Uerdinggen, M.; Kiwi-Minsker, L., Ionic liquid synthesis in a microstructured reactor for process intensification. *Chem. Eng. Proc.* **2007,** 46, (9), 840–845.

9.    Yoswathananont, N.; Nitta, K.; Nishiuchi, Y.; Sato, M., Continuous hydrogenation reactions in a tube reactor packed with Pd/C. *Chem. Commun.* **2005**, (1), 40–42.

10.   Kobayashi, J.; Mori, Y.; Kobayashi, S., Triphase hydrogenation reactions utilizing palladium-immobilised capillary column reactors and a demonstration of suitability for large scale synthesis. *Adv. Synth. Catal.* **2005,** 347, (15), 1889–1892.

11.   Kobayashi, J.; Mori, Y.; Okamoto, K.; Akiyama, R.; Ueno, M.; Kitamori, T.; Kobayashi, S., A microfluidic device for conducting gas-liquid-solid hydrogenation reactions. *Science* **2004,** 304, (5675), 1305–1308.

12.   Kobayashi, J.; Mori, Y.; Kobayashi, S., Hydrogenation reactions using $scCO_2$ as a solvent in microchannel reactors. *Chem. Commun.* **2005**, (20), 2567–2568.

13.   Yeong, K. K.; Gavriilidis, A.; Zapf, R.; Hessel, V., Catalyst preparation and deactivation issues for nitrobenzene hydrogenation in a microstructured falling film reactor. *Catal. Today* **2003,** 81, (4), 641–651.

14.   Bavykin, D. V.; Lapkin, A. A.; Kolaczkowski, S. T.; Plucinski, P. K., Selective oxidation of alcohols in a continuous multifunctional reactor: Ruthenium oxide catalysed oxidation of benzyl alcohol. *Appl. Catal. A: Gen.* **2005,** 288, (1–2), 175–184.

15.   Plucinski, P. K.; Bavykin, D. V.; Kolaczkowski, S. T.; Lapkin, A. A., Liquid-phase oxidation of organic feedstock in a compact multichannel reactor. *Ind. Eng. Chem. Res.* **2005,** 44, (25), 9683–9690.

16.   Plucinski, P. K.; Bavykin, D. V.; Kolaczkowski, S. T.; Lapkin, A. A., Application of a structured multifunctional reactor for the oxidation of a liquid organic feedstock. *Catal. Today* **2005,** 105, (3–4), 479–483.

17.   van Dam, H. E.; van Bekkum, H., Preparation of platinum on activated carbon. *J. Catal.* **1991,** 131, (2), 335–349.

18. Kiwi-Minsker, L.; Yuranov, I.; Holler, V.; Renken, A., Supported glass fibers catalysts for novel multi-phase reactor design. *Chem. Eng. Sci.* **1999,** 54, (21), 4785–4790.

19. Baidossi, M.; Joshi, A. V.; Mukhopadhyay, S.; Sasson, Y., Pd/C-catalysed transfer-hydrogenation of benzaldehydes to benzyl alcohols using potassium formate as the selective hydrogen donor. *Syn. Commun.* **2004,** 34, (4), 643-650.

20. Nijhuis, T. A.; Kreutzer, M. T.; Romijn, A. C. J.; Kapteijn, F.; Moulijn, J. A., Monolithic catalysts as more efficient three-phase reactors. *Catal. Today* **2001,** 66, (2–4), 157–165.

21. Dudukovic, M. P.; Larachi, F.; Mills, P. L., Multiphase catalytic reactors: A perspective on current knowledge and future trends. *Catal. Rev.* **2002,** 44, (1), 123–246.

22. Weisz, P. B.; Prater, C. D., Interpretation of measurements in experimental catalysis. *Adv. Catal.* **1954,** 6, 143–196.

23. vannice, M. A., *Kinetics of Catalytic Reactions*. 1st ed.; Springer: New York, 2005.

24. *Hydrogen and Deuterium*. 1st ed.; Pergamon: Oxford, 1981; Vol. 5–6.

25. Singh, U. K.; Vannice, M. A., Kinetics of liquid-phase hydrogenation reactions over supported metal catalysts – a review. *Appl. Catal. A: Gen.* **2001,** 213, (1), 1–24.

26. Verevkin, S. P.; Vasiltsova, T. V., Thermochemistry of benzyl alcohol: Reaction equilibria involving benzyl alcohol and *tert*-alkyl ethers. *J. Chem. Eng. Data* **2004,** 49, (6), 1717–1723.

27. Vatani, A.; Mehrpooya, M.; Gharagheizi, F., Prediction of standard enthalpy of formation by a QSPR model. *Int. J. Mol. Sci.* **2007,** 8, (5), 407–432.

28. Thomas, S.; Pushpavanam, S.; Seidel-Morgenstern, A., Performance improvements of parallel-series reactions in tubular reactors using reactant dosing concepts. *Ind. Eng. Chem. Res.* **2004,** 43, (4), 969–979.

# Chapter 4

# Potential of 'nanofluids' to further intensify microreactors

Recent discovery of high enhancement of heat transfer in nanofluids may be applicable to the area of process intensification of chemical reactors through integration of the functionalities of reaction and heat transfer in compact multifunctional reactors.  This may lead to the reduction in the processes footprint and energy intensity over the process Life Cycle, allow easier implementation of highly exothermic and endothermic reactions, and enable rapid quenching of reactions.  A nanofluid based on benign $TiO_2$ material dispersed in ethylene glycol has been studied in an integrated reactor-heat exchanger.  An up to 35 % increase in the overall heat transfer coefficient was measured in the steady state continuous experiments.  This resulted in a closer temperature control in the reaction of selective reduction of an aromatic aldehyde by molecular hydrogen and very rapid change in the temperature of reaction under dynamic reaction control. This chapter is based on the paper: X. Fan, H. Chen, Y. Ding, P. K. Plucinski, A. A. Lapkin, *Green Chem.*, 2008, 10, 670–677.

## 4. 1 Introduction

Process Intensification (PI), a term coined in 1980s,[1-3] encompasses the many different approaches leading ultimately to chemical processes that are: inherently safe, reduce or eliminate the need for on-site inventory of toxic/hazardous compounds, energy efficient and are characterised by a small footprint.[4, 5] Some examples of PI approaches include intensification of mass and heat transfer in microreactors[6-8] and high shear reactors, *e.g.*, spinning disk[9] and impinging jets, the use of neoteric solvents, *e.g.*, sc-$CO_2$[10] and ionic liquids.[11] Amongst many PI approaches, ionic liquids and compact reactors/heat exchangers are being commercialised at a very rapid pace.[12]

The principle of intensification in microreactors and compact reactors is in the reduction of the length scales across which mass and heat transfer should occur, which allows performing highly exothermic and endothermic reactions safely, and to couple reactions with different heat effects. For example, selective oxidation of aromatic alcohols by molecular oxygen has been demonstrated at up to 24 atm undiluted oxygen pressure, which was enabled by (*i*) highly efficient heat removal in an integral micro-heat exchanger and (*ii*) the absence of gas-phase volume in which an explosive mixture of hydrocarbon vapour and oxygen may be produced.[6]

The main mechanisms by which an enhancement of heat transfer is achieved in a microstructured heat exchangers, compared with conventional heat exchangers, are (*i*) the reduction of the material of construction conduction resistance (very thin barrier between the process fluid and the heat transfer medium), and (*ii*) by enhancing the convective heat transfer coefficient, the latter being achieved through design of the geometry of the 100s of microns width scale heat transfer fluid channels.[13] Taking this concept to extreme will give a design with very thin walls and very narrow channels. The resulting heat transfer fluid pressure drop and, consequently, high pumping power, will negate the increase in the effectiveness of heat transfer, by increasing the overall process energy requirement. Thus, there exists an upper bound

in efficiency of microreactors, given by the overall process energy optimisation. The remaining possibilities in further increasing the efficiency of micro-heat exchangers are the modification of the surface[14] or an enhancement in the thermal properties and behaviour of the heat transfer fluid itself.

The latter approach has recently attracted a significant interest through the emergence of a new field of 'nanofluids', the term coined at Argonne National Labs.[15] A nanofluid is a stable dilute suspension of nanoparticles in a heat transfer fluid, which alters the heat transfer characteristics of the base fluid. According to the classic effective medium (mean field or Maxwell) theory of heat transfer, an increase in the volume fraction of nanoparticles with a higher thermal conductivity than that of the base fluid, results in an increase in the effective thermal conductivity, as given by Hamilton and Crosser:[16]

$$\frac{k_{nf}}{k_f} = \frac{k_P + 2k_f - 2\phi\left(k_f - k_P\right)}{k_P + 2k_f + 2\phi\left(k_f - k_P\right)} \tag{4.1}$$

where $k_{nf}$, $k_f$ and $k_p$ are thermal conductivities of the nanofluid, base fluid and suspended particle, respectively, and $\phi$ is the particle volume fraction.

According to Eq. (4.1) only a marginal increase in the thermal conductivity of a nanofluid could be expected. For example, a typical volume fraction of nanoparticles of 1 vol.% gives an enhancement in thermal conductivity of *ca*. 3 %. However, experimental results can be found in the literature with significantly better[17-19] and significantly worse[20] $k_{nf}/k_f$ ratios, as well as those supporting the basic Maxwell theory.[21] The exciting unexpectedly high increase in the thermal conductivity above the prediction of the classic theory resulted in a sharp increase in the interest to nanofluids. Fig. 4.1 summarises some recent literature data of thermal conductivity of nanofluids (the shaded area shows the overlap in experimental data between nanofluids based on nanomaterials with high effective thermal conductivity, such as metal nanoparticles, and low thermal conductivity, such as oxides).[22]
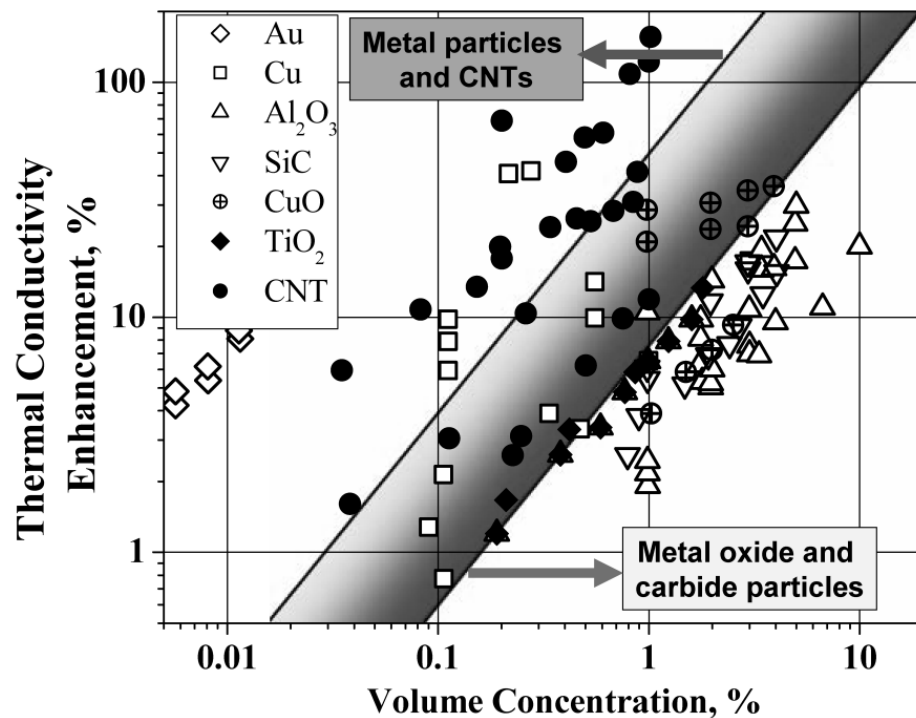
**Fig. 4.1** Recent research data on the thermal conductivity of nanofluids. Adopted from ref. 22.

A number of theories were proposed to explain this phenomenon.[23, 24] The emerging consensus among the nanofluids community, however, is that if clustering of nanoparticles is taken into account and the volume fraction is adjusted for the effective density/volume of the cluster, the heat conduction enhancement fits well to that predicted by Eq. (4.1).[25, 26] The deterioration of heat conduction below the mean field theory has been shown to result from a significant interfacial heat transfer resistance in the case of poor wetting of nanoparticles by the base fluid.[27] Therefore, the chemistry of nanoparticles and fundamental knowledge of nanoparticle aggregation behaviour are the key to designing new and effective nanofluids for heat transfer applications. There remains a possibility of higher enhancement of conductive heat transfer, if particle-to-particle conduction pathways are generated above the percolation threshold in the case of the high aspect ratio nanoparticles, such as carbon nanotubes.[28-30]

In most practical applications heat transfer fluid is not stationary as in the case of heat conduction measurements described above. Convective heat transfer coefficient

becomes more important and, according to the fundamental theory, heat transfer may be enhanced, remain unchanged or even be worse in the presence of nanoparticles, depending on how affected are the three parameters: heat conductivity of nanofluids ($k_{nf}$), thermal boundary layer thickness ($\delta_t$) and properties of the heat transfer surface, where the effects of the former two parameters are shown, for the case of turbulent flow, by Eq. (4.2):

$$h = k_{nf} / \delta_t \tag{4.2}$$

*where h* is the convective heat transfer coefficient. The effect of the heat transfer surface properties is reflected in the total heat flux.

There is very little experimental or theoretical data on the convective heat transfer of nanofluids in micro-heat exchangers. It was shown experimentally, that an enhancement in heat transfer efficiency, expressed as thermal resistance ($K\ W^{-1}$), of *ca.* 13 % can be achieved only at low heat transfer fluid flow-rate.[31] Pronounced fouling of micro-heat exchanger by nanoparticles at higher flow-rates was shown to be responsible for poor performance of nanofluids. In another study, a more pronounced enhancement of the heat transfer coefficient was found in the entrance region of a laminar flow in a microchannel.[32] Theoretical calculations not based on convective heat transfer theory are underestimating the enhancement in the flow regime, even if high conductive heat transfer enhancement is assumed.[33]

To the best knowledge of the authors, there have been no studies concerning application of nanofluids in chemical microreactors until now. The aim of this study is to evaluate performance of nanofluids in a structured compact reactor/heat exchanger. Enhancement of the overall heat transfer coefficient, stability of nanofluids and feasibility of rapid reaction quenching were studied in detail and comparison of the increased efficiency *versus* the penalty of higher pumping power was made.

## 4. 2   Experimental

### 4.2.1      *Formulation of TiO₂-EG nanofluids*

Nanofluids preparation was done at the University of Leeds.  The following content in this section was advised by the colleagues from Professor Ding Yulong's group at the University of Leeds.

Dry titanium dioxide nanoparticles and pure ethylene glycol (EG) were used to make nanofluids.  The nanoparticles (P25 $TiO_2$, purity better than 99.5 %) were purchased from Degussa and ethylene glycol (> 99.0 %) was from Alfa Aesar.  Both were used as received.  The primary nanoparticles are spherical with approximately 25 nm diameter (by SEM and HRTEM).  However, they are in the form of large agglomerates.  The method of preparation of nanofluids employed in this work is described in details elsewhere.[34, 35]  EG-$TiO_2$ nanofluids with concentrations of 0.5, 2.0 and 4.0 % by weight, corresponding respectively to 0.10, 0.43 and 0.86 % by volume, were produced.  As the dry $TiO_2$ nanoparticles were in the form of agglomerates, an ultrasonic bath (Nickel Electro Ltd, UK) was used to break the agglomerates.  The average particle size of the resulting nanofluids was measured to be 50–150 nm by using dynamic light scattering (Malvern Nanosizer, Malvern Instruments), suggesting the presence of agglomerates in the colloid, rather than well separated seed particles.  The EG-$TiO_2$ nanofluids were found to be stable for over two months at ambient temperature.
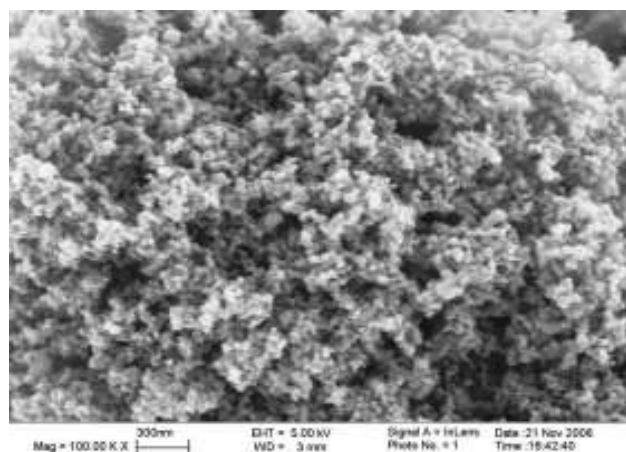


**Fig. 4.2** SEM image of $TiO_2$ nanoparticles as received. Adopted from ref. 36.

### *4.2.2    Structured compact reactor*

Details of the reactor and the experimental were disclosed in Chapter 3 (Fig. 3.1 and 3.2, section 3.2.2 and 3.2.3) and elsewhere.[6, 36]   In this study a square reaction channel with side of 3 mm and length of 100 mm was packed with 0.1 g of 3 wt.% Pt/C catalysts produced by Engelhard, using microspherical (particle diameter: 110–130 μm) mesoporous carbon support developed by MAST Carbons Ltd (UK).   The catalyst was diluted with glass spheres (150–212 μm diameter, Sigma–Aldrich) to fill the reaction channel completely.   The experimental system (only heat transfer section of the rig) for performing convective heat transfer experiments (steady state/dynamic heat transfer experiments) and hydrogenation reaction is shown schematically in Fig. 4.3   Heat transfer fluid was heated and pumped into compact heat exchange module by re-circulating bath (RCB, Haake DC30, DC10).   A needle valve (with scale, Hoke, Circor Instrumentation Ltd) was used to control flow-rate of heat transfer fluid.   Four K-type thermocouples (WATLOW) were used to measure temperature of heat transfer fluid inlet ($T_1$), outlet ($T_2$), process liquid inlet ($T_3$) and outlet ($T_4$).   Three thermo-wells were placed along the length of each reaction channel at 13, 48 and 80 % ($T_5$–$T_7$) from the inlet respectively.   The thickness of the metal plate between thermocouples and the reaction channel was 100 μm, ensuring a reasonably quick response.   Micro-thermocouples (Tempcon Instrumentation, UK) were used to measure temperature of the reaction channel wall.

In hydrogenation experiments, a 0.2 M benzaldehyde solution in 2-propanol was placed in the stainless steel feed vessel connected to a pump (Kontron Instruments, HPLC pump 422).   Hydrogen flow-rate was controlled by mass flow controllers (MFC, Brooks 5850s).   The outlet from the compact reactor was connected via a low dead-volume six-way valve to a receiving vessel, which also served as a gas-liquid separator.   The feed and receiving vessels were connected in order to equalise the pressure.   The operating pressure was set by a back pressure regulator (BPR, Brooks 5866) and the pressure drop across the reactor was measured using a Bronkhorst differential pressure transducer (DPT).
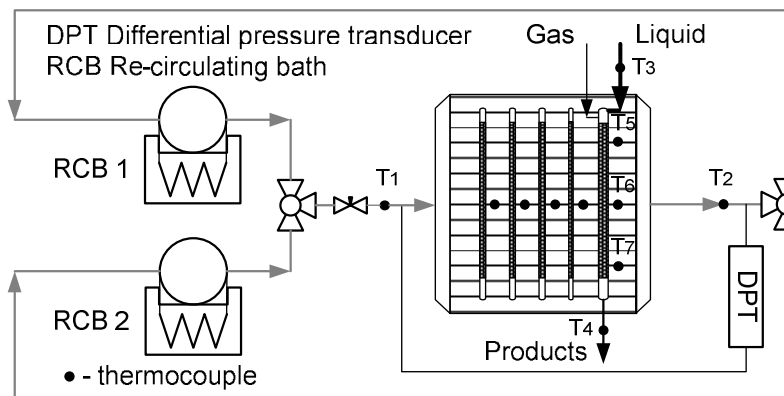
**Fig. 4.3** Experimental rig for heat transfer and hydrogenation of benzaldehyde experiments.

### *4.2.3    Characterisation of physical and thermal properties of nanofluids*

Nanofluids characterisation was performed at the University of Leeds.    The following content in this subsection was advised by the colleagues from Professor Ding Yulong's group at the University of Leeds.

The thermal conductivity was measured by using a KD2 thermal property metre (Labcell Ltd., UK), which is based on the transient hot wire method.  The KD2 metre has a probe with 60 mm length and 0.9 mm diameter, which integrates in its interior a heating element and a thermo-resistor, and is connected to a microprocessor for controlling and conducting the measurements.  The KD2 metre was calibrated by using distilled water and pure EG before any set of measurements.  A thermostat bath (GD 120-S12, Grant, UK) was used to maintain the temperature uniformity within 0.02 K.   At least five measurements were taken for each concentration of the nanofluids at a given temperature to ensure the uncertainty of measurements within 3 %.  Fig. 4.4 shows the relative thermal conductivity of nanofluids against the pure EG as a function of nanoparticle concentration together with the prediction of the conventional Maxwell equation at ambient temperature.   It can be seen that the thermal conductivity of nanofluids increases with increasing nanoparticle concentration.  The measured thermal conductivity of the nanofluids is higher than the predictions of the Maxwell equation (Eq. (4.1)) even with the experimental error taken into account.
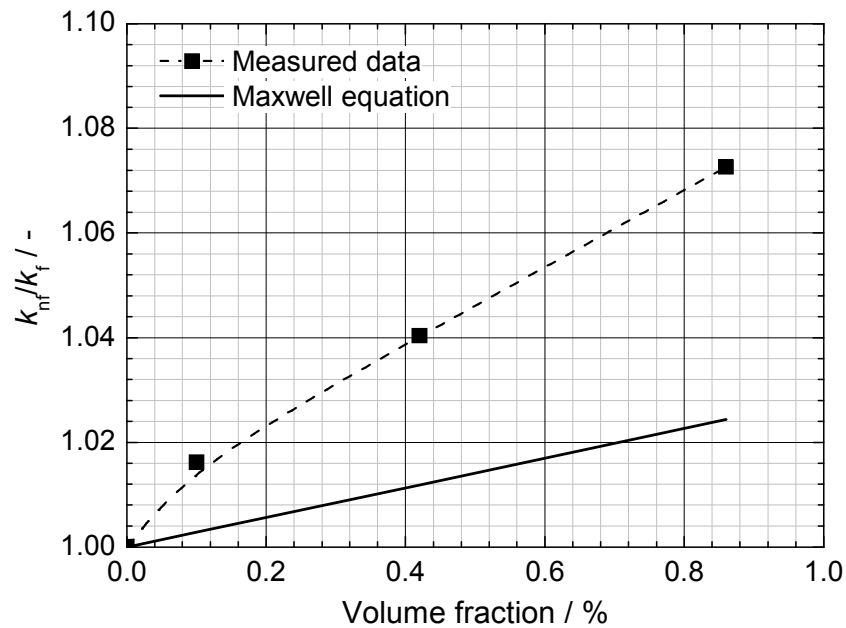
**Fig. 4.4** Relative thermal conductivity of nanofluids ($k_{nf}/k_f$) as a function of nanoparticle volume fraction.

A Bohlin CVO rheometre (Malvern Instruments, UK) was used to measure nanofluids viscosity. Over the shear rate range (1–3000 s$^{-1}$) used in the measurements, EG-TiO$_2$ nanofluids were confirmed as Newtonian fluids. Calibrations were conducted against standard solutions on weekly basis over the duration of this work to ensure accurate measurements of nanofluid viscosity. Three measurements were taken for each test and the maximum uncertainty of viscosity was found to be ~2.0 %. The measured relative viscosity of nanofluids is plotted against nanoparticle volume fraction in Fig. 4.4. It can be seen that the viscosity of nanofluids increases with the increase of nanoparticle volume fraction. Also included in Fig. 4.5 is the prediction of the Einstein equation for dilute non-interacting suspensions of spherical particles ($\mu_{nf}/\mu_f = 1 + 2.5\phi$), showing that the Einstein equation under predicts the experimental data.
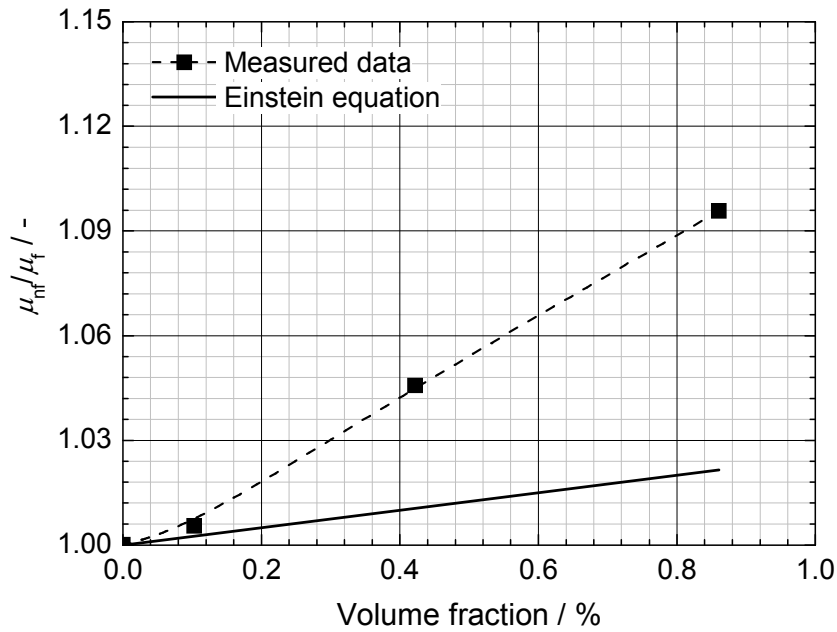
**Fig. 4.5** Relative viscosity of nanofluids ($\mu_{nf}/\mu_f$) as a function of nanoparticle volume fraction.

Based on the nanoparticle and base fluid densities, the nanofluid density is calculated as Eq. (4.3).[37]

$$\rho_{nf} = \varphi \rho_p + (1-\varphi)\rho_f \qquad (4.3)$$

where $\phi$ is the volumetric fraction of nanoparticles and the subscripts p, f and nf refer to the nanoparticles, base liquid and nanofluids, respectively.

Assuming that the nanoparticles and the base liquid fluid are in thermal equilibrium, the specific heat capacity of the nanofluid can be estimated by:

$$c_{p,nf} = \varphi \frac{\rho_p}{\rho_{nf}} c_{p,Particle} + (1-\varphi)\frac{\rho_f}{\rho_{nf}} c_{P,f} \qquad (4.4)$$

Table 4.1 shows the properties of the base liquid as well as for different concentrations of $TiO_2$. It can be seen that the density and the heat capacity of nanofluids are very close to those of the base liquid.

**Table 4.1** Thermal and physical properties of TiO$_2$-EG nanofluids at 303 K and 100 kPa.

| Thermal properties | nanoparticle volume fraction in base liquid | | | |
| --- | --- | --- | --- | --- |
| | $\varphi = 0$ % | $\varphi = 0.10$ % | $\varphi = 0.43$ % | $\varphi = 0.86$ % |
| $\rho$ (kg m$^{-3}$) | 1110 | 1113 | 1123 | 1137 |
| $c_p$ (kJ kg$^{-1}$ K$^{-1}$) | 2.430 | 2.423 | 2.391 | 2.370 |
| $\mu$ (kg m$^{-1}$ s$^{-1}$) | $1.410 \times 10^{-2}$ | $1.418 \times 10^{-2}$ | $1.474 \times 10^{-2}$ | $1.545 \times 10^{-2}$ |
| $k$ (W m$^{-1}$ K$^{-1}$) | 0.2530 | 0.2571 | 0.2632 | 0.2714 |

TiO$_2$ properties: $\rho_{TiO_2} = 4200$ kg m$^{-3}$, $C_{P,TiO_2} = 0.54$ kJ kg$^{-1}$ K$^{-1}$, $k_{TiO_2} = 11.70$ W m$^{-1}$ K$^{-1}$

### *4.2.4 Evaluation of the heat transfer performance of nanofluids.*

The overall experimental heat transfer coefficient, $h_{(exp)}$, was used to evaluate the heat transfer performance of different heat transfer fluids. Based on energy conservation equation:

$$\dot{q}\left[ J \cdot s^{-1} \right] = c_{p,HTF} \cdot \dot{m}_{HTF}(T_2 - T_1) = c_{p,P} \cdot \dot{m}_P(T_4 - T_3) = h_{(exp)} \cdot A \cdot f_t \cdot \Delta\vartheta_m \tag{4.5}$$

And then $h_{(exp)}$ can be calculated as Eq. (4.6):

$$h_{(exp)}\left[ J \cdot s^{-1} \cdot m^{-2} \cdot K^{-1} \right] = \frac{c_{p,P} \cdot \dot{m}_P \cdot (T_4 - T_3)}{A \cdot f_t \cdot \Delta\vartheta_m} \tag{4.6}$$

In Eqs. (4.5) and (4.6), subscripts *HTF* and *P* refer to heat transfer fluid and process liquid, $c_p$ is the specific heat capacity, $\dot{m}$ is the mass flow-rate, *A* is the effective heat transfer area, and $\Delta\vartheta_m$ is the log-mean temperature difference, defined as:

$$\Delta\vartheta_m = \frac{(T_1 - T_4) - (T_2 - T_3)}{\ln\left[ (T_1 - T_4)/(T_2 - T_3) \right]} \tag{4.7}$$

Log mean temperature is usually defined for counter flow heat exchangers. Therefore, a correction factor $f_t$ was introduced in Eq. (4.6) to account for the cross flow heat exchange process used in this study. Derivation of $f_t$ can be found in the literature.[38] For the position of T$_1$–T$_4$, refer to Fig. 4.3.

## 4. 3   Results and discussion

### *4.3.1   Enhancement of the heat transfer in the micro-heat exchanger*

The potential enhancement of the overall heat transfer coefficient was studied in the steady state experiments in the absence of reaction with only water as a process fluid. Fig. 4.6 shows the recorded process fluid temperature at outlet (measured by $T_4$, see Fig. 4.3) as a function of overall mass flow-rate of heat transfer fluid (HTF) for both, the base liquid and the EG-TiO$_2$ nanofluids.
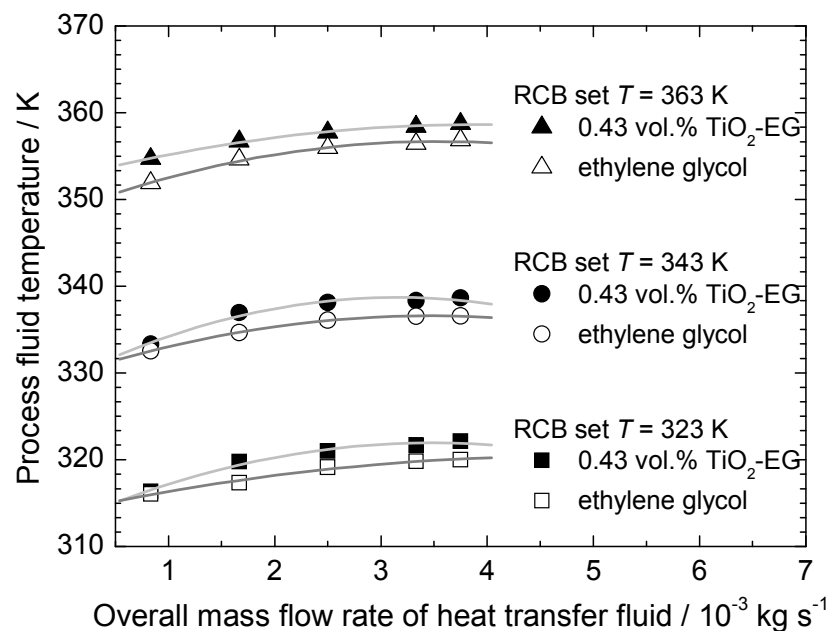


**Fig. 4.6** Process fluid (water) temperature at reactor outlet as a function of overall mass flow-rate of the heat transfer fluid, Water flow-rate = $1.66 \times 10^{-4}$ kg s$^{-1}$.

As it can be seen, the increase in $T_4$ with increasing of the overall HTF mass flow-rate follows a similar pattern for both, pure EG and EG-TiO$_2$ nanofluids. Higher temperatures ($T_4$) were achieved using nanofluids as HTF compared with those using pure EG at the same flow-rates. This indicates that more heat was transferred to the process fluid, according to Eq. (4.5), by introducing nanoparticles into the base liquid. Therefore, convective heat transfer was improved by using nanofluids (note that the

heat capacity and density of nanofluids are approximately the same as those of the based liquid due to low particle concentrations, see Table 4.1).
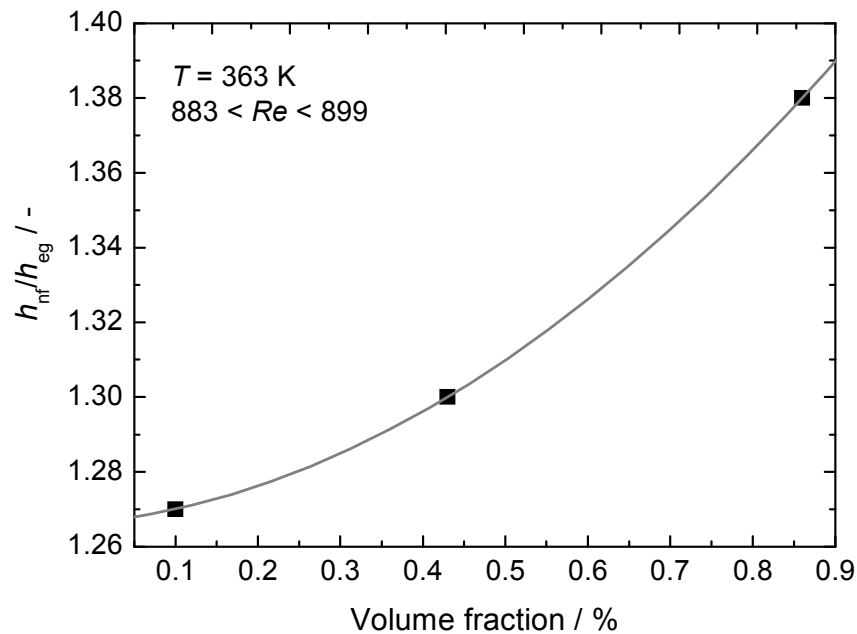


**Fig. 4.7** Increment of overall relative heat transfer coefficient as a function of $TiO_2$ nanoparticle volume fraction.

Fig. 4.7 shows the measured relative heat transfer coefficient of nanofluids (calculated by Eq. (4.6)) as a function of $TiO_2$ nanoparticle volume fraction. The heat transfer coefficient of nanofluids increased rapidly with increasing nanoparticle concentration under the conditions used in this work.

Fig. 4.8 shows the temperature dependence of the measured overall heat transfer coefficient of nanofluids. The higher the temperature, the higher is the relative enhancement over pure EG. This is likely to be associated with an increase in convective heat transfer due to a decrease in viscosity of the base liquid with increasing temperature. Recent study[39] showed that $TiO_2$ (P25)-EG nanofluid behaves as a Newtonian fluid over 0–8 wt.% concentration of nanoparticles, and the presence of nanoparticles does not affect the temperature dependence of the shear viscosity of the base EG fluid. The temperature dependent enhancement can be

explained, at least qualitatively, by Eq. (4.2). An increase in temperature leads to a decrease in viscosity, and hence a decrease in the thermal boundary layer. An increase in temperature also increases thermal conductivity.[28, 39] These factors, according to Eq. (4.2), result in an increase in heat transfer, which corresponds to our observations.
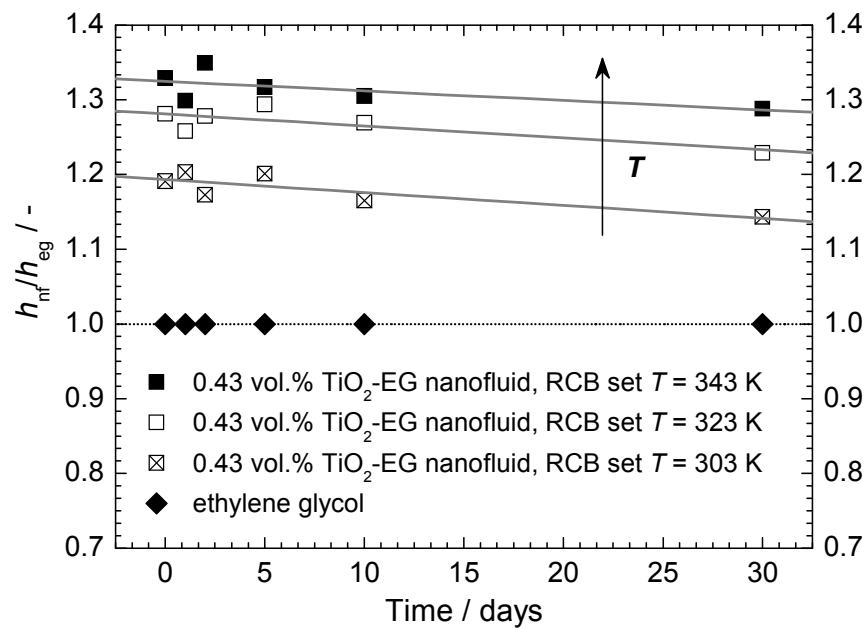


**Fig. 4.8** Overall relative heat transfer coefficient of 0.43 vol.% $TiO_2$-EG nanofluid as a function of time, overall mass flow-rate $= 5 \times 10^{-3}$ kg s$^{-1}$.

The enhancement in the heat transfer coefficient is slowly degrading over time. Fig. 4.8 shows the results over a period of 30 days, which give *ca.* 0.15 % day$^{-1}$ loss in the enhancement effect for the 0.43 vol.% nanofluid. The exact reasons for this requires further investigation but it is believed to be associated with the gradual clustering of nanoparticles and sedimentation of the larger clusters in the low shear areas of the heat transfer system, most likely in the recirculating bath. This is supported by the dynamic light scattering measurements of the nanofluids, which showed an increased average particle size after 30 days.

There was no noticeable deposition of nanoparticles on the micro-heat exchanger surfaces as evidenced by the retention of the enhancement upon change from the older nanofluid samples to a fresh sample. However, it was also noticed that elevated temperatures significantly accelerated aggregation and if strongly aggregated suspension of nanoparticles was circulated through the micro-heat exchanger structure, serious fouling of surfaces occurs, requiring long sonication to remove the deposits.

### 4.3.2    *Pressure drop and pumping power*

As shown above, heat transfer process in the micro channel heat exchanger was intensified considerably using nanofluids. However, the enhanced heat transfer coefficient came with a small penalty of pressure increase, arising from a few percents of viscosity increase (Fig. 4.5). With conventional heat transfer fluids, an increase of heat transfer coefficient by a factor of 100 % typically incurs a pressure drop penalty of ~1000 %.[40] By using nanofluids, the penalty could be greatly reduced.

In comparison with pure base heat transfer liquid, introduction of nanoparticles leads to the increase in pressure drop and hence pumping power (see Fig. 4.9). Therefore, the overall system energy efficiency must be considered, since the enhancement in the heat transfer may be negated by the increase in the required pumping power. Given that replacement of heat transfer fluid leaves the rest of the system unchanged, we can compare the ratio of the heat transfer enhancement to the pumping power penalty, expressed as performance factor $\zeta_{PF}$, see Eq. (4.8). Thus, if performance factor is equal or above unity, the introduction of nanofluids will have a positive effect on the overall energy balance of the system. Performance factors of nanofluids with different $TiO_2$ concentrations are plotted against overall mass flow-rate in Fig. 4.10.

$$\xi_{PF} = \Delta\dot{q}\Big/\Delta P_{Pumping} = \left(\dot{q}_{nf} - \dot{q}_f\right)\Big/\left(P_{Pumping,nf} - P_{Pumping,f}\right) \tag{4.8}$$

where $\dot{q}$ is the heat transferred to the process liquid, calculated by Eq. (4.5) and $P_{\text{Pumping}}$ is pumping power, calculated by:

$$P_{Pimping} = \Delta p \cdot \dot{v} \tag{4.9}$$

where $\dot{v}$ is the average volumetric flow-rate of the HTF.

As shown in Fig. 4.10, $\zeta_{\text{PF}}$ degrades with the increase in $TiO_2$ nanoparticle concentration for a given flow-rate, as well as with increasing of the overall flow-rate for a given concentration of nanoparticles. Performance factors remain above unity for most of the flow-rates and nanofluids concentrations, which means the whole system is more energy efficient with the nanofluids as compared with a pure base liquid. The results show that the heat transfer increase in the compact reactor-heat exchanger due to nanofluids can be obtained with a moderate increase in the pumping power within a certain range of mass flow-rates. However, it should be understood, that the energy demand for the manufacture of nanoparticles should also be included in the overall energy assessment, considering the process within the wider Life Cycle system boundary. A lower than unity value of the performance parameter, obtained at high nanofluid flow-rate and with high concentration of nanoparticles shows the regime under which the use of nanofluids is less economical.

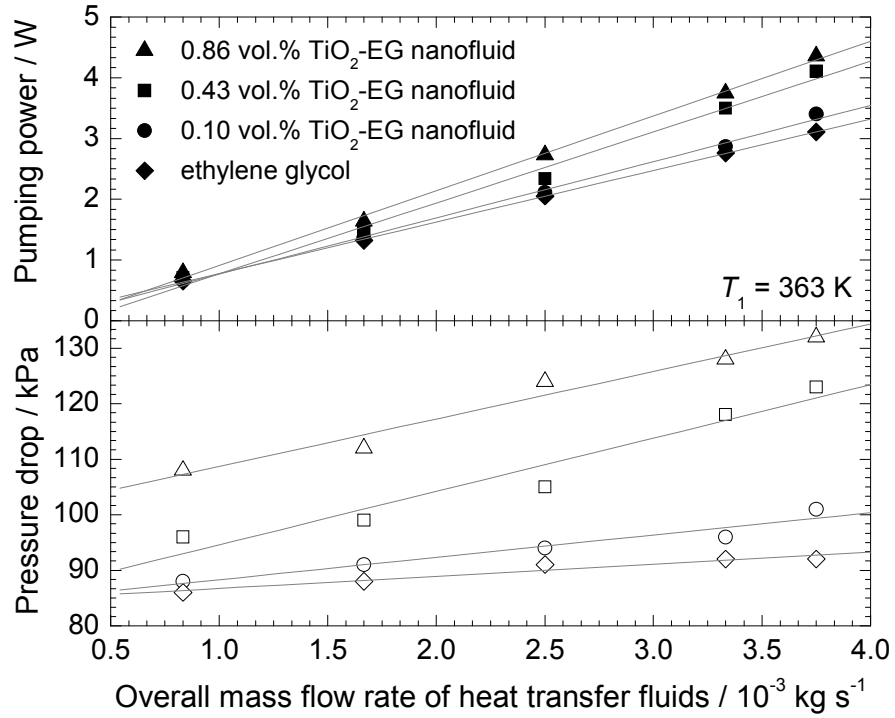**Fig. 4.9** Dependence of pressure drop across micro-heat exchange module and of pumping power on the overall mass flow-rate and nanoparticle concentration of the heat transfer fluids. The pressure drop was measured across the whole device and includes the effects of inlet and outlet headers.
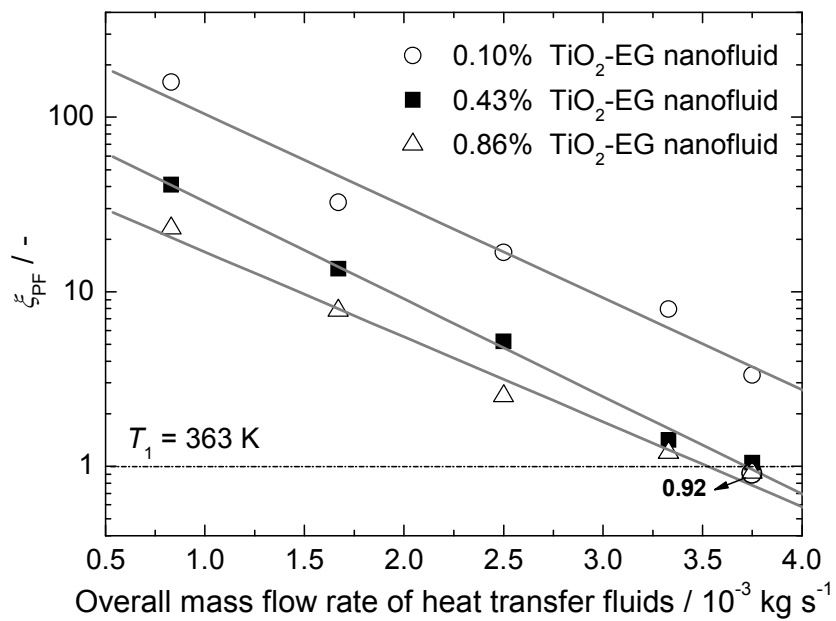


**Fig. 4.10** Performance factor ($\zeta_{PF}$) of TiO$_2$-EG nanofluids as a function of overall mass flow-rate of HTF.

### 4.3.3    *Dynamic experiments*

In the dynamic experiments the two re-circulating baths, containing either EG or TiO$_2$-EG nanofluids and set at two different temperatures, were rapidly switched between them to direct a heat transfer fluid with a different temperature into the reactor system, as shown in Fig. 4.3. The dynamics of quenching of the process fluid, water, is shown in Fig. 4.11. In dynamic experiments, the lower temperature set by RCB2 for different HTFs was always 303 K. The off-set from the lower set temperature is due to the thermal mass of the reactor. Cooling of the reactor itself is under a different and much slower dynamics, which does not affect the dynamics of the process fluid quenching.

Eq. (4.10) describes the reactor wall temperature change over time in the dynamic quenching experiments:

$$T_w = T_\infty + \left(T_0 - T_\infty\right)e^{-t/\tau}$$
(4.10)

where $T_w$, $T_0$ and $T_\infty$ are instantaneous reactor wall temperature, initial reactor wall temperature and reactor wall temperature at the final steady state; $\tau$ is the process time constant. The fit of the Eq. (4.10) for pure EG and the 0.43 vol.% TiO$_2$-EG nanofluid to the experimental data and the calculated time constants are shown in Fig. 4.11.
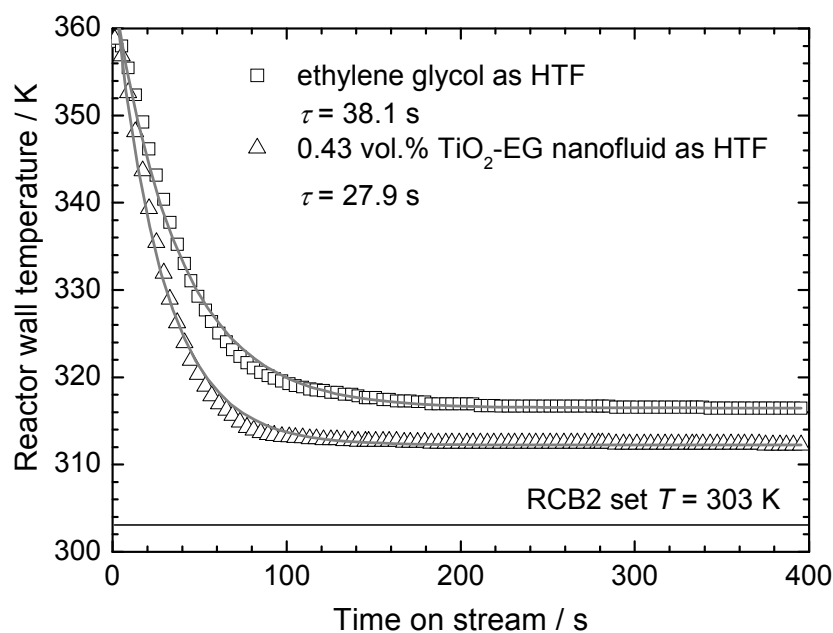
**Fig. 4.11** Comparison of the temperature profiles of the quenching experiment based on EG and 0.43 vol.% TiO$_2$-EG nanofluid.  Symbols – experimental data points, solid lines – model fit curves.

Time constants calculated from this model are 27.9 s for the TiO$_2$-EG nanofluid and 38.1 s for pure EG.  Smaller $\tau$ of the system with nanofluid compared with pure EG means the reactor responds quicker to the temperature change.  The apparent rate of cooling of the working fluid with EG only is 0.7 K s$^{-1}$, whereas with the nanofluid it is increased to 1.1 K s$^{-1}$, which is a 57 % increase.  Such an increase in the rate of temperature change should also have a pronounced effect on the rate of quenching of chemical reactions, since the temperature effect is enhanced by the exponential dependence of reaction rate on temperature.

To investigate the potential dynamic quenching of a chemical reaction in the compact reactor, the reaction of selective reduction of benzaldehyde to benzyl alcohol (refer to Scheme 3.1 in Chapter 3) was studied.  Experiments showed that the benzyl alcohol yield has a reversible dependence on the reaction temperature over the range of 300–360 K (refer to Fig. 3.8 and section 3.3 in Chapter 3).  Therefore, this effect is being exploited to demonstrate the dynamic switch between reaction regimes.

Fig. 4.12 shows results of the experiment in which temperature of the heat transfer fluid was changed step-wise from 353 to 303 K and response of reaction was followed by taking samples at the interval of 120 s. Based on the data one can estimate the rate of transition from one steady state to the second, assuming the rate processes to be first order. Thus, in the case of ethylene glycol only the rate is *ca.* 1.1 $10^{-4}$ mol $L^{-1}$ $s^{-1}$, whereas in the case of the nanofluid this rate increased to *ca.* 3.9 $10^{-4}$ mol $L^{-1}$ $s^{-1}$. It is worth emphasizing that the rate of change between the two steady states is significantly under-estimated, since due to the slow sampling technique it was unable to collect the concentration data sufficiently fast to obtain the data-points in the transient regime. The likely actual rate of this transition is expected to be even higher.



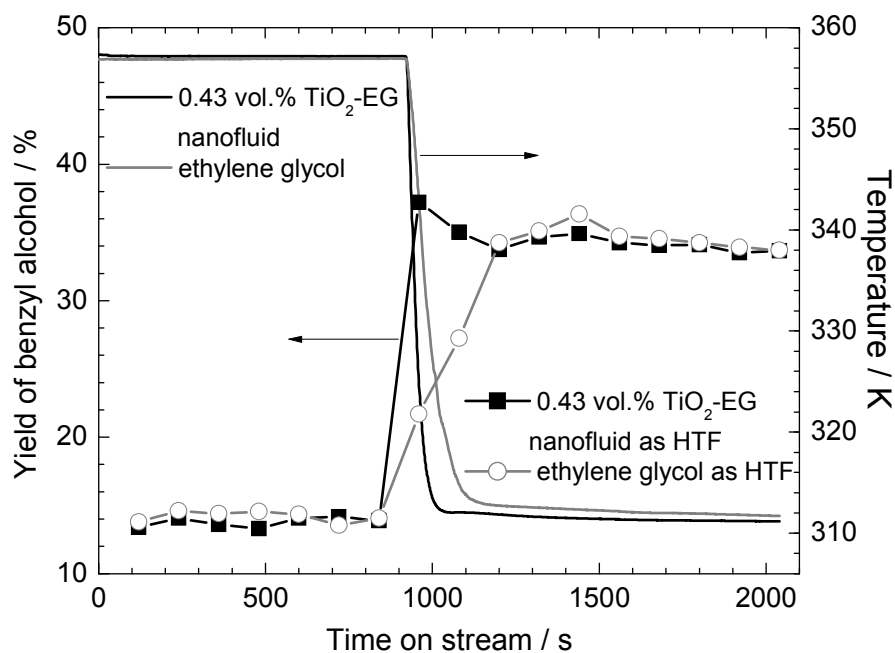**Fig. 4.12** Benzyl alcohol concentration in the outlet of the reactor as a function of the reaction temperature. $P = 8$ barg, $F_{Gas} = 2.66 \times 10^{-3}$ kg m$^{-2}$ s$^{-1}$.

The significant increase in the rate of response of chemical reaction to the change in temperature of the working fluid may open interesting new opportunities for rapid

quenching of chemical reactions in compact multifunctional systems. This should be especially important for the development of sequential transformations in a single unit operation, or for inducing rapid phase changes in the process stream.

## 4. 4  Conclusions

Further intensification of heat transfer in compact reactor/heat exchanger with nanofluids was confirmed and enhancement in the overall heat transfer coefficient of up to *ca.* 35 %, compared with the corresponding base fluid, was observed studying the specific case of $TiO_2$ nanoparticles in ethylene glycol. Nanoparticle agglomeration was believed to be responsible for the slow decrease in performance of $TiO_2$-EG nanofluids.

The penalty for introduction of nanoparticles due to the increased pressure drop was shown to be small, and considerable increase in the overall energy efficiency can be attained. This is in strong contrast with conventional heat exchangers. Results showed that the compact reactor/heat exchanger system became more efficient with nanofluids for most of the condition used in present study.

The results of dynamic experiments demonstrated that the compact reactor/heat exchanger has a significantly faster dynamic response when nanofluids are used. The quick dynamic response of the reactor can be employed for rapid switching of reaction conditions, *e.g.*, rapid quenching of reactions, which was shown in the example of temperature dependent reaction selectivity.

There is a significant potential of nanofluids for new applications in flow chemistry and catalytic reaction engineering, and the minimum feasible outcome is the significant reduction in the overall process energy requirement.

## Acknowledgements

## Reference

1.   Cross, W. T.; Ramshaw, C., Process intensification − Laminar-flow heat-transfer. *Chem. Eng. Res. Des.* 1986, 64, 293–301.

2.   Jenck, J. F.; Agterberg, F.; Droescher, M. J., Products and processes for a sustainable chemical industry: A review of achievements and prospects. *Green Chem.* 2004, 6, (11), 544–556.

3.   Stankiewicz, A. I.; Moulijn, J. A., Process Intensification: Transforming chemical engineering. *Chem. Eng. Prog.* 2000, 96, 22–34.

4.   Becht, S.; Franke, R.; Geisselmann, A.; Hahn, H., Micro process technology as a means of process intensification. *Chem. Eng. Technol.* 2007, 30, (3), 295–299.

5.   Tonkovich, A.; Kuhlmann, D.; Rogers, A.; McDaniel, J.; Fitzgerald, S.; Arora, R.; Yuschak, T., Microchannel technology scale-up to commercial capacity. *Chem. Eng. Res. Des.* 2005, 83, (A6), 634–639.

6.   Bavykin, D. V.; Lapkin, A. A.; Kolaczkowski, S. T.; Plucinski, P. K., Selective oxidation of alcohols in a continuous multifunctional reactor: Ruthenium oxide catalysed oxidation of benzyl alcohol. *Appl. Catal. A: Gen.* 2005, 288, (1–2), 175–184.

7.   Ehrfeld, W.; Hessel, V.; Löwe, H., *Microreactors*. WILEY−VCH: Weinheim, 2000; p 288.

8.   Phillips, C. H.; Lauschke, G.; Peerhossaini, H., Intensification of batch chemical processes by using integrated chemical reactor-heat exchangers. *Appl. Thermal Eng.* 1997, 17, (8–10), 809–824.

9.   Aoune, A.; Ramshaw, C., Process intensification: Heat and mass transfer characteristics of liquid films on rotating discs. *Int. J. Heat Mass Transfer* 1999, 42, (14), 2543–2556.

10.  Jessop, P. G., Homogeneous catalysis using supercritical fluids: Recent trends and systems studied. *J. Supercrit. Fluids* 2006, 38, (2), 211–231.

11.  Wasserscheid, P.; Welton, T., *Ionic liquids in Synthesis*. 2nd ed.; Wiley–VCH: Weinheim, 2007.

12.  Freemantle, M., BASF'S smart ionic liquid. *Chem. Eng. News* 2003, p 9.

13.  Tuckerman, D. B.; Pease, R. F. W., High-performance heat sinking for VLSI. *IEEE Electron Device Lett.* 1981, EDL-2, (5), 126–129.

14.  Kays, W. M.; London, A. L., *Compact Heat Exchangers*. McGraw–Hill: USA, 1984.

15.  Eastman, J. A.; Choi, S. U. S.; Li, S.; Yu, W.; Thompson, L. J., Anomalously increased effective thermal conductivities of ethylene glycol-based nanofluids containing copper nanoparticles. *Appl. Phys. Lett.* 2001, 78, (6), 718-720.

16.  Hamilton, R. L.; Crosser, O. K., Thermal Conductivity of Heterogeneous Two Component Systems. *Ind. and Eng. Chem. Fundamentals* 1962, 1, 187-191.

17.  Eastman, J. A.; Choi, S. U. S.; Li, S.; Yu, W.; Thompson, L. J., Anomalously increased effective thermal conductivities of ethylene glycol-based nanofluids containing copper nanoparticles. *Appl. Phys. Lett.* 2001, 78, (6), 718–720.

18.  Lee, S.; Choi, S. U. S.; Li, S.; Eastman, J. A., Measuring thermal conductivity of fluids containing oxide nanoparticles. *J. Heat Transfer – Transactions of The ASME* 1999, 121, (2), 280.

19.  Wen, D. S.; Ding, Y. L., Experimental investigation into convective heat transfer of nanofluids at the entrance region under laninar flow conditions. *Int. J. Heat Mass Transfer* 2004, 47, (24), 5181–5188.

20.  Das, S. K.; Putra, N.; Roetzel, W., Pool boiling characteristics of nano-fluids. *Int. J. Heat and Mass Transfer* 2003, 46, 851-862.

21.  Das, S. K.; Choi, S. U. S.; Patel, H. E., Heat Transfer in Nanofluids-A Review. *Heat Transfer Eng.* 2006, 27, 3-19.

22.  Ding, Y. L.; Chen, H. S.; Wang, L.; Wang, C.; He, Y. R.; Yang, W.; Lee, W.; Zhang, L. L.; Huo, R., Heat transfer intensification using nanofluids. *KONA – Powder and Particle* 2007, 25, 23–38.

23.  Keblinski, P.; Phillpot, S. R.; Choi, S. U. S.; Eastman, J. A., Mechanisms of heat flow in suspensions of nano-sized particles (nanofluids). *Int. J. Heat Mass Transfer* 2002, 45, (4).

24. Prasher, P.; Evans, W.; Meakin, P.; Fish, J.; Phelan, P.; Keblinski, P., Effect of aggregation on thermal conduction in colloidal nanofluids. *Appl. Phys. Lett.* 2006, 89, (14), 143119.

25. In *Nanofluids: Fundamentals and Applications*, Copper Mountain, Colorado, USA, 2007.

26. Eapen, J.; Williams, W. C.; Buongiorno, J.; Hu, L. W.; Yip, S.; Rusconi, R.; Piazza, R., Mean-field versus microconvection effects in nanofluid thermal conduction. *Phys. Rev. Lett.* 2007, 99, (9), article number: 095901.

27. Shenogin, S.; Xue, L. P.; Ozisik, R.; Keblinski, P.; Cahill, D. G., Role of thermal boundary resistance on the heat flow in carbon-nanotube composites. *J. Appl. Phys.* 2004, 95, (12), 8136–8144.

28. Ding, Y. L.; Alias, H.; Wen, D. S.; Williams, R. A., Heat transfer of aqueous suspensions of carbon nanotubes (CNT nanofluids). *Int. J. Heat Mass Transfer* 2006, 49, (1–2), 240–250.

29. Hong, H. P.; Wensel, J.; Liang, F.; E., B. W.; Roy, W., Heat transfer nanofluids based on carbon nanotubes. *J. Thermophysics and Heat Transfer* 2007, 21, (1), 234–236.

30. Wen, D. S.; Ding, Y. L., Effective thermal conductivity of aqueous suspensions of carbon nanotubes (carbon nanotubes nanofluids). *J. Thermophys. Heat Transfer* 2004, 18, (4), 481–485.

31. Chein, R. Y.; Chuang, J., Experimental microchannel heat sink performance studies using nanofluids. *Int. J. Thermal Sci.* 2007, 46, (1), 57–66.

32. Lee, J.; Mudawar, I., Assessment of the effectiveness of nanofluids for single-phase and two-phase heat transfer in micro-channels. *Int. J. Heat and Mass Transfer* 2007, 50, 452-463.

33. Jang, S. P.; Choi, S. U. S., Cooling performance of a microchannel heat sink with nanofluids. *Appl. Thermal Eng.* 2006, 26, (17–18), 2457–2463.

34. Zhu, H. T.; Lin, Y. S.; Yin, Y. S., A novel one-step chemical method for preparation of copper nanofluids. *J. Colloid Interface Sci.* 2004, 277, (1), 100–103.

35. Wen, D. S.; Ding, Y. L., Formulation of nanofluids for natural convective heat transfer applications. *Int. J. Heat Fluid Flow* 2005, 26, (6), 855–864.

36. Plucinski, P. K.; Bavykin, D. V.; Kolaczkowski, S. T.; Lapkin, A. A., Liquid-phase oxidation of organic feedstock in a compact multichannel reactor. *Ind. Eng. Chem. Res.* 2005, 44, (25), 9683–9690.

37. Pak, B. C.; Cho, Y. I., Hydrodynamic and heat transfer study of dispersed fluids with submicron metallic oxide particles. *Exp. Heat Transfer* 1998, 11, (2), 151–170.

38. Janna, W. S., *Engineering Heat Transfer*. PWS Pub.: Boston, 1986.

39.     Chen, H. S.; Ding, Y. L.; He, Y. R.; Tan, C. Q., Rheological behaviour of ethylene glycol based titania nanofluids. *Chem. Phys. Lett.* 2007, 444, 333–337.

40.     Choi, S. U. S., In *2nd Korean – American Scientists and Engineers Association Research Trend Study Project Review and the Korea – U.S. Technical Conference on Strategic Technologies*, Vienna, VA, USA, 1998.

# Chapter 5

# Coupling of Heck and hydrogenation reactions in the compact reactor

A continuous multi-step synthesis of 1,2-diphenylethane was performed sequentially within the structured compact reactor. This process involved a Heck C-C coupling reaction followed by the addition of hydrogen to perform reduction of the intermediate obtained in the first step. Both of the reactions were catalysed by microspherical carbon supported Pd catalysts. Due to the integration of the micro heat exchanger, the static mixer, and the mm-scale packed-bed reaction channel, the compact reactor was proven to be an intensified tool for promoting the reactions. In comparison with the batch reactor, this flow process in the compact reactor was more efficient as: (*i*) the reaction time was significantly reduced (*ca.* 7 min *vs.* several hours), (*ii*) no additional ligands were used, and (*iii*) the reaction was run at lower operational pressure and temperature. Pd leached in the Heck reaction step was shown to be effectively recovered in the following hydrogenation reaction section and the catalytic activity of the system can be mostly retained by reverse flow operation. This chapter is based on the paper: X. Fan, M. G. Manchon, K. Wilson, S. Tennison, A. Kozynchenko, P. K. Plucinski, A. A. Lapkin*, J. Catal.*, 2009, 267, 114–120.

## 5.1    Introduction

Microreactor technology (reaction volume ranging in the scale range from nanolitre to millilitre), has gained enormous interest recently in both academic research and practical applications, especially for the fine chemical and pharmaceutical industry.[1] For practical chemical transformations, this engineering technology offers chemistry a potential solution to circumvent limitations of batch processes, such as (*i*) temperature runaway and poor selectivity in dealing with exothermic reactions, (*ii*) hot spots due to inefficient mixing, in flow systems, which is often called 'flow chemistry'.

The advantages of switching conventional batch operations to small flow systems are readily apparent. A prominent benefit of this technology is high surface-to-volume ratio which enables a narrow temperature profile along the reactor and efficient cooling. This feature offers the opportunity to successfully execute highly exothermic/endothermic chemical transformations which are usually inhibited in larger batch reactors. Gross *et al.*[2] demonstrated the use of a flow reactor in synthesis of NBI-75043 (an anti-insomnia drug) to promote the key halogen-metal exchange step whose highly exothermic nature limited this total synthesis route in a large scale batch. Small reaction volume also endows microreaction technology with the inherent safety, which allows us to perform hazardous reactions and reactions using toxic reagents, for instance, selective oxidation of aromatic alcohols by molecular oxygen at up to 24 atm undiluted oxygen pressure[3] and ring-expansion reaction involved diazo compound as a reactant.[4] Another additional interest in flow reactor technology is that, in comparison with batch operation, multi-step synthesis can be more facile to achieve in flow process by dosing reactants in different reaction stages to promote the whole process without either losing valuable unstable intermediates, product isolation at intermediate stages or at least interrupting the whole process. Based on this concept, Baxendale *et al.*[5] developed a micro-flow process, which involves various packed columns containing immobilised reagents, catalysts, scavengers or catch and release agents, for the multi-step synthesis of the

alkaloid natural product oxomaritidine. Moreover, an important advantage of flow chemistry over batch processing is the significant reduction of footprint of transferring technology to production scale due to the principle of numbering-up, *i.e.* productivity is increased by simply adding more identical reactors instead of expanding the volume of the reactor.[1, 6]

In the former studies, the use of a multichannel mm-scale flow compact reactor as a versatile tool for designing practical heterogeneous catalysis process with reasonable throughput was demonstrated. This compact reactor integrated the static mixer and the microchannel heat exchanger which enabled an excellent mixing and heat management ability for efficiently and safely running different kinds of reactions. Several practical examples have been successfully demonstrated with this compact reactor, such as (*i*) selective oxidation[3] and hydrogenation[7] with pure oxygen and hydrogen at elevated pressures, (*ii*) the staged dosing of gas along the length of the catalytic channel to increase product yield,[3, 7] (*iii*) the kinetic study for fast reactions.[3, 7] Furthermore, by integrating nanofluids with the micro-heat exchanger, rapid dynamic quenching of chemical reactions was also demonstrated.[8]

Following from the previous study, in this chapter the extension in functionality of the compact reactor was investigated, *i.e.* developing an alternative strategy for continuous multi-step synthesis of 1,2-diphenylethane (an important intermediate for synthesizing flame retardants[9]) which is conventionally obtained by a 'one-pot' reaction combining Heck coupling and hydrogenation reactions, Scheme 5.1.
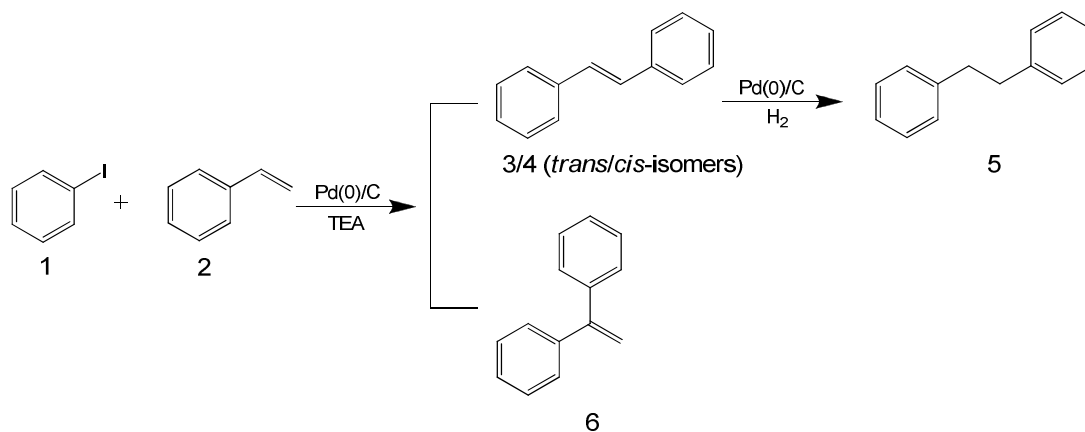


**Scheme 5.1** Consecutive synthesis of 1,2-diphenylethane (5).

## 5.2    Experimental

### *5.2.1    Preparation and characterisation of Pd/C catalyst*

The carbon support (~150 μm particle diameter, synthetic carbon manufactured from phenolic resins, MAST Carbon Ltd. Guildford, UK) was dispersed in distilled water (20 mL $H_2O$ for 1.5 g carbon) at a moderate stirring rate under $N_2$ for 30 min. Aqueous hydrogen tetrachloropalladate (II) ($H_2PtCl_4$, 50 mL, 14.1 mM, corresponding to 5 wt.% of Pd) solution was introduced by portion (10 mL each time) dropwise into the slurry and followed by the addition of aqueous sodium borohydride solution (25 mL, 145 mM, 5 mL each time) under stirring.  This sequential introduction of Pd solution and reducing agent was performed incrementally with a 10 minutes break between each addition.  The slurry was left for two hours under a nitrogen atmosphere and gentle stirring.  Following impregnation, the suspension was filtered and washed with distilled water several times.  The remaining solution was analysed by the atomic absorption spectroscopy (AAS, Perkin Elmer) to determine the quantity of deposited palladium.  The catalyst was dried under vacuum at 353 K overnight and stored in a desiccator prior to being used for the reaction studies.

The gas adsorption analysis was performed using a Micrometrics ASAP 2010 analyser ($N_2$ as probing gas) for obtaining nitrogen adsorption isotherms to evaluate the specific surface area ($S_{BET}$), average pore diameter ($d_{ave}$), and pore volume ($V_p$) of the carbon support and catalyst.  A relative pressure range of 0.05–0.20 was used to calculate the BET surface area.[10]  The median pore diameter was calculated from the adsorption branch of the isotherm[11] using the original Barrett-Joiner-Halenda (BJH) method which, assumes all pores are open-ended cylindrical pores[12] (using the relative pressure range 0.8–0.9; refer to section II in Appendix).

The phase analysis and the determination of the average crystallite size were carried out by X-ray diffraction (XRD) using a Bruker AXS D8 Discover X-ray diffractometre, with Cu$K_\alpha$ radiation $\lambda = 0.145$ nm and a graphite monochromator, in the 2θ range of 30°–55°.  The average size of the metal particle was calculated using

the Scherrer equation. X-ray photoelectron spectroscopy (XPS) was performed by using a Kratos Axis XPS analyser (equipped with a Mg$K\alpha$ X-ray source and charge neutraliser) for determining the elemental composition of the catalysts and chemical state of the metal on the support. Spectra are acquired by using a pass energy of 20 eV with an X-ray power of 169 w.

### 5.2.2    Procedure for batch Heck reactions

8 mL of solvent (anhydrous dimethylformamide, DMF) was first added in a two-necked flask and de-aerated by $N_2$ flow for 10 minutes, then 8 mmol of iodobenzene, 12 mmol of styrene, 10 mmol of triethylamine (TEA) and 0.1 mol% of Pd (as heterogeneous catalyst) were introduced into the reactor. The reactor (equipped with a condenser) was placed in a preheated oil bath at 413 K and vigorously stirred for 4.5 h. Samples were taken at time intervals for off-line GC analysis. All chemicals were purchased from Sigma–Aldrich and used as received.

### 5.2.3    Compact reactor and continuous experiment procedure

Details of the compact reactor and the catalytic system were disclosed in Chapter 3 (Fig. 3.1 and 3.2, section 3.2.2 and 3.2.3) and elsewhere.[3, 13] The reaction channel configuration for consecutive multi-step analysis is shown schematically in Fig. 5.1. Liquid reagents were premixed and placed in the feed vessels. A HPLC pump (422, Kontron Instruments) was used to flow liquid feed through packed-bed reaction channels, and the product was collected in another vessel via a low dead-volume six-way valve (Valco Instruments) equipped with a 250 μL sample loop. The temperature of the reactor was controlled by using a re-circulating bath (Haake DC30 with Haake B3 tank) to circulate heat transfer fluid (glycerol) through the micro-heat exchangers which were located underneath and above all the reaction channels. Thus, all reaction channels have an even temperature field (the measured temperature differences along the reactor were less than 0.5 K). Each channel was equipped with standard Swagelok® fittings for connecting the liquid and the gas feed lines. The system was pressurised by purging gas (either $N_2$ or $H_2$) through the reaction

channels and the operating pressure was set by a back pressure regulator (Brooks 5866). Details of the design concepts and the hydrodynamic characteristics of the compact reactor and details of the rig are specified elsewhere.[3, 13]
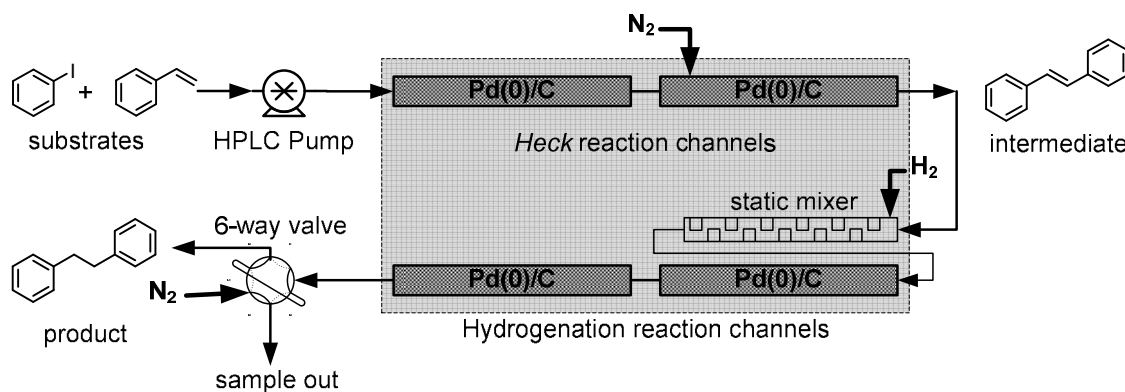


**Fig. 5.1** A schematic diagram of the channel configuration of the compact reactor for consecutive C–C coupling/hydrogenation. The shaded area corresponds to the two micro-heat exchangers located underneath and above all the reaction channels.

### 5.2.4    Sample analysis

The analyses of the samples' composition were performed using a Varian chromatograph (CP-3800) equipped with a FID detector and a 15 m capillary column (CP Sil 5 CB, 0.25 mm × 0.25 μm, Varian).

### 5.2.5    Determination of Pd leaching

Aliquots of the reaction filtrate (in batch experiments the post-reaction mixture was filtered to remove the solids) or the liquid product (in continuous experiments the mesh closing the reaction channel prevented macroscopic removal of the catalyst) were collected in a round bottomed flask (20 mL). The samples were evaporated to remove organic compounds, dissolved in *Aqua Regia* and diluted with distilled water to a certain volume, and then analysed by A Varian (AA-275 series) spectrometre.

## 5.3    Results and Discussion

### 5.3.1    *Catalyst characterisation*

The porous structure characteristics of the carbon and the prepared Pd/C catalyst are reported in Table 5.1. The synthesised catalyst uses a new synthetic carbon support (mesoporous), specifically designed for deposition of metal nanoparticles with a controlled particle size distribution. Pore size distribution of carbon support and Pd/C catalyst is shown in Fig. 5.2. The plots show sharp peaks at the median pore diameter ($d_{ave}$) of 13.3 nm for carbon support and 10.2 nm for Pd/C catalyst. In comparison with carbon support, the area in the size range of the peak was also found smaller for Pd/C, which indicates the decrease of pore volume in that range (refer to $V_p$ in Table 5.1) after Pd deposition. The prepared Pd/C catalyst has a specific surface area of 727 $m^2$ $g^{-1}$, which is lower than that of the carbon support (1070 $m^2$ $g^{-1}$), that is, the support lost 32 % of its area after impregnation of the palladium. It might be that the surface area loss is due to the pore blocking by the palladium nanoparticles. The XRD spectra showed the characteristic bands of the palladium phase for the prepared Pd/C catalyst and the calculated average particle size was *ca.* 4.8 nm (refer to section IV in Appendix), which corresponds well with the TEM analysis (Fig 5.3). Such nanoparticles can easily block micropores of activated carbon support, which are in the range of *ca.* 0.8 nm diameter[14] and therefore reduce the area of the catalyst substantially.

**Table 5.1** The porous structure characterisations of the carbon support and the prepared Pd/C catalyst.

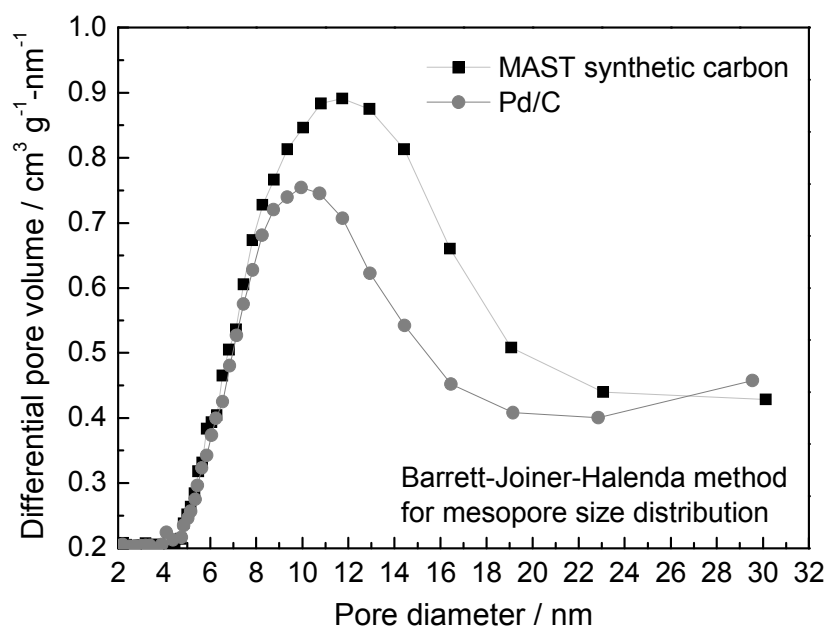|  | $S_{BET}$ / $m^2$ $g^{-1}$ | $d_{ave}$ / nm | $V_p$ / $cm^3$ $g^{-1}$ |
|---|---|---|---|
| Carbon support | 1070 | 13.3 | 0.195 |
| Pd/C (5 wt.%) | 727 | 10.2 | 0.111 |

**Fig. 5.2** Pore size distribution plots for carbon support and Pd/C catalyst ($0.3 < p/p^0 < 0.9$, assuming all the pores are open-ended cylindrical pores, *i.e.* the fraction of open-ended cylindrical pores = 1 in BJH model).
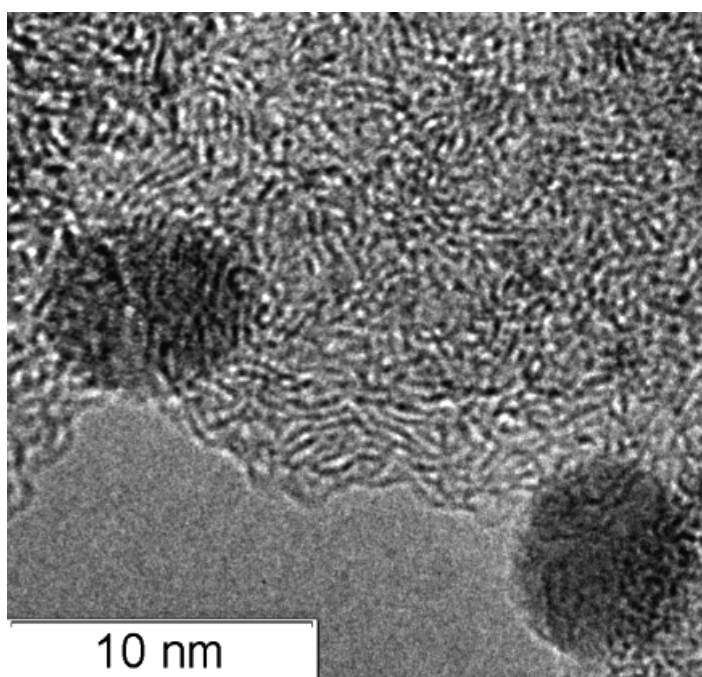


**Fig. 5.3** TEM image of Pd nanoparticles on synthetic carbon support.

### 5.3.2    *Evaluation of the catalytic reactivity for Heck C-C coupling reaction*

In order to test the activity and selectivity of the synthesised 5 wt.% palladium on the carbon catalyst (Pd/C) in the Heck reaction, batch experiments were performed initially.  For comparison purposes, a commercial palladium on an activated carbon catalyst (5 wt.%, obtained from Sigma–Aldrich) was employed as well.  The results of the batch Heck reaction (Table 5.2) show that the two catalysts have a similar performance in terms of selectivity to the main Heck coupling product (3).  However, the reaction catalysed by the commercial catalyst achieved a 97 % of substrate (1) conversion and a 81 % yield of product (3) in 4.5 h, which were higher than that for the synthesised Pd/C catalyst (Table 5.2 and Fig. 5.4).  The faster reaction kinetics of the commercial Pd/C catalyst may be attributed to its smaller size and therefore a smaller contribution of intraparticle diffusion.

**Table 5.2** Results of batch Heck reaction[a] performed using Pd/C (5 wt.%) catalysts.

| Catalysts | Conversion of (1) / % | Yield of (3)[b] / % | Selectivity to (3) / % | Pd leaching / ppm[c] |
|---|---|---|---|---|
| Pd/C, Sigma | 97 | 81 | 85 | 11 |
| Pd/C, this work | 87 | 74 | 85 | 6 |

[a] Temperature ($T$) = 413 K; reaction time ($t_R$) = 4.5 h; in dimethylformamide (DMF); TEA as base.
[b] no *cis*-stilbene (3) was found in the product.
[c] aqueous solution was prepared immediately after the reaction.

According to the mechanism of C–C coupling reactions using aryl iodides as reactants and catalysed by supported Pd catalysts, Pd(0) metal particles on the supports are in fact only precursors for the soluble palladium species that are the real catalysts in this system.[15-20]  The activated carbon support of the commercial catalyst is in the form of a fine powder with the mean particle size of 20 μm which might make it much easier to release Pd species into the reaction mixture as compared with the Pd/C where *ca*. 150 μm particles were used as the support.  This hypothesis was confirmed by measuring the Pd content in the reaction solutions after the reactions.  The Pd concentration was measured by atomic absorption in the cold or hot filtrates once the reaction period was completed.
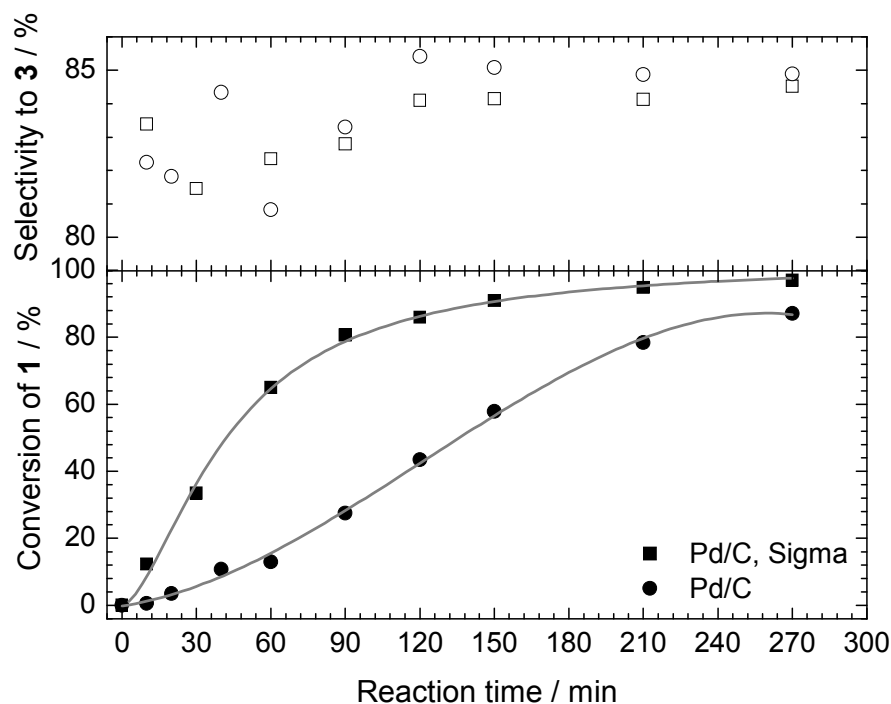
**Fig. 5.4** Batch Heck C–C coupling reaction catalysed by supported palladium catalysts. Reaction conditions: 8 mmol of (1); 12 mmol of (2); 10 mmol of TEA; and 0.1 mol% Pd in 8 mL of DMF; $T = 413$ K, under $N_2$.

11 ppm of palladium was measured in the filtrate of the commercial catalyst, which corresponded to 10 % Pd leaching in respect to the initial loading of Pd onto the activated carbon. This was found to be greater than the corresponding value of the Pd/C catalysts synthesised in this work (6 ppm, corresponding to 6 % Pd leaching). Because of the mechanism of the Pd catalysed Heck reaction,[18-20] which appears to require the presence of leached Pd, it is questionable whether a continuous Heck reaction is a feasible option. However, palladium should re-deposit on the surface of a support after the completion of the reaction due to: (*i*) the absence of aryl halides for oxidative addition, *i.e.* the absence of driving force for Pd to leave the support, and (*ii*) the instability of the soluble Pd complexes. The solubilisation/redeposition process was also found to be controllable by adjusting the reaction conditions.[16, 18-20] Thus, Pd recovery might be achievable under flow conditions by using a bed of "empty" support (which could be subsequently used as an additional catalyst bed) following the bed of a supported Pd catalyst or by using an additional metal scavenger module.[16]

### 5.3.3    *Compact reactor performance in Heck C-C coupling reaction*

The continuous Heck coupling reaction was conducted in a packed-bed compact reactor. In these experiments only the catalyst synthesised in this work was used; the Sigma Pd/C catalyst, due to small size of the particles, generated too high pressure drop across the reactor. Fig. 5.5 shows the reactor performance (as yield and selectivity) for the Heck coupling reaction as a function of the liquid feed rate. A clear dependence of the coupling products yield on the liquid flow-rate was found in this study. For the very first continuous Heck coupling experiment with a fresh catalyst, the yield of 58 % to coupling products (66 % conversion of (1)) was measured at the flow-rate of 0.25 mL min$^{-1}$, whereas, only 18 % yield (20 % conversion of 1) was obtained for the flow-rate of 2 mL min$^{-1}$. The variation of the residence time of liquid substrates in the reaction channels is due to the change of flow-rate (calculated residence time of the liquid substrates in the reaction channels reduces from *ca.* 3 min to *ca.* 0.5 min by increase flow-rate from 0.25 mL min$^{-1}$ to 2 mL min$^{-1}$). The decrease in the residence time is the only explanation for the observed results, since the Heck coupling reactions are usually quite "slow" under batch conditions.
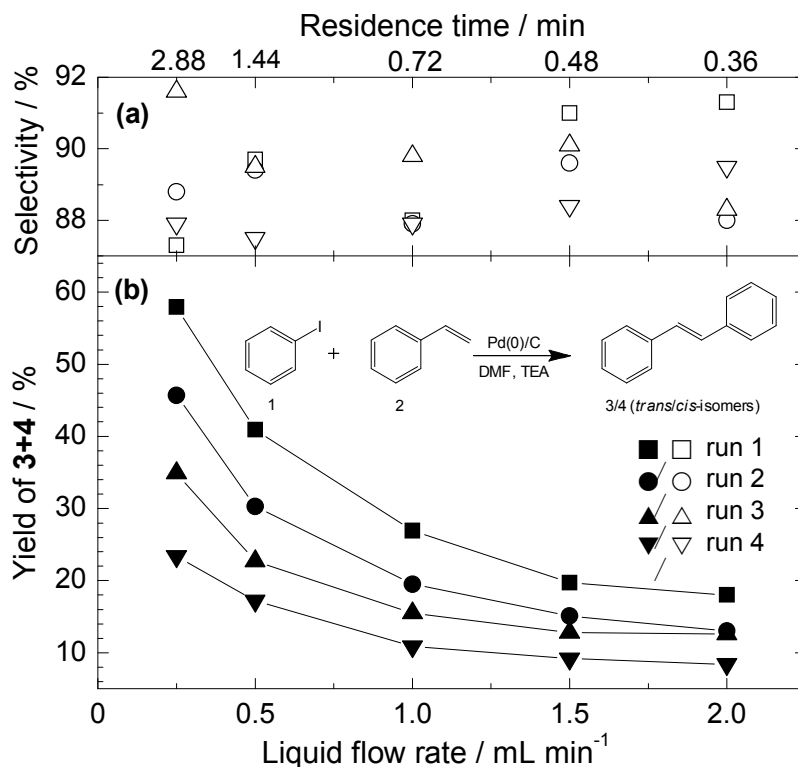
**Fig. 5.5** Continuous Heck coupling reaction in the compact reactor. (a) selectivity to 3+4, (b) yield of 3+4. Reaction conditions: $C_{1,0}$ = 0.5 mol L$^{-1}$; $C_{2,0}$ = 0.75 mol L$^{-1}$; $C_{TEA,0}$ = 0.6 mol L$^{-1}$; DMF as solvent; $T$ = 390 K; 2 channels in series; approx. 0.9 g catalyst.

The selectivity to coupling products ((3) + (4)) in the continuous mode was found to be slightly higher than in the batch one (89 % for the flow reactor *vs.* 85 % for the batch reactor). However, in the case of the flow reactor, *cis*-stilbene (4) was detected in the product stream, whereas only *trans*-stilbene (3) was found under batch conditions. It seems that the conditions of the continuous reactor with different mass and heat transfer characteristics compared to the batch reactor, promoted the synthesis of *cis*-stilbene (4). However, the ratio of *cis* to *trans* product was very low and equal to *ca*. 1 : 40.

The higher conversions in the continuous reactor compared to the batch one (*e.g.* 58 % of conversion for the residence time $t$ = 2.88 min in the continuous reactor (Fig. 5.4) compared to *ca*. 150 min necessary for the same conversion in the batch reactor (see Fig. 5.4) resulted from a much higher catalyst loading in the continuous reactor (500 mg of catalyst per cm$^3$ of the channel volume compared to 2.2 mg of catalyst per cm$^3$ of organic phase in the batch reactor).

Significant catalyst deactivation was found in subsequent experiments, with yields dropping by *ca.* 60 % for 0.25, 0.5, and 1 mL min$^{-1}$ liquid flow-rates, and by *ca.* 53 % for the 1.5, and 2 mL min$^{-1}$ flow-rates. This is related to the reaction mechanism since Pd must be leached from the support and thus is no longer available for consecutive catalytic runs. Pd was detected at different levels in the products collected from continuous experiments.

### 5.3.4 *Compact reactor performance in alkene hydrogenation*

The Pd/C catalysed hydrogenation of intermediates (3) to the final product (5) (see the reaction scheme in Fig. 5.6) in the compact reactor was performed under different conditions, than the C–C coupling reaction, to test the catalytic activity for alkene hydrogenation and to verify the effects of experimental parameters on productivity (different flow-rates, two-phase system, higher pressure). Fig. 5.6 shows the molar flow-rate of 1,2-diphenylethane (5) in the outlet of the reactor (measured at steady state) as a function of H$_2$ flow-rate for the three initial substrate concentrations.

The Pd/C catalyst showed remarkable activity in the packed bed continuous-flow system. Furthermore, the yields of product (5) were found to correlate very well with the theoretical hydrogen supply to the system. This indicates that efficient gas/liquid mixing (mass transfer) was achieved by the integral static mixer within the reactor structure. Compared with the previous literature that used a batch reactor,[15] the continuous flow packed-bed flow reactor enables a more efficient overall hydrogenation process: a lower temperature (398 K *vs.* 413 K), a lower pressure (8 barg *vs.* 20 barg), and a much shorter reaction time (*ca.* 6 min to achieve steady state with *ca.* 100 % conversion *vs.* 20 h reaction time).
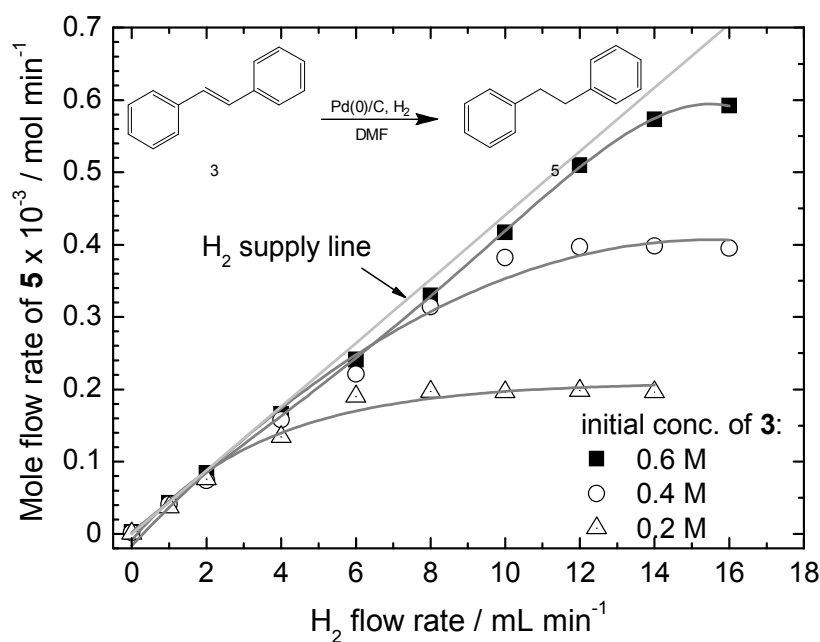
**Fig. 5.6** Continuous alkene hydrogenation in the compact reactor. Reaction conditions: $T = 397$ K; $P = 8$ barg; $F_{Liquid} = 1$ mL min$^{-1}$; two channels in series; approx. 0.9 g catalyst in the two channels.

### 5.3.5    *Consecutive synthesis of 1,2-diphenylethane in a compact reactor*

To evaluate the feasibility of consecutive Heck coupling and hydrogenation reactions under flow conditions, the reaction of 1,2-diphenylethane synthesis in four consecutively connected channels of the compact reactor was studied. The results are shown in Table 5.3. Compared with alkene hydrogenation, the Heck coupling reaction is the slower step of the two. A liquid flow-rate of 0.25 mL min$^{-1}$, therefore, was used in the consecutive synthesis experiments in order to promote Heck coupling reaction.

The catalytic system was not found to be effective for producing the main desirable product (5) by using hydrogen to pressurise the system (Runs 1 to 3). Benzene (dehalogenation product of substrate (1)) and ethylbenzene (hydrogenation product of substrate (2)) were detected in the final product. This result indicates that H$_2$ can back-flush into the Heck reaction channel and the Heck coupling reaction was suppressed due to the absence of substrates caused by their consumption in the side

reactions. This hypothesis was supported by the measured significant increase in the amount of benzene with the increase of system pressure, *i.e.* $H_2$ pressure (Table 5.3, condition b).

In order to eliminate the effect of side reactions, nitrogen was used to pressurise the whole system instead of hydrogen. After pressurising the system, a small stream of nitrogen (1 mL min$^{-1}$) was kept to flow through the reaction channels for providing an inert atmosphere for the Heck reaction. Then, a hydrogen stream was introduced into the hydrogenation channels. (refer to Fig. 5.1) The system became more efficient for synthesizing the target product. The complete conversion of the substrate (1) was achieved and a significant increase in the product yield (*ca.* 80 % selectivity to final product) was measured (Runs 4 and 5). This result suggested that a stepwise conversion of the substrates/intermediate occurred in the continuous process. Compared with the system under condition (b) the target product yield became less dependent on the total pressure for condition (c). The same level of product yield can be achieved using moderate total pressure. High pressure is not essential for achieving high product yield.

**Table 5.3** Optimisation of the flow chemistry[a] in the compact reactor for a desirable multi-step organic synthesis (Scheme 5.1).

| Run | Pressure / barg | Solvent | PhI conversion / % | Selectivity / % | | |
|-----|-----------------|---------|--------------------|-----------------------------------------------------|------------------------------|-----------------------------|
| | | | | *trans*/*cis*-stilbene (3/4) intermediate | 1,2-diphenylethane (5) product | benzene byproduct[e] |
| 1 | 1[b] | DMF | 83 | 38 | 38 | 23 |
| 2 | 4[b] | DMF | 96 | 0 | 18 | 81 |
| 3 | 8[b] | DMF | 100 | 0 | 5 | 95 |
| 4 | 4[c] | DMF | 99 | 1 | 80 | 15 |
| 5 | 8[c] | DMF | 100 | 0 | 82 | 13 |
| 6 | 4[d] | EtOH | 100 | 0 | 83 | 13 |
| 7 | 8[d] | EtOH | 100 | 0 | 83 | 12 |

[a] reaction conditions: $C_{1,0} = 0.4$ mol L$^{-1}$; $T = 393$ K; $F_{Liquid} = 0.25$ mL min$^{-1}$; $F_{Gas,\ hydrogen} = 8$ mL min$^{-1}$; four channels in series, approx. 0.9 g catalyst for the Heck reaction, approx. 0.75 g catalyst for the alkene hydrogenation.
[b] system was pressurised with $H_2$.
[c] system was pressurised with $N_2$.
[d] system was pressurised with $N_2$, ethanol was used as solvent.
[e] analysis of the reaction did not include production of ethylbenzene due to the excess of styrene in the system.

One disadvantage of the present system is the use of DMF as a solvent which is toxic and difficult to evaporate during the following workup. Therefore, finding a suitable substitute to replace DMF is essential to make the whole system more environmentally benign. Ethanol is innocuous and less expensive and was considered in this study. Furthermore, due to the flow reactor being pressurised, solvents with lower boiling points can be held in reaction channels as superheated liquids to promote the reaction. In our experiments (Table 5.3 condition d), ethanol was used as a solvent for the hydrogenation reaction, Scheme 5.1, at 393 K and elevated pressure under continuous flow (Runs 6 and 7). The process with ethanol was as effective and efficient as the one using DMF, *i.e.* the same level of substrate conversion and yield of product (5) were obtained.

### 5.3.6    *Retention of Pd in a flow reactor*

The aforementioned solubilisation/redeposition was well studied and supported by several investigations performed under batch conditions.[16, 18-21] Even in a flow reactor, this mechanism was employed as well for retrieving leached species from the continuous Heck reactions (by inserting a column containing the metal scavenger resin after the reaction column).[22] In the present flow reactor, the subsequent hydrogenation channels can actually serve as scavengers to re-capture the leached Pd species from the Heck reaction channels. Theoretically, the catalytic activity of the system could be maintained for both reactions by reversing the flow direction[23-24] under carefully chosen conditions. The channel arrangement for this concept is shown in Fig. 5.7. This hypothesis was proven by the experimental results in Fig. 5.8 (only one set of results from forward/reverse runs was shown in Fig. 5.8, the same reaction profiles as for reverse run were obtained in consecutive two experiments). The reuse of the catalyst is viable without major deactivation by obverse/reverse running of the two reactions in each other's reaction channels. Most of the leached Pd species were found to re-deposit on the support during hydrogenation under the conditions used in this study, which was proven by XPS analysis. (refer to section IV in Appendix) Compared with the fresh catalyst in Channel 4, Pd species on the carbon surface were found to have increased by 79 % (from 1.4 % to 2.5 %) after one experiment.

Accordingly, a decrease of oxygen on the carbon surface from 26.2 % to 22.3 % was measured which indicates the consumption of oxygen containing surface groups by redeposition of Pd in hydrogenation channel. Zhao[18-20] and Heidenreich[16] confirmed this reversible transfer of Pd species between solvent and support in their studies and asserted that a unique process is tuneable by carefully choosing reaction conditions and base. Therefore, further investigation is needed to optimise the present catalytic system for minimizing the Pd leaching or promoting the rapid re-deposition of Pd species on the support.
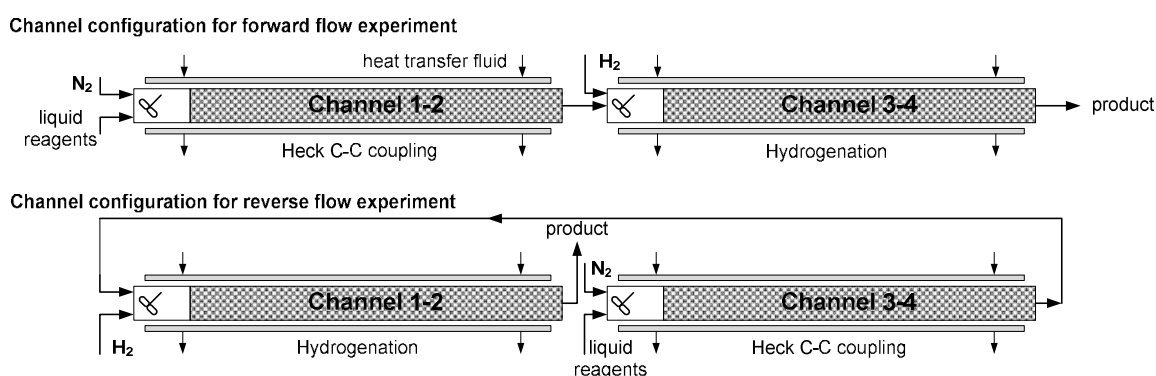
**Fig. 5.7** Channel configurations for normal/reverse flow experiments.

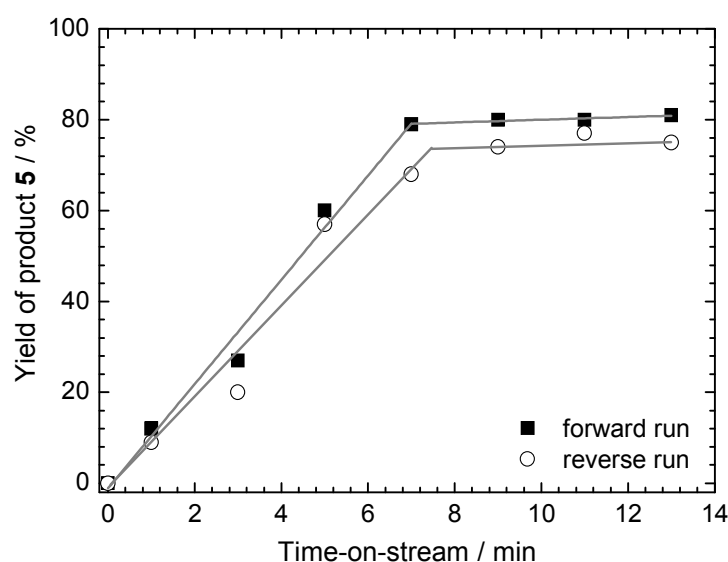**Fig. 5.8** Time yield of 1,2-diphenylethane 5 for the normal flow direction and the reverse flow direction runs. Reaction conditions: $C_{1,0} = 0.4$ mol $L^{-1}$; $T = 393$ K; $P = 4$ barg; $F_{Liquid} = 0.20$ mL $min^{-1}$; $F_{Gas,\,hydrogen} = 8$ mL $min^{-1}$; EtOH as solvent; 4 channels in series; approx. 0.9 g catalyst for Heck reaction; approx. 0.75 g catalyst for the alkene hydrogenation.

## 5.4 Conclusions

The suitability of a compact multichannel reactor for multi-step organic synthesis was investigated using a conventional 'one-pot' reaction, *i.e.* a Heck C–C coupling reaction followed by hydrogenation for synthesizing 1,2-diphenylethane. Compared with conventional batch reactors, the compact reactor promoted a more intensified Heck reaction and alkene hydrogenation. 1,2-diphenylethane was synthesised using the flow compact reactor within minutes of residence time with a lower operating temperature and pressure. In comparison, the conventional batch synthesis took several hours for a similar yield. A stepwise conversion of the substrates to the final product was achieved in the compact multichannel reactor by coupling the Heck reaction and hydrogenation. Compared with the batch reactor, this flow chemistry process in the compact reactor features some advantages such as: (*i*) being more intensified (much shorter residence time) due to the high catalyst/substrates ratio, (*ii*) being operated under benign conditions, *i.e.* lower temperature and pressure, (*iii*) using superheated ethanol at elevated pressure which makes the process greener.

Leached Pd species were believed to be active for igniting and promoting the Heck reaction. Due to (*i*) the reversible transfer mechanism of Pd species between solvent and support, and (*ii*) the unique mass transfer of Pd in different reaction channels, catalytic activity of the system can be mostly maintained by reverse running the two reactions in one another's reaction channels. This continuous catalytic system might be a promising alternative to replacing the conventional batch reactor for multi-step synthesis.

The present investigation demonstrated that a compact reactor is capable of performing the multi-step synthesis in one stream. Considering the specific reaction used in this study, *i.e.* C–C coupling reactions, however, there is still much room left for optimising this flow catalytic system with compact reactor. Therefore, future studies on C–C coupling reactions in this flow reactor system are suggested to focus on (*i*) developing the ligand-free catalytic system which is capable of effectively and efficiently catalyzing C–C coupling reactions involving aryl bromides and aryl chlorides (less active, more practical and economical substrates), (*ii*) minimizing the

Pd leaching by either optimising present flow catalytic system or engineering new supported Pd catalysts for true surface catalysis. The optimisation of styrene concentration is also necessary to reduce the formation of byproducts (ethylbenzene).

## Acknowledgements

## References

1.      Ehrfeld, W.; Hessel, V.; Löwe, H., *Microreactors*. WILEY–VCH: Weinheim, 2000; p 288.

2.      Gross, T. D.; Chou, S.; Bonneville, D.; Gross, R. S.; Wang, P.; Campopiano, O.; Ouellette, M. A.; Zook, S. E.; Reddy, J. P.; Moree, W. J.; Jovic, F.; Chopade, S., Chemical development of NBI-75043. Use of a flow reactor to

circumvent a batch-limited metal-halogen exchange Reaction. *Org. Proc. Res. Dev.* 2008, 12, (5), 929–939.

3.    Bavykin, D. V.; Lapkin, A. A.; Kolaczkowski, S. T.; Plucinski, P. K., Selective oxidation of alcohols in a continuous multifunctional reactor: Ruthenium oxide catalysed oxidation of benzyl alcohol. *Appl. Catal. A: Gen.* 2005, 288, (1–2), 175–184.

4.    Zhang, X.; Stefanick, S.; Villani, F. J., Application of microreactor technology in process development. *Org. Proc. Res. Dev.* 2004, 8, (3), 455–460.

5.    Baxendale, I. R.; Deeley, J.; Griffiths-Johns, C. M.; Ley, S. V.; Saaby, S.; Tranmer, G. K., A flow process for the multi-step synthesis of the alkaloid natural product oxomaritidine: A new paradigm for molecular assembly. *Chem. Commun.* 2006, (24), 2566–2568.

6.    Becht, S.; Franke, R.; Geisselmann, A.; Hahn, H., Micro process technology as a means of process intensification. *Chem. Eng. Technol.* 2007, 30, (3), 295–299.

7.    Fan, X. L.; Lapkin, A. A.; Plucinski, P. K., Continuous selective hydrogention of aromatic aldehydes in a structured compact reactor. *Org. Proc. Res. Dev.* 2009, submitted.

8.    Fan, X. L.; Chen, H. S.; Ding, Y. L.; Plucinski, P. K.; Lapkin, A. A., Potential of 'nanofluids' to further intensify microreactors. *Green Chem.* 2008, 10, (6), 670–677.

9.    Ye, L.; Meng, X.; Liu, X.; Tang, J.; Li, Z., Flame-retardant and mechanical properties of high-density rigid polyurethane foams filled with decabrominated dipheny ethane and expandable graphite. *J. Appl. Polym. Sci.* 2009, 111, (5), 2372–2380.

10.   Brunauer, S.; Emmett, P. H.; Teller, E., Adsorption of gases in multimolecular layers. *J. Am. Chem. Soc.* 1938, 60, (2), 309–319.

11.   Gregg, S. J.; Sing, K. S. W., *Adsorption, surface area and porosity.* Academic Press: London, 1982.

12.   Barrett, E. P.; Joyner, L. G.; Halenda, P. P., The determination of pore volume and area distributions in porous substances. I. Computations from nitrogen isotherms. *J. Am. Chem. Soc.* 1951, 73, (1), 373–380.

13.   Plucinski, P. K.; Bavykin, D. V.; Kolaczkowski, S. T.; Lapkin, A. A., Liquid-phase oxidation of organic feedstock in a compact multichannel reactor. *Ind. Eng. Chem. Res.* 2005, 44, (25), 9683–9690.

14.   Tennison, S. R., Phenolic-resin-derived activated carbons. *Appl. Catal. A: Gen.* 1998, 173, 289–311.

15. Gruber, M.; Chouzier, S.; Koehler, K.; Djakovitch, L., Palladium on activated carbon: a valuable heterogeneous catalyst for one-pot multi-step synthesis. *Appl. Catal. A: Gen.* 2004, 265, 161–169.

16. Heidenreich, R. G.; Köhler, K.; Krauter, J. G. E.; Pietsch, J., Pd/C as a Highly Active Catalyst for Heck, Suzuki and Sonogashira Reactions. *Synlett.* 2002, (7), 1118–1122.

17. Pigamo, A.; Besson, M.; Blanc, B.; Gallezot, P.; Blackburn, A.; Kozynchenko, O.; Tennison, S.; Crezee, E.; Kapteijn, F., Effect of oxygen functional groups on synthetic carbons on liquid phase oxidation of cyclohexanone. *Carbon* 2002, 40, (8), 1267–1278.

18. Zhao, F.; Bhanage, B. M.; Shirai, M.; Arai, M., Heck reactions of iodobenzene and methyl acrylate with conventional supported palladium catalysts in the presence of organic and/or inorganic bases without ligands. *Chem. Eur. J.* 2000, 6, (5), 843–848.

19. Zhao, F.; Murakami, K.; M., S.; Arai, M., Recyclable homogeneous/heterogeneous catalytic systems for Heck reaction through reversible transfer of palladium species between solvent and support. *J. Catal.* 2000, 194, 479–483.

20. Zhao, F.; Shirai, M.; Ikushima, Y.; Arai, M., The leaching and re-deposition of metal species from and onto conventional supported palladium catalysts in the Heck reaction of iodobenzene and methyl acrylate in N-methylpyrrolidone. *J. Mol. Catal. A: Chem.* 2002, 180, 211–219.

21. Zhao, F.; Shirai, M.; Arai, M., Palladium-catalysed homogeneous and heterogeneous Heck reactions in NMP and water-mixed solvents using organic, inorganic and mixed bases. *J. Mol. Catal. A: Chem.* 2000, 154, (1–2), 39–44.

22. Nikbin, N.; Ladlow, M.; Ley, S. V., Continuous flow ligand-free Heck reactions using monolithic Pd [0] nanoparticles. *Org. Proc. Res. Dev.* 2007, 11, (3), 458–462.

23. Bailey, J. E., Periodic operation of checmial reactos: A review. *Chem. Eng. Commun.* 1973, 1, 111–124.

24. Matros, Y. S., *Catalytic Processes under Unsteady State Conditions*. Elsevier Science Pulishers: Amsterdam, The Netherlands, 1989.

# Chapter 6

# Preliminary study on developing Pd catalysts based on mesoporous synthetic carbon for flow catalysis in a structured compact reactor

A synthetic carbon derived from phenolic resin was used as a support for Pd hydrogenation and hydrodehalogenation catalysts which were employed in the compact structured flow reactor. Bimodal meso- and micro porous structure of the synthetic carbon was characterised and confirmed by $N_2$ adsorption analysis. HR-TEM, XRD and XPS analyses were performed for characterising the synthesised catalysts. Continuous liquid-phase hydrogenation and hydrodehalogenation of various substrates in liquid phase with molecular hydrogen was performed in a multifunctional compact reactor at mild conditions and residence time of *ca.* 40 s. For all model reactions investigated, the catalysts show high activity and selectivity as well as a high stability and reproducibility.

## 6. 1    Introduction

Driven by the demand of industry for cleaner and intensified chemical processes, structured reactors such as micro-, compact[1-4] and monolith reactors[5] emerged with a potential to replace the conventional catalytic chemical technologies, *e.g.* the stirred tanks and trickle bed reactors.  In comparison with the conventional reactors, one of the most important advantages of the structured reactors is the integration of various functionalities in one unit: heat transfer, mixing and even specific responsive functionalities, for example a 'chemical valve membrane' for controllable delivery of reactants.[6] This often produces improved safety, higher throughput and lower operating cost of the new technologies.  Integrating heat exchangers into the structured reactors is a common measure to improve thermal efficiency of the chemical processes, to avoid hot spots formation, thermal runaways and to minimise heat losses, which helps to improve the overall process efficiency.[2, 3, 7-9]  One example demonstrated in the early investigations is the continuous oxidation with molecular oxygen in a compact reactor–micro heat exchanger.[2]  Structured chemical reactor-heat exchangers also promote the development of new, otherwise impossible, chemical processes.  For instance, coupling the endothermic steam reforming reaction with an exothermic catalytic combustion in a mm-scale structured monolith reactor.[8, 9]

Most of the studied structured reactors use reaction channels with hydraulic diameters in the range of 0.05 to 5 mm,[1, 2, 7-9] which promote the intensification of heat and mass transfer and safe plant operation.  It should be stressed that the intensified heat and mass transfer are important for the practical heterogeneous catalysis.  The absence of transport limitations is critical for obtaining reliable quantitative kinetics[10] and is essential for increasing yield and selectivity.  In conventional reactors, however, especially in large-scale batch reactors, reaction conditions free from heat and mass transfer limitations are hard to achieve.

Small intensive reactors, from the industrial point of view, are also advantageous due to the elimination of the traditional scale-up procedure. In conventional process chemistry a bench-top synthesis must be re-designed for industrial throughput, whereas a method known as 'numbering-up' of microreactors involves addition of identical units to achieve the desired throughput.[1, 11]

Microreactors, however, are not without their own drawbacks. One of the concerns is the issue of channel-clogging which might be induced by *e.g.* precipitate formation or in processing of solids.[11] For heterogeneous catalytic microreaction systems another problem is the immobilisation of catalysts in the reaction channels. The most popular method is coating catalysts onto reactor walls.[12-14] This method, however, produces a single-use catalytic reactors, due to difficult replacement of catalytic coating in the case of catalyst deactivation. Moreover, catalytic wall-coating would have to be optimised for each particular catalyst/reaction, offering little operational flexibility.

An alternative approach is to use catalytic packed-bed in micro-reaction channels,[15] which features an easier catalyst handling (unloading and repacking) and less chance of channel clogging. Catalysts used in the mm-scale packed beds can be developed by well-understood conventional methods. There are different requirements for heterogeneous catalysts for microreactors though, due to a markedly different hydrodynamics on the macro and micro scale, the need to operate in the kinetic reaction regime, and the need for a simple catalyst loading procedure.

The channel size, the particle sizes in micro-packed beds would necessarily approach tens or hundreds of micrometres, thus resulting in a significant pressure drop across the reactor, especially in liquid- and multiphase processes of interest in this study. Therefore, there is a requirement towards catalyst particle shape that would minimise pressure drop. It was shown earlier, that microspherical catalytic particles produce lower pressure drop in a three-phase reaction and result in a faster establishment of a steady-state regime following initial catalyst bed re-packing.[16]

Due to intensified mass and heat transfer the reaction rates in microreactors are expected to be higher than in conventional batch reactors. Therefore, catalyst structure that would lead to the kinetic reaction regime, without internal mass transfer limitations is even more critical. This requires optimisation of a catalyst internal structure in terms of site activity, stability, number and accessibility.

In the early investigations, the use of a mm-scale packed-bed reactor for several practical applications has been demonstrated, *i.e.* oxidation,[2, 4, 16] hydrogenation,[17] and multi-step synthesis.[18] Synthetic mesoporous carbons were used as supports and were found to be suitable for catalysts specifically for compact, mm-scale, packed-bed reactors. Mesoporous materials for catalysis, such as mesoporous zeolites, silicas, and carbons received much attention in recent years, especially in liquid-phase systems, due to the reduced mass transfer limitation in comparison with microporous solid hosts.[19] Apart from the enhanced diffusion of reactants and products to and from the catalytic sites, mesoporous hosts also allow the reaction with larger molecules[19-21] and promote preparation of heterogeneous catalysts with controlled particle sizes.

In this work, Pd catalysts were developed by conventional methods based on the mesoporous synthetic carbons. Preliminary characterisation of the synthetic carbon pore structure and Pd supported catalysts was studied. Performance of the flow catalytic system in terms of conversion, selectivity, and space-time yield for continuous hydrogenation and hydrodehalogenation of different substrates was evaluated.

## 6. 2   Experimental

### *6.2.1   Synthetic carbon and reagents*

The carbon support used in this study was mesoporous phenolic resin derived synthetic carbon[22, 23] and was kindly provided by MAST Carbon (UK). The synthetic carbons possess a tailored pore structure (a bimodal micro and meso-pore

structure) and were produced in the form of beads. A SEM image of microspherical carbon supports is shown in Fig. 6.1. Besides microspherical carbon particles (with different particle diameters), debris and aggregates of very small particles are found altogether. Therefore, preliminary treatment of synthetic carbon, *i.e.* sonication in methanol to break up aggregates and sieving, was performed for producing a carbon support with a uniform diameter. In this study, particle fraction with diameters 110– 150 microns was used. The synthetic carbon possesses very high attrition and physical strength and is suitable for application as a catalyst support. [22]
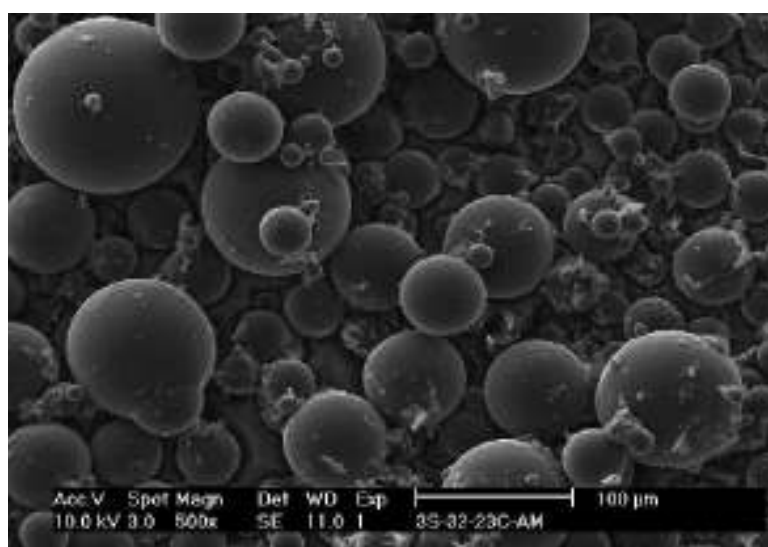


**Fig. 6.1** SEM image of synthetic carbons with bead structures. Adapted from ref. 23.

All chemicals used in this study were obtained from Sigma-Aldrich and Fisher, and used without further purification (reagents are of *ReagentPlus®* grade and solvents are of HPLC grade).

### 6.2.2    *Preparation of Pd/C catalysts*

### 6.2.2.1   **Deposition–reduction**

The synthetic carbon was dispersed in distilled water (20 mL $H_2O$ for 1.5 g carbon) at a moderate stirring rate under $N_2$ for 30 min. Aqueous hydrogen tetrachloropalladate (II) ($H_2PdCl_4$, 50 mL, 14.1 mM, corresponding to 5 wt.% of Pd)

solution was introduced into the slurry dropwise in 10 mL portions at a time and followed by the addition of aqueous sodium borohydride solution (25 mL, 145 mM, 5 mL each time) under stirring. This sequential introduction of Pd solution and reducing agent was performed incrementally with a 10 minutes break between each addition. The slurry was left for two hours under nitrogen atmosphere and gentle stirring. Following impregnation, the suspension was filtered and washed with distilled water several times. The remaining solution was analysed by the atomic absorption spectroscopy (AAS, Perkin Elmer) to determine the quantity of deposited palladium. The catalyst was dried under vacuum at 353 K overnight and stored in a desiccator prior to being used for reaction studies.

### 6.2.2.2   Anaerobic incipient wetness

An anaerobic incipient wetness method was used to prepare approximately 3 %wt Pd/C catalysts utilizing standard Schlenk techniques.[24] Palladium actylactonate, $Pd(C_5H_7O_2)_2$, dissolved in dried, degassed tetrahydrofuran (THF, 1.5 mL, corresponds to the pore volume possessed by 1 g synthetic carbon) was used as the precursor to produce Cl-free catalysts. The precursor solution was added into carbon support $N_2$ and the incipient wetting impregnation was carried out at room temperature for 24 hrs. The catalysts were evacuated overnight at 300 K, then at 323 K for 2 h to remove any THF, and transferred to a desiccator. Catalyst was packed in reaction channel and reduced *in-situ* with hydrogen flow at 333 K.

### *6.2.3   Materials characterisation*

High-resolution transmission electron microscopy (HRTEM) images were obtained using a JEOL JEM-2010 system (200 kV accelerating voltage, with the resolution limit of 0.14 nm). Low temperature nitrogen adsorption experiments were performed using a Micromeritics ASAP-2010 volumetric system with $N_2$ as probing gas. XPS measurements were performed on a Kratos Axis HSi instrument equipped with Mg $K_\alpha$ X-ray source and charge neutraliser. High resolution spectra were recorded at

normal emission using an analyser pass energy of 40 eV and an X-ray power of 225 W.  Energy referencing was employed using the valence band and adventitious carbon at 285 eV.  Spectra were Shirley background-subtracted across the energy region and fitted using CasaXPS Version 2.3.15.  XRD analysis was performed by using a Philips 4 kW X-ray generator (PW1730) with a Cu $K_\alpha$ X-ray source ($\lambda$ = 0.154 nm) and the diffractometre goniometre (PW1820) controlled via Philips (PW1877 PC-APD) software).

### 6.2.4    Structured compact reactor

Details of the structured multichannel reactor and of the auxiliary continuous catalytic system used are given in Chapter 3 and elsewhere.[2, 16, 17, 25] Gas chromatography (GC, Varian CP-3900, CP Sil 5 CB column, flame ionisation detector) was used to analyse reaction products.

## 6. 3    Results and discussion

### 6.3.1    Characterisation of synthetic carbon and Pd/C catalysts

The isotherms of low temperature $N_2$ adsorption/desorption on synthetic carbons (Fig. 6.2) showed a two-step increase in the amount of nitrogen adsorbed over the whole relative pressure range, which indicates the presence of micro and meso-porous structure.  The sharp linear increase in the sorbed amount of nitrogen and the round knee in the isotherm at low relative pressures ($p/p^0$ < 0.05) represent the presence of micropores.  The well-developed mesoporous structure of the synthetic carbons was evidenced by the consecutive increase in the amount of adsorbed $N_2$ at medium and high relative pressures (0.05 < $p/p^0$ < 0.42), and the hysteresis loop in the pressure range of 0.42–0.90.  Mesopores represent the larger part of the bimodal pore structure: the mesopore volume ($V_{meso}$, BJH adsorption cumulative pore volume of pores) is considerably higher than the micropore volume ($V_{micro}$, by $t$-plot method using slit-shaped pore model). Furthermore, contribution of the external surface area ($S_{ext}$, defined as the surface of the pores larger than micropores; determined by $t$-plot

method) towards the total surface area determined by BET model ($S_{BET}$) is larger than that of micropores, see Table 6.1. Calculation of the median mesopore size (relative pressure range 0.8–0.9 from the adsorption branch of isotherms[26] using BJH model) shows that the synthetic carbons have an average pore diameter ($d_{ave}$) of *ca.* 13.3 nm. The microstructure of the carbons, which was derived from the void spaces between small (~4 nm) spherical resin domains generated during the initial polymer curing step,[22] shows a very narrow pore distribution with a mean pore size of *ca.* 0.5 nm (by original Harvoth-Kawazoe method,[27] slit-shaped pore geometry, see inset in Fig. 6.3).

Following the deposition of Pd, the amount of adsorbed nitrogen is decreased as shown in Fig. 6.2. Meso- and micropore size distributions of the synthetic carbon and Pd/C catalysts are illustrated in Fig. 6.3. In comparison with the neat carbon support, the reduction in the mesopore diameters and the external surface area ($S_{ext}$) was found for both Pd/C catalysts after Pd impregnation, but also the micropore volume was reduced (see pore diameter range in Fig. 6.3 for and the calculated average pore diameters in Table 6.1). This suggests that Pd is deposited both in micro and in mesopores. This was further confirmed by the decrease in the micropore and mesopore volumes with the palladium deposition, *i.e. ca.* 22 % for mesopore volumes and *ca.* 40 % for micropores, as well as by HR-TEM imaging (see later text on HR-TEM analysis and Fig.6.4).
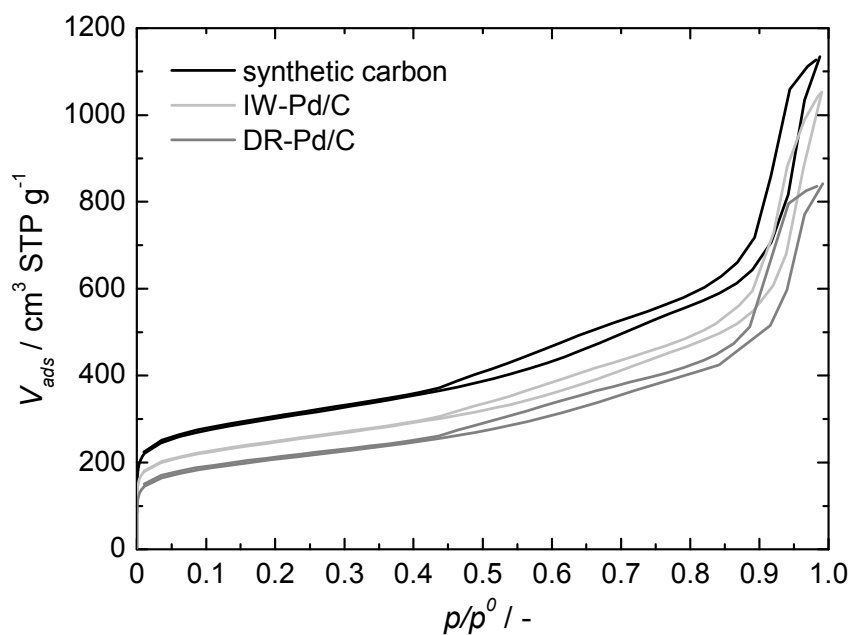
**Fig. 6.2** Nitrogen adsorption/desorption isotherms measured at 77 K for synthetic carbons and prepared catalysts.
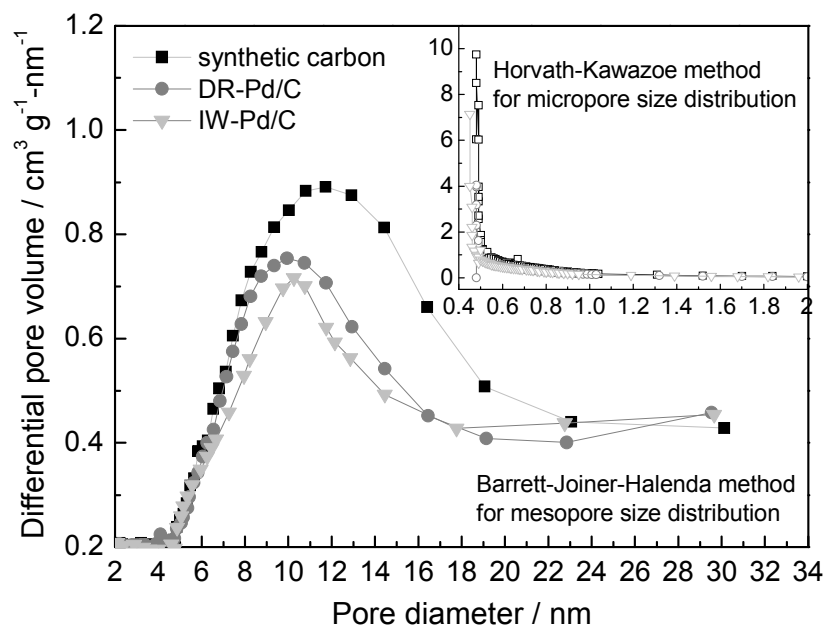


**Fig. 6.3** Pore size distributions derived from nitrogen adsorption data using the BJH model (for mesopores, open-ended cylindrical pore model) and Horvath-Kawazoe method (for micropores, inset).

**Table 6.1** Porous structure characterisation data (by nitrogen adsorption at 77 K) for synthetic carbons and Pd/C catalysts.

| | Pd loading / wt.% | $S_{BET}{}^a$ /m$^2$ g$^{-1}$ | $S_{ext}{}^b$ / m$^2$ g$^{-1}$ | $V_{meso}{}^c$ / cm$^3$ g$^{-1}$ | $V_{micro}{}^b$ / cm$^3$ g$^{-1}$ | $d_{ave}{}^c$ / nm |
|---|---|---|---|---|---|---|
| Carbon support | – | 1070 | 619 | 1.43 | 0.195 | 13.3 |
| DR–Pd/C | 5 | 727 | 477 | 1.09 | 0.111 | 10.2 |
| IW–Pd/C | 3 | 870 | 523 | 1.16 | 0.152 | 11.9 |

[a] Total surface area, calculated using a relative pressure range of 0.05–0.20 (to ensure positive BET constants to be obtained by using BET equation).
[b] Calculated using $t$-plot method. $t$-plot estimates of micropore volume and external surface area correspond here to the slit-shaped pore model.
[c] Determined from adsorption branch of isotherms using BJH method. The ($4V/A$) term was used in estimation of average pore diameters, which corresponds to the assumed cylindrical model of pores.

The structure and distribution of Pd nanoparticles on the catalysts were analysed by HR-TEM microscopy. Carbon microspheres were mechanically ground, dispersed in ethanol and sonicated; a sample droplet was placed onto the TEM sample grid. In DR-Pd/C catalyst Pd species of three different sizes are found. The smallest particles detected are around 1 nm. Crystal lattice of these clusters cannot be obtained, since it does not necessarily corresponds to FCC packing of atoms at this size of particles. Tightly packed clusters of 1 nm particles are detected: there are about 10 clusters in a 10 × 10 nm image area, see Fig. 6.4a. The larger particles are about 5 nm diameter. There are many evenly distributed particles of this size, Fig 6.4b. Then, there are microblock particles looking like hedgehogs with the mean size about 50 nm, see Fig 6.4c.

Small clusters and particles of 5 nm are spread across the sample very evenly. It is suspected that the larger particle aggregates, the 'hedgehogs', are formed on the particle surface. On the surface of carbon particles also found are few very large crystals of about 1 μm size. The formation of the larger particles is most likely due to the high concentration of the precursor metal salt solution.

For the Pd/C catalyst prepared by anaerobic incipient wetness method, HR-TEM analysis showed that the predominant particle size is *ca.* 5 nm and there are only few particles that are aggregated, see Fig. 6.4c. Pd particles are distributed evenly within

the sample, however, the particles concentration is much lower than in the case of DP/Pd catalyst.
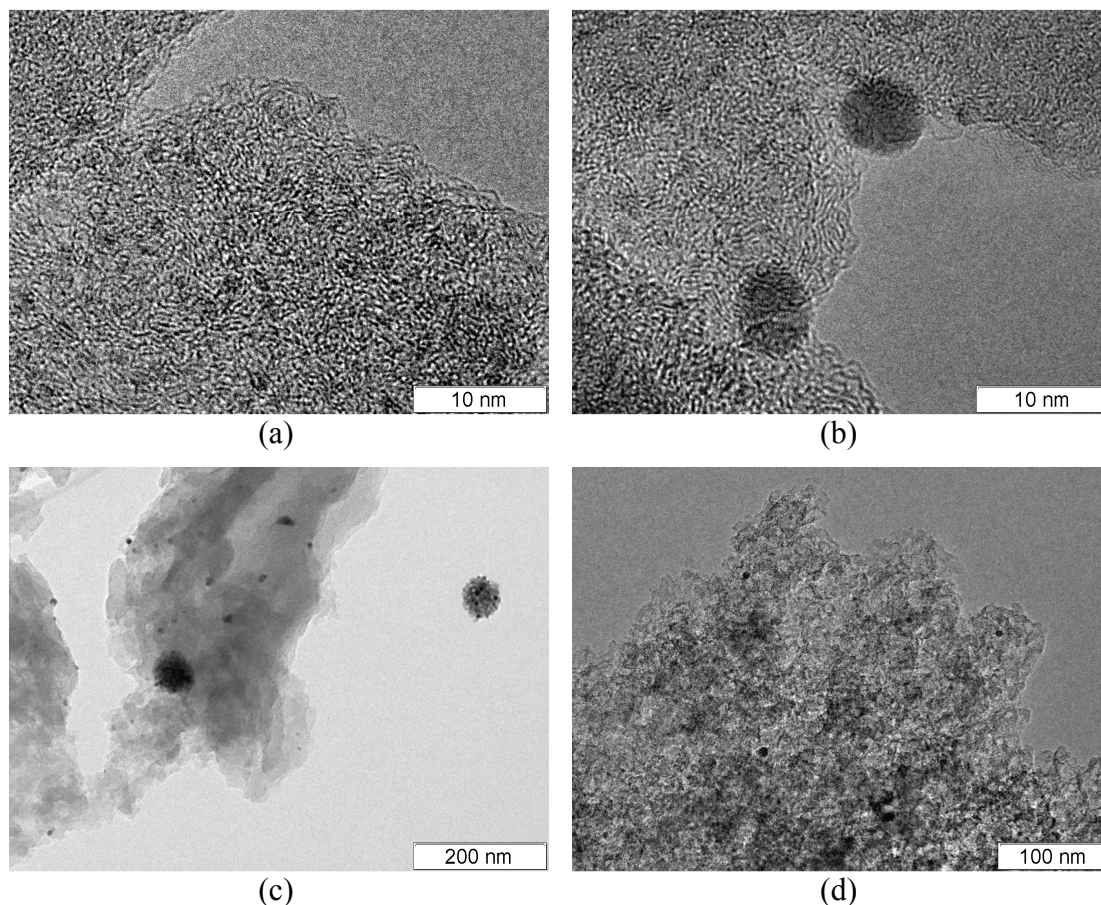


**Fig. 6.4** HR-TEM microscopic images of Pd nanoparticles on synthetic carbon support. (a-c) DR-Pd/C catalyst, (d) IW-Pd/C catalyst.

XRD analysis was performed to estimate the average Pd particle size on each catalyst. All the samples were scanned over the $2\theta$ range of 30°–55° at a rate of 0.01° step$^{-1}$ with a scan time of 1.25 s step$^{-1}$. As one can see in Fig. 6.5, Pd phase on synthetic carbon was revealed with two peaks at $2\theta = 40.1°$ (plane 111) and 46.7° (plane 200). Average Pd particle diameters for each catalyst were analysed using integral breadth analysis and Scherrer formula,[28-29] the results as shown in Table 6.2. For DR–Pd/C, XRD analysis yielded an average Pd particle diameter of 4.8 nm which is in the range of 1–5 nm (for majority of Pd particles) confirmed by HRTEM analysis. For IW–Pd/C, the estimated average particle size by XRD, *i.e.* 5.2 nm, which corresponds well with the result based on HR-TEM analysis.
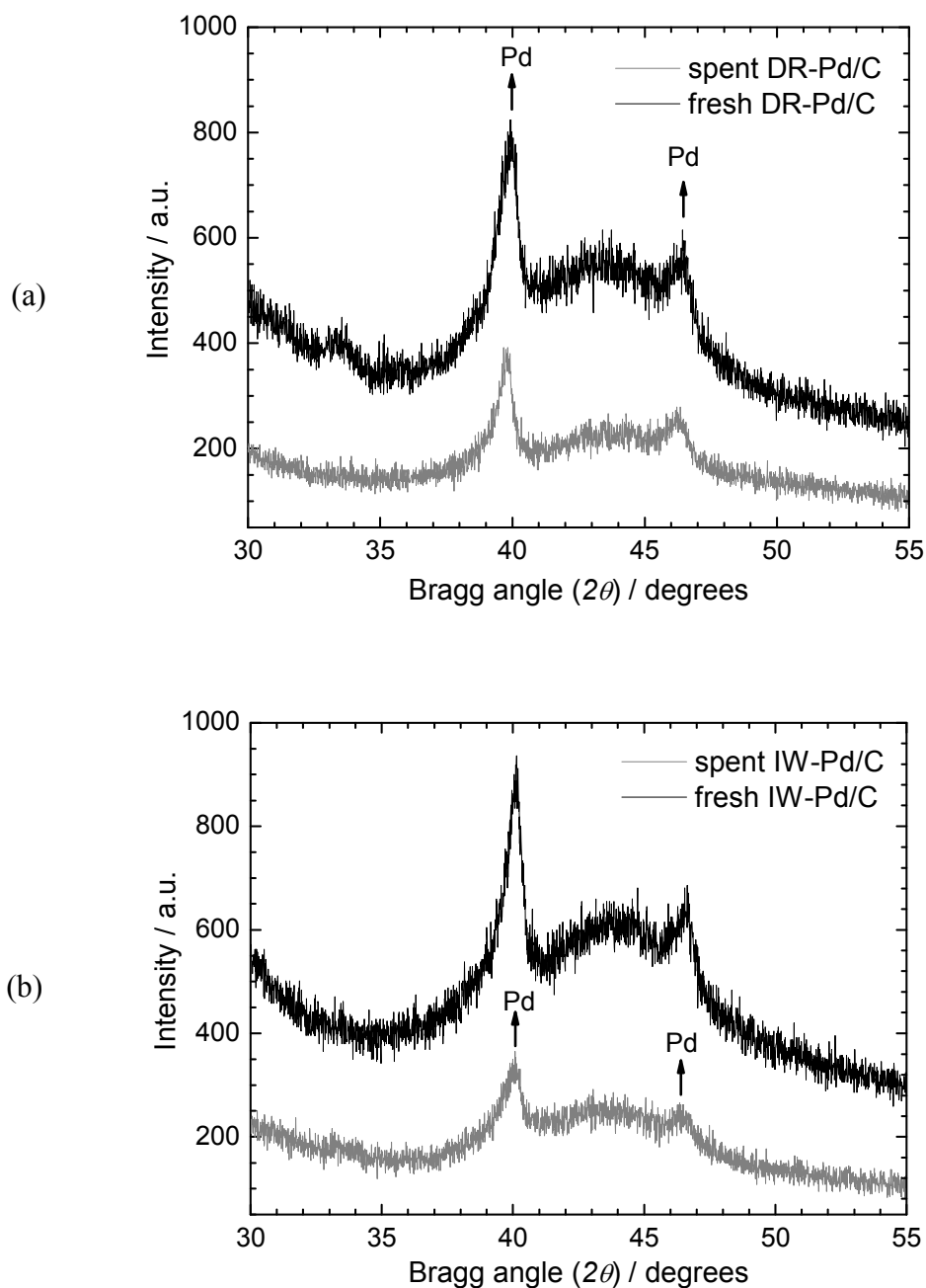
**Fig. 6.5** XRD patterns of Pd/C catalysts: (a) DR–Pd/C and (b) IW–Pd/C.

**Table 6.2** Average Pd particle diameter by XRD analysis (Scherrer equation).

| Catalyst | Average Pd particle diameter ($d$) / nm |
|---|---|
| Fresh DR–Pd/C | 4.8 |
| Spent DR–Pd/C | 5.7 |
| Fresh IW–Pd/C | 5.2 |
| Spent IW–Pd/C | 5.5 |

Results of XPS quantitative analysis of prepared Pd/C catalysts are shown in Table 6.3. As it can be seen, carbon and oxygen are main components on the surface for both the samples. The DR–Pd/C and IW–Pd/C catalyst showed the amount of surface Pd deposition equals 2.53 wt.% and 1.02 wt.%, respectively. The lower surface Pd concentration corresponds well with the HRTEM imaging, showing sparsely distributed particles throughout the sample.

**Table 6.3** Mass surface concentration obtained by XPS quantitative analysis and distribution of the different phosphorus and palladium surface groups.

| | XPS quantitative analysis of surface composition / wt.% | | | Theoretical Pd deposition / wt.% |
|---|---|---|---|---|
| | C 1s | O 1s | Pd 3d | |
| DR–Pd/C | 81.6 | 15.9 | 2.53 | 5 |
| IW–Pd/C | 88.1 | 10.9 | 1.02 | 3 |

### 6.3.2  *Results of continuous-flow catalytic reactions*

Hydrogenation of various substrates in the compact flow reactor was carried out to evaluate catalytic performance of Pd supported onto mesoporous synthetic carbon; results are summarised in Table 6.4 (entries 1–5). As it can be seen the Pd/C based catalysts showed high efficiency in hydrogenating alkenes and alkynes to alkanes. For hydrogenation of non-hindered double bond in styrene and triple bond in phenylacetylene, 100 % conversion with 100 % selectivity to ethylbenzene were achieved by both Pd-supported on synthetic carbon catalysts in a single pass with *ca.* 40 s residence time. Reactions were performed in a slight excess of hydrogen to ensure full conversion, *e.g.* mole flow rate of substrate was $2.5 \times 10^{-4}$ mol min$^{-1}$ whereas mole flow rate of hydrogen (for styrene hydrogenation) was *ca.* $2.9 \times 10^{-4}$ mol min$^{-1}$ under the conditions used (see note 'a' in Table 6.4). Due to consumption of hydrogen in the reactions very little gas was detected in the exit stream upon sampling.

Hydrogenation of carbonyl groups (aldehyde and ketone) was conducted and the results are shown as entries 3 and 4. High selectivities to primary and secondary alcohols (> 98 %) with fairly good conversions were achieved by using this flow

catalytic system. No over-hydrogenated products and hydrogenolysis products were detected (by GC) for the two model reactions under the conditions used. The possible reasons for the observed high selectivity can be attributed to the advantages of the multifunctional compact reactor, as discussed in Section 3.3.4.

Hydrogenation of nitrobenzene to aniline was also carried out in the compact reactor. This model reaction is known as a highly exothermic reaction with a reaction enthalpy of 545 kJ mol$^{-1}$.[12] Good temperature control is essential to produce aniline and avoid generating intermediates which are formed in several parallel and consecutive reactions as suggested by Yeong *et al.*[12] and Höller *et al.*[30] All catalysts showed high selectivity towards the final amine product with excess supply of hydrogen and 40 s residence time. Hydrogenation of side-chain nitro group was found proportional to hydrogen supply and step conversion of nitro group to amine was detected by GC analysis, *i.e.* the presence of intermediates in the product mixture under hydrogen starvation regime. However, no ring hydrogenation products and side reaction products were detected under the reaction conditions used.
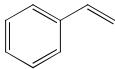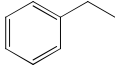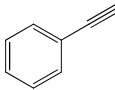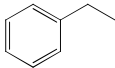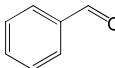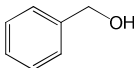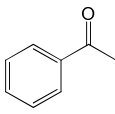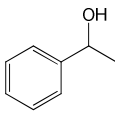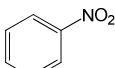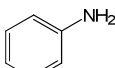
The integrated micro heat exchangers showed high efficiency for removing the heat release by the reaction. The expected adiabatic temperature rise ($\Delta T_{ad}$) for the conditions used (0.5 mol L$^{-1}$ concentration, 100 % conversion, 0.5 mL min$^{-1}$ liquid flow rate, 40 s residence time) was *ca.* 260 K (estimated by Eq. (6.1)), whereas a temperature rise of < 2 K was measured along the reaction channel, and isothermal condition was ensured during the reaction. In comparison with another study of this reaction using a microstructured falling film reactor (0.1 mol L$^{-1}$ initial concentration, 333 K, 1 bar, 0.5 mL min$^{-1}$ liquid flow-rate),[12] a significant increase in aniline yield (max. *ca.* 70 % *vs.* 98 %) was achieved with a similar space-time yield (16.4 mol h$^{-1}$ L$^{-1}$ *vs.* 16.7 mol h$^{-1}$ L$^{-1}$) in the case of the packed-bed compact reactor (0.5 mol L$^{-1}$ initial concentration, 333 K, 9 bar, 0.5 mL min$^{-1}$ liquid flow-rate). In the present study, the production rate of the compact reactor (for nitro benzene hydrogenation) was limited by the mass flow controller, *i.e.* 20 mL(STP) min$^{-1}$ maximum flow-rate (theoretical hydrogen consumption for reducing 0.5 mol L$^{-1}$ nitrobenzene under conditions used is *ca.* 18 mL(STP) min$^{-1}$).

$$\Delta T_{ad} = Q/(m \cdot c_p) \qquad\qquad (6.1)$$

where $Q$ is the total heat liberated from the reaction ($Q$ is calculated from the reaction enthalpy, initial substrate concentration, conversion and flow rate); $m$ is the mass of catalyst bed (0.5 g); $c_p$ is the specific heat capacity of catalyst (0.7 J g$^{-1}$K$^{-1}$).

The synthesised Pd/C catalyst also showed high activity in hydrodehalogenation of aryl halides. Investigation of the liquid phase hydrodehalogenation was carried out using DR–Pd/C and results are shown in Table 6.4, entry 6. High conversion was achieved in dehalogenation of iodobenzene and bromobenzene with high selectivity to benzene, *i.e.* 97 %. For less reactive chlorobenzene, a *ca.* 59 % yield of benzene was obtained at 40 s residence time. Concerning safety and simplicity of operation, this liquid-phase process using molecular hydrogen is more advantageous in comparison with conventional batch operations which either require high temperature and pressure[31, 32] or hours of reaction time.[33]

**Table 6.4** Results of flow hydrogenation and hydrodehalogention of different substrates in the packed-bed (Pd/C catalysts) compact reactor.

| Entry | Substrate | Catalyst | Conversion | Product | Selectivity[e] |
|---|---|---|---|---|---|
| 1[a] | styrene | DR–Pd/C | 100 % | ethylbenzene | 100 % |
|  |  | IW–Pd/C | 100 % |  | 100 % |
| 2[a] | phenylacetylene | DR–Pd/C | 100 % | ethylbenzene | 100 % |
|  |  | IW–Pd/C | 100 % |  | 100 % |
| 3[b] | benzaldehyde | DR–Pd/C | 61 % | benzyl alcohol (OH) | 99 % |
|  |  | IW–Pd/C | 56 % |  | 98 % |
| 4[b] | acetophenone | DR–Pd/C | 57 % | 1-phenylethanol (OH) | 100 % |
|  |  | IW–Pd/C | 50 % |  | 100 % |
| 5[c] | nitrobenzene ($NO_2$) | DR–Pd/C | 100 % | aniline ($NH_2$) | 99 % |
|  |  | IW–Pd/C | 98 % |  | 99 % |
| 6[d] | R = I, Br, Cl | DR–Pd/C | 100 % | benzene | 97 % |
|  |  |  | 98 % |  | 97 % |
|  |  |  | 60 % |  | 98 % |

[a] reaction conditions: $C_{Initial}$ = 0.5 mol L$^{-1}$; $T$ = 331 K; $P$ = 9 barg; $F_{Liquid}$ = 0.5 mL min$^{-1}$; $F_{Gas}$ = 6 mL(STP) min$^{-1}$ (for styrene hydrogenation); $F_{Gas}$ = 14 mL(STP) min$^{-1}$ (for phenylacetylene hydrogenation); ethanol as solvent.

[b] reaction conditions: $C_{Initial}$ = 0.5 mol L$^{-1}$; $T$ = 318 K (for benzaldehyde hydrogenation); $T$ = 328 K (for acetophenone hydrogenation); $P$ = 9 barg; $F_{Liquid}$ = 0.5 mL min$^{-1}$; $F_{Gas}$ = 8 mL(STP) min$^{-1}$; ethanol as solvent.

[c] reaction conditions: $C_{Initial}$ = 0.5 mol L$^{-1}$; $T$ = 333 K; $P$ = 9 barg; $F_{Liquid}$ = 0.5 mL min$^{-1}$; $F_{Gas}$ = 20 mL(STP) min$^{-1}$; ethanol as solvent.

[d] reaction conditions: $C_{Initial}$ = 0.2 mol L$^{-1}$; $T$ = 328 K (for iodobenzene and bromobenzene hydrodehalogenation); $T$ = 348 K (for chlorobenzene hydrogenation); $P$ = 8 barg; $F_{Liquid}$ = 0.5 mL min$^{-1}$; $F_{Gas}$ = 6 mL(STP) min$^{-1}$; triethylamine as additive, ethanol or DMF as solvent.

[e] for all GC analyses, mass balance ≥ 98.5.

Stability and deactivation of catalysts were studied in extended continuous runs. Results are shown in Fig. 6.6. For the IW-Pd/C catalysed alkene hydrogenation, the product yield stabilised at *ca.* 100 % at 5 min after start-up of the system and remained at that level for almost 7 h of continuous run. The DR-Pd/C catalyst also showed good stability: no noticeable catalyst deactivation was measured in carbonyl reduction over 6 h on stream as evidenced in Fig. 6.6. Both the IW-Pd/C and the DR-Pd/C catalysts used in the long experiments were not fresh catalysts. Both

catalysts have been used several times (up to 50 h of cumulative reaction time) in previous experiments for reducing different substrates and only solvent washing was employed after each reaction to regenerate the catalyst bed. It should be noted, that the potential activity compensation effect due to the reaction exotherm, especially at 100% conversion is negligible in this case. The reactor was operated effectively in isothermal regime. Furthermore, since the catalysts were used for over 50 h of reaction in previous tests, any activity loss would have been apparent.
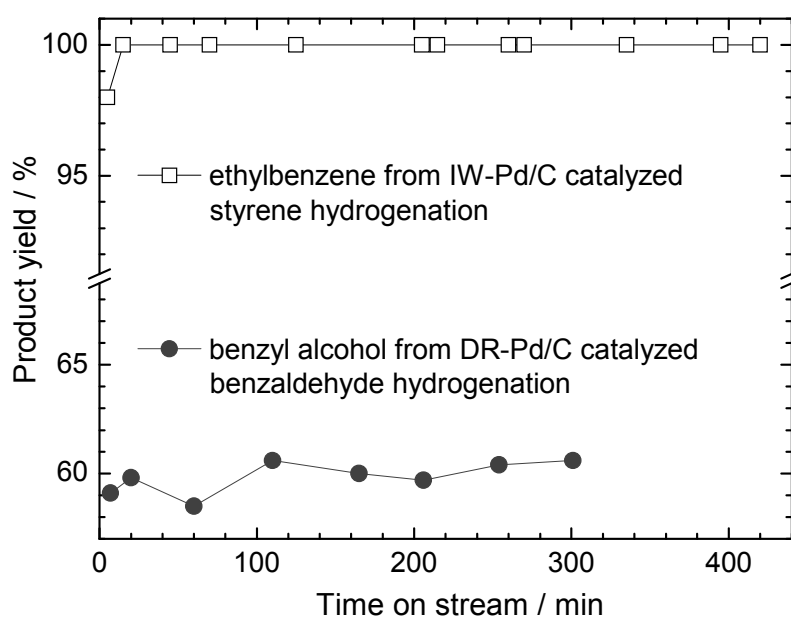
**Fig. 6.6** Ethylbenzene and benzyl alcohol yield as a function of reaction time. Conditions: see notes (a) and (b) in Table 6.3.

## 6. 4   Conclusions

Synthetic carbon, with the pore structure specifically tailored for preparation of metal nanoparticles catalysts, was used as a support for preparation of Pd catalysts by deposition-reduction and anaerobic incipient wetness methods. N$_2$ adsorption analyses showed the synthetic carbon possesses a developed micro-mesoporous bimodal pore structure. HR-TEM analysis of the fresh catalysts showed that Pd particles were well dispersed within IW–Pd/C with a homogeneous size of *ca.* 5 nm,

whilst DR–Pd/C catalyst also contained very small Pd nanoparticles of less than 1 nm diameter.

Pd supported on mesoporous carbon catalysts were evaluated in liquid phase hydrogenation and hydrodehalogenation reactions in a structured compact reactor. The combination of integrated intensified reactor and specifically designed catalysts results in rapid and efficient reduction of double and triple unsaturated bonds, carbonyl and nitro group, as well as direct reduction of aromatic halides under mild conditions. Due to the intensified heat transfer in the compact reactor, isothermal conditions were maintained for ensuring good selectivity and eliminating inherent hazards of exothermic reactions. The catalysts in the flow reactor system could be regenerated by solvent washing after the reaction. Both catalysts demonstrated good stability in long runs. No deactivation of catalysts was detected 7 hour continuous runs. Both catalysts were reused up to 50 hours under flow conditions without loss of activity.

Both catalysts used showed high activity and selectivity as well as high stability and reproducibility for all model reactions. Based on the preliminary results obtained in this study more questions arise in order to fully understand the reasons behind high activity and especially good stability of the developed catalysts. Therefore, further analyses ($N_2$ adsorption, XPS, XRD and HRTEM) on catalysts' morphology and metal transportation/transformation following the reactions are needed.

## Acknowledgements

(Department of Chemistry, University of Cardiff, UK) for performing the XPS analysis, Mr Harry Bone (Department of Physics, University of Bath, UK) for performing the XRD analysis, Dr. Vladimir I. Zaikovski (Boreskov Institute of Catalysis, Russia) for performing the HRTEM analysis. I am grateful to Dr. Victor Sans (School of Engineering, University of Warwick, UK) for the instructive discussions. The assistance of Mr. Fernando Acosta (Department of Chemical Engineering, University of Bath, UK) on nitrogen adsorption experiments is acknowledged**.**

## References

1.    Ehrfeld, W.; Hessel, V.; Löwe, H., *Microreactors*. WILEY–VCH: Weinheim, 2000; p 288.

2.    Bavykin, D. V.; Lapkin, A. A.; Kolaczkowski, S. T.; Plucinski, P. K., Selective oxidation of alcohols in a continuous multifunctional reactor: Ruthenium oxide catalysed oxidation of benzyl alcohol. *Appl. Catal. A: Gen.* **2005,** 288, (1–2), 175–184.

3.    Ferrouillat, S.; Tochon, P.; Peerhossaini, H., Micromixing enhancement by turbulence: Application to multifunctional heat exchangers. *Chem. Eng. Proc.* **2006,** 45, (8), 633–640.

4.    Plucinski, P. K.; Bavykin, D. V.; Kolaczkowski, S. T.; Lapkin, A. A., Application of a structured multifunctional reactor for the oxidation of a liquid organic feedstock. *Catal. Today* **2005,** 105, (3–4), 479–483.

5.    Kreutzer, M. T.; Kapteijn, F.; Moulijn, J. A.; Heiszolf, J. J., Multiphase monolith reactors: Chemical reaction engineering of segmented flow in microchannels. *Chem. Eng. Sci.* **2005,** 60, (22), 5895–5916.

6.    Julbe, A.; Farrusseng, D.; Cot, D.; Guizard, C., The chemical valve membrane: a new concept for an auto-regulation of $O_2$ distribution in membrane reactors. *Catal. Today* **2001,** 67, (1–3), 139–149.

7.  Kolb, G.; Schurer, J.; Tiemann, D.; Wichert, M.; Zapf, R.; Hessel, V.; Lowe, H., Fuel processing in integrated micro-structured heat-exchanger reactors. *J. Power Sour.* **2007,** 171, (1), 198–204.

8.  Frauhammer, J.; Eigenberger, G.; von Hippel, L.; Arntz, D., A new reactor concept for endothermic high-temperature reactions. *Chem. Eng. Sci.* **1999,** 54, (15–16), 3661–3670.

9.  Kolios, G.; Frauhammer, J.; Eigenberger, G., Efficient reactor concepts for coupling of endothermic and exothermic reactions. *Chem. Eng. Sci.* **2002,** 57, (9), 1505–1510.

10. Singh, U. K.; Vannice, M. A., Kinetics of liquid-phase hydrogenation reactions over supported metal catalysts – a review. *Appl. Catal. A: Gen.* **2001,** 213, (1), 1–24.

11. Poe, S. L.; Cummings, M. A.; Haff, M. P.; McQuade, D. T., Solving the clogging problem: Precipitate-forming reactions in flow. *Angew. Chem. Int. Ed.* **2006,** 45, (10), 1544–1548.

12. Yeong, K. K.; Gavriilidis, A.; Zapf, R.; Hessel, V., Catalyst preparation and deactivation issues for nitrobenzene hydrogenation in a microstructured falling film reactor *Catal. Today* **2003,** 81, (4), 641–651.

13. Kobayashi, J.; Mori, Y.; Okamoto, K.; Akiyama, R.; Ueno, M.; Kitamori, T.; Kobayashi, S., A microfluidic device for conducting gas-liquid-solid hydrogenation reactions. *Science* **2004,** 304, (5675), 1305–1308.

14. Kobayashi, J.; Mori, Y.; Kobayashi, S., Triphase hydrogenation reactions utilizing palladium-immobilised capillary column reactors and a demonstration of suitability for large scale synthesis. *Adv. Synth. Catal.* **2005,** 347, (15), 1889–1892.

15. Losey, M. W.; Schmidt, M. A.; Jensen, K. F., Microfabricated multiphase packed-bed reactors: Characterisation of mass transfer and reactions. *Ind. Eng. Chem. Res.* **2001,** 40, (12), 2555–2562.

16. Plucinski, P. K.; Bavykin, D. V.; Kolaczkowski, S. T.; Lapkin, A. A., Liquid-phase oxidation of organic feedstock in a compact multichannel reactor. *Ind. Eng. Chem. Res.* **2005,** 44, (25), 9683–9690.

17.    Fan, X. L.; Lapkin, A. A.; Plucinski, P. K., Liquid phase hydrogenation in a structured multichannel reactor. *Catal. Today* **2009,** 147S, S313–S318.

18.    Fan, X. L.; Manchon Gonzalez, M.; Karen, W.; Tennison, S. R.; Kozynchenko, A.; Plucinski, P. K.; Lapkin, A. A., Coupling of Heck and hydrogenation reactions in a continuous compact reactor. *J. Catal.* **2009,** 267, 114–120.

19.    Taguchi, A.; Schuth, F., Ordered mesoporous materials in catalysis. *Micropor. Mesopor. Mater.* **2005,** 77, (1), 1–45.

20.    Tamai, H.; Nobuaki, U.; Yasuda, H., Preparation of Pd supported mesoporous activated carbons and their catalytic activity. *Mater. Chem. Phys.* **2009,** 114, (1), 10–13.

21.    Tamai, H.; Ogawa, J.; Yasuda, H., Simple preparation and catalytic activity of Pd particles dispersed mesoporous carbons from poly(VDC/MA) containing Pd and Y compounds. *J. Colloid Interface Sci.* **2003,** 260, (2), 312–316.

22.    Tennison, S. R., Phenolic-resin-derived activated carbons. *Appl. Catal. A: Gen.* **1998,** 173, 289–311.

23.    Pigamo, A.; Besson, M.; Blanc, B.; Gallezot, P.; Blackburn, A.; Kozynchenko, O.; Tennison, S.; Crezee, E.; Kapteijn, F., Effect of oxygen functional groups on synthetic carbons on liquid phase oxidation of cyclohexanone. *Carbon* **2002,** 40, (8), 1267–1278.

24.    Krishnanakutty, N.; Vannice, M. A., The effect of pretreatment on Pd/C catalysts. 1. Adsorption and absorption properties. *J. Catal.* **1995,** 155, (2), 312–326.

25.    Fan, X. L.; Chen, H. S.; Ding, Y. L.; Plucinski, P. K.; Lapkin, A. A., Potential of 'nanofluids' to further intensify microreactors. *Green Chem.* **2008,** 10, (6), 670–677.

26.    Groen, J. C.; Perez-Ramirez, J., Critical appraisal of mesopore characterisation by adsorption analysis. *Appl. Catal. A: Gen.* **2004,** 268, (1–2), 121–125.

27.    Horvath, G.; Kawazoe, K., Method for the calculation of effective pore size distribution in molecular sieve carbon. *J. Chem. Eng. Jpn* **1983,** 16, (6), 470–475.

28.    Patterson, A. L., The scherrer formular for X-ray particle size determination. *Phys. Rev. Lett.* **1939,** 56, (10), 978–982.

29.    Langford, J. L.; Wilson, A. J. C., Scherrer after 60 Years: A survey and some new results in the determination of crystallite size. *J. Appl. Cryst.* **1978,** 11, (April), 102–113.

30.    Höller, V.; Wegricht, D.; Yuranov, I.; Kiwi-Minsker, L.; Renken, A., Three-phase nitrobenzene hydrogenation over supported glass fiber catalysts: Reaction kinetics study. *Chem. Eng. Technol.* **2000,** 23, (3), 251–255.

31.    Konuma, K.; Kameda, N., Effect of substituents on the hydrodechlorination reactivity of para-substituted chlorobenzenes. *J. Mol. Catal. A: Chem.* **2002,** 178, (1-2), 239–251.

32.    Forni, P.; Prati, L.; Rossi, M., Catalytic dehydrohalogenation of polychlorinated biphenyls – Part II: Studies on a continuous process. *Appl. Catal. B: Environ.* **1997,** 14, (1–2), 49–53.

33.    Alonso, F.; Beletskaya, I. P.; Yus, M., Metal-mediated reductive hydrodehalogenation of organic halides. *Chem. Rev.* **2002,** 102, (11), 4009–4091.

# Chapter 7

# Summary, evaluation and future work

In this chapter, the results presented in the thesis are summarised. The contribution of the work to the area of reactor engineering and catalysis is evaluated. In addition future work as a continuation of the present study is suggested.

## 7. 1 Introduction

Microreactors have been gradually recognised as a new branch of chemical reactor technology and chemistry[1, 2] and the application of microstructured chemical reactors has been widely investigated for a variety of reactions.[3] The benefits of microreactors stem from the nature of reduced characteristic dimensions where a chemical reaction happens. The microreactors therefore, in comparison with conventional batch or semi-batch reactors, lead to better performance in terms of effective heat management, fast mixing, and narrow residence time. The use of microreactors for three-phase catalytic reactions is beneficial because of the enhanced transport phenomena, which ensure the absence of heat- and mass-transfer limitations and improved yield and selectivity. In this investigation, a structured compact multifunctional reactor with mm-scale packed-bed reaction channels was presented and its application in continuous-flow catalytic reactions was studied. Hydrogenations, which are regarded as important class of reactions due to their various applications in synthesis of fine chemicals and pharmaceuticals,[4] were used as model reactions in this study for evaluating the performance of the reactor. The results obtained in this investigation were summarised and evaluated in the following sections. Future research within this subject was also suggested.

## 7. 2 Summary and evaluation

### 7.2.1. *Selective hydrogenation of aromatic aldehydes*

The continuous liquid phase hydrogenation of benzaldehyde to benzyl alcohol over Pt/C catalyst was demonstrated by using the structured compact reactor (**Chapter 3**). The enhanced mass transport was achieved in the reactor which in return ensured the operation in the reaction-limited regime. This can be attributed to the integration of heat transfer, mixing and reaction functionalities into a single reactor. Performing the reactions in the reaction-limited regime is important for attaining maximum reaction

throughput and for studying reaction kinetics. When compared to a reported monolith reactor with the same substrate,[5] a more intensified process was attained by the compact reactor. Consequently, a 41 % yield, corresponding to a space-time yield of product of *ca.* 34 mol $L_{reactor}^{-1} h^{-1}$, was achieved at 317 K for a single pass through the reaction channel with undiluted catalyst bed for *ca.* 40 second residence time. Some deactivation of the catalysts occurred due to formation of an insoluble byproduct. The catalytic activity can, however, be recovered by solvent washing of the catalyst. The staged injection of hydrogen was shown to be beneficial for this model reaction, which was attributed to a better hydrodynamic regime.

### *7.2.2.    Nanofluids heat transfer in the compact reactor–micro heat exchanger*

Effective heat transfer of integrated micro heat exchangers has been demonstrated in the early study.[6, 7] The possibility of further intensification of heat transfer in compact reactor/heat exchanger with thermal nanofluids was studied in this thesis (**Chapter 4**). The results showed that the enhancement in the overall heat transfer coefficient of up to *ca.* 35 %, compared with the corresponding base heat transfer fluid, was achieved with $TiO_2$-ethylene glycol nanofluids. The thermal intensified system showed a significantly faster dynamic response. This characteristic of the thermal system enabled the rapid quenching of reactions. The increased demand on pumping power was confirmed after introducing nanoparticles in heat transfer fluids. The overall energy analysis of the system therefore is essential to obtain a true picture of the whole system energy efficiency.

### *7.2.3.    Multi-step synthesis in the compact reactor*

The investigation of the feasibility of performing multi-step catalytic reactions in the compact multichannel reactor was presented in **Chapter 5**. Synthesis of 1,2-diphenylethane through Heck C–C coupling reaction and hydrogenation was employed as a model reaction. A stepwise conversion of the substrates to the final product was achieved in the compact multichannel reactor by coupling the Heck reaction and hydrogenation. Furthermore, compared with the conventional 'one-pot'

synthesis in a batch reactor (several hours to attain a similar yield),[8] the compact reactor promoted a more intensified Heck reaction and alkene hydrogenation, *i.e.* the target product was synthesised in the flow compact reactor within minutes of residence time; with a lower operating temperature and pressure.    Activity of the catalytic system can be mostly maintained by periodic reverse running operation of the two reactions.  The established tandem synthesis in flow compact reactor showed that this compact reactor might be a suitable alternative to replacing the conventional batch reactor for laboratory-scale multi-step synthesis.

### *7.2.4.    Developing Pd supported on mesoporous synthetic carbon catalysts for flow catalysis*

Pd supported on mesoporous synthetic carbon catalysts were proven to be highly efficient for flow hydrogenation and hydrodehalogenation reactions in the structured compact reactor (in **Chapter 6**).  The synthetic carbon and two Pd/C catalysts were characterised preliminarily using $N_2$ adsorption, HR-TEM, XRD and XPS analysis. The high efficiency of the continuous-flow catalytic system was believed to be linked with (*i*) intensified atmosphere in the structured compact reactor due to the integration of functionalities and reduction of characteristic dimensions and (*ii*) well-dispersed active sites on the mesoporous surface and reduced diffusion resistance in mesoporous structures.    Additionally, the continuous-flow catalytic system demonstrated a high stability and catalyst longevity.  The Pd/C catalysts were used for up to 50 hours (for different reactions and substrates) under flow conditions without significant loss of activity.

## 7. 3   Dissemination

Some of the results obtained from this investigation have been published in peer-reviewed journals and others are being prepared, the information of these articles is shown in section 7.3.1.  Several oral and poster presentations, with regard to the scientific aspects of this research, were made at a number of international

conferences. The information of these presentations and conferences is listed in section 7.3.2.

### 7.3.1.   *Publications*

The following set of publications have resulted from this research:

- Chen H. S.; Ding Y. L.; Lapkin A. A.; Fan X. L., Rheological behaviour of ethylene glycol-titanate nanotube nanofluids. *J. Nanopart. Res.* 2009, 11(6), 1513-1520.

- Fan, X. L.; Manchon, M.; Wilson, K.; Tennison, S.; Kozynchenko, A.; Lapkin A. A.; Plucinski, P. K., Coupling of Heck and hydrogenation reactions in a continuous compact reactor. *J. Catal.* 2009, 267 (2), 114–120.

- Fan, X. L.; Plucinski, P. K.; Lapkin A. A., Liquid phase hydrogenation in a structured multichannel reactor. *Catal. Today* 2009 (147S), S313–S318.

- Fan, X. L.; Chen H. S.; Ding Y. L.; Plucinski, P. K.; Lapkin A. A., Potential of 'nanofluids' to further intensify microreactors. *Green Chem.* 2008, 10 (6), 670–677.

### 7.3.2.   *Oral and poster presentations*

The following oral and poster presentations were made:

- Poster presentation by Pawel Plucinski, 'Liquid phase hydrogenation in a structured multichannel reactor' in the 3rd International Conference on Structured Catalysts and Reactors, Naples, Italy, 27–30 September 2009.

- Oral presentation by Xiaolei FAN, 'A promising flow reactor technology: applications of a structured compact reactor in catalytic flow chemistry' in EuropaCat IX Congress, Salamanca, Spain, 30 August–04 September 2009.

- Oral presentation by Xiaolei FAN, 'Coupling of Heck and hydrogenation reactions in a continuous compact reactor' in the 8th World Congress of Chemical Engineering (WCCE8), Montreal, Canada, 23–27 August 2009.

- Oral presentation by Alexei Lapkin, 'Nanofluids: thermal and rheological properties and application in microfluidics and chemical reactors' and poster presentation by Xiaolei Fan, 'Structured compact reactors for catalytic flow chemistry' in ACHEMA 2009, International Exhibition-Congress on Chemical Engineering, Environmental Protection and Biotechnology, Frankfurt, Germany, 11–15 May 2009.

- Poster presentation by Xiaolei FAN, 'The use of a compact multichannel reactor for contiguous multi-step organic synthesis' in IChemE Catalysis Subject Group 2008 Student Conference (Applied Catalysis: Towards Sustainable Chemical Industry), Bath, UK, 12 November 2008.

- Oral presentation by Xiaolei FAN, 'Intensification of heat transfer in compact reactor/heat exchanger by $TiO_2$-ethylene glycol nanofluids' in the 20th International Symposium on Chemical Reaction Engineering (ISCRE 20), Kyoto, Japan, 7–10 September 2008.

- Oral presentation by Alexei Lapkin, 'Heat transfer nanofluids in compact and microreactors' in Engineering Conference International (ECI): Nanofluids-Fundamentals and Applications, Colorado, USA, 16-19 September 2007.

## 7. 4   Future work

The results of this investigation have shown that further research within this area is recommended for optimising the continuous-flow reactor technology and extending its applicability for different processes.

The structured compact reactor showed how efficient it is for transferring some conventional heterogeneous catalytic processes in continuous flow. When considering the multiphase systems in micro and compact reactors, full understanding of the hydrodynamics of individual phases and the interfacial transport phenomena in the microreaction system is necessary for further optimising the present design or developing new types of micro and compact reactors. Subsequently, further experimental work together with necessary CFD simulation on these two aspects is recommended.

Catalysts developed based on mesoporous synthetic carbons seem promising (refer to Chapter 6) for their preliminary application in flow reactor systems. New catalysts development using mesoporous synthetic carbons, especially for micro and compact reactors, for extending their versatility in heterogeneous catalysis may open more opportunities for exploiting new processes in flow regime, such as regioselective, stereoselective, and enantioselective catalysis which is of particular importance for fine chemical and pharmaceutical industries.

## References

1.    Janowska, I. W.; Liu, Y.; Carvalho, A.; Edouard, D.; Keller-Spitzer, V.; Leller, N.; Ledoux, M. J.; Pham-Huu, C., CNTs - microreactor concept for chemical processes. In *E-MRS Fall Meeting 2008, Symposium D: Novel synthesis processes and design of nanomaterials for catalytic applications*, Warsaw University of Technology, Warsaw, Poland, 2008.

2.    Martinez-Latorre, L.; Ruiz-Cebollada, P.; Monzón, A.; García-Bordejé, E., Preparation of stainless steel microreactors coated with carbon nanofiber

layer: Impact of hydrocarbon and temperature. *Catal. Today* **2009,** 147, (Supplement 1), S87–S93.

3.  Ehrfeld, W.; Hessel, V.; Löwe, H., *Microreactors*. WILEY–VCH: Weinheim, 2000; p 288.

4.  Kulkarni, A. A.; Kalyani, V. S., Two-phase flow in minichannels: Hydrodynamics, pressure drop, and residence time distribution. *Ind. Eng. Chem. Res.* **2009,** 48, (17), 8193–8204.

5.  Nijhuis, T. A.; Kreutzer, M. T.; Romijn, A. C. J.; Kapteijn, F.; Moulijn, J. A., Monolithic catalysts as more efficient three-phase reactors. *Catal. Today* **2001,** 66, (2–4), 157–165.

6.  Bavykin, D. V.; Lapkin, A. A.; Kolaczkowski, S. T.; Plucinski, P. K., Selective oxidation of alcohols in a continuous multifunctional reactor: Ruthenium oxide catalysed oxidation of benzyl alcohol. *Appl. Catal. A: Gen.* **2005,** 288, (1–2), 175–184.

7.  Plucinski, P. K.; Bavykin, D. V.; Kolaczkowski, S. T.; Lapkin, A. A., Liquid-phase oxidation of organic feedstock in a compact multichannel reactor. *Ind. Eng. Chem. Res.* **2005,** 44, (25), 9683–9690.

8.  Gruber, M.; Chouzier, S.; Koehler, K.; Djakovitch, L., Palladium on activated carbon: a valuable heterogeneous catalyst for one-pot multi-step synthesis. *Appl. Catal. A: Gen.* **2004,** 265, 161–169.

# Appendix

# I      Gas chromatography (GC) and GC method

*Gas chromatography (GC)*

Gas chromatography (GC) analysis was carried out to determine the product distribution and conversion during catalytic experiments.     Two Varian chromatographs (CP-3800/CP-3900) were employed in this study, and both equipped with Flame Ionisation Detectors (FID), CP 8400 autosamplers (Varian), and split injectors.  A non-polar capillary column (CP Sil 5 CB, fused silica model, 15 m, 0.25 mm, 0.25 μm, Varian) was used in this study.  The CP-Sil 5 CB column contains a 100 % dimethylpolysiloxane phase.  Separation is almost entirely based on boiling points making this column suitable for a wide range of applications, *i.e.* aromatic hydrocarbons, halogenated hydrocarbons, hydrocarbons, *etc.*, with a broad temperature range.  Samples taken from the experiments were analysed without further preparation but with dilution in some cases.  Split mode was used with a split ratio of 50, *i.e.* 1/50th of the volume of the injected sample was sent for analysis during sample injection.  Preliminary analyses with pure compounds were performed to determine the retention times and obtain detector calibration coefficients.  The internal standard method was also used in GC analysis to quantify the components of the sample.

The internal standard is a compound added to a sample in known concentration to provide a relative measure of concentration of the sample components.   Either dihexyl ether or dodecane were employed as internal standards in this study for different reactions.   Preliminary GC analyses showed that both of the internal standard elute in a proper position on the chromatogram that does not interfere or merge with any of the substrates, intermediates and products.   Standard samples with known concentrations of analytes and internal standards were prepared for calibration.   The calibration curves (one instance as shown in Fig. a.1) can be obtained by plotting the ratio of the analyte signal to the internal standard signal (peak area) as a function of the analyte concentration of the standards.   This was done to correct for the loss of analyte during sample preparation or sample inlet.
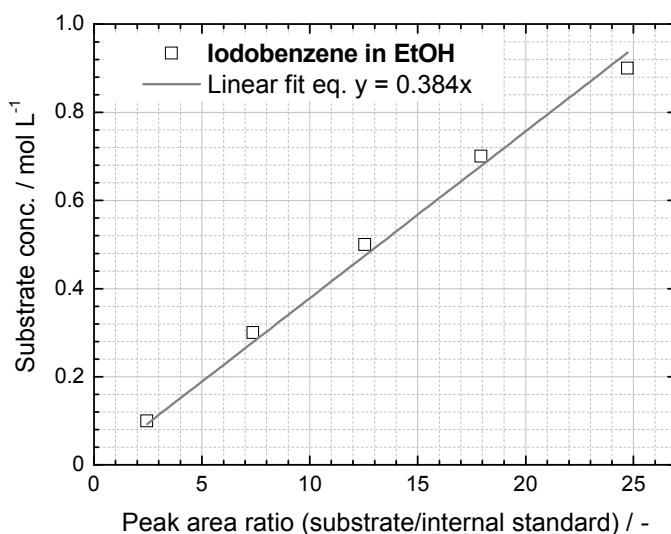
**Fig. a.1** Calibration sample curve of GC analysis.  Iodobenzene in ethanol.

*GC method*

Information on developing GC methods for this study is listed as below.

 **Autosampler**

Syringe size – 10 μL.

Injection mode: std split/splitless.

Sample depth – 90 %.

Solvent depth – 90 %.

**Injector**

Select injector (only apply to GC 3800) – middle injector (connected with capillary column and FID detector, for most applications).

Injector coolant – set as 'off'.

Split ratio –50.

Injector temperature – 10 K higher than the highest boiling point of the compounds in the sample.

**Detector**

Select detector (only apply to GC 3800) – middle (FID detector, for most applications).

Detector oven – set as 'on'.

Electronics – set as 'on'.

Time – set as 'initial'.

Range – set as '12' (most sensitive mode).

Attenuation – set as '1'. (only apply to GC 3900)

Autozero – set as 'yes'.

EFC type – set as 'type 11' (only apply to GC 3900, flow-rates of make-up gas, $H_2$, and air can be specified here, refer to B. Set up the flow-rates for make-up gas (30 mL min$^{-1}$), air (300 mL min$^{-1}$), $H_2$ (30 mL min$^{-1}$) and septum purge line (in the range of 1–5 mL min$^{-1}$).

Detector temperature – 10 K higher than injector temperature (in order to avoid the condensation of compounds in detector).

Time constant – set as 'fast'.

**Flow/pressure (only apply to GC 3800)**

EFC type – set as 'type 1, for (1079/1177 injectors)'.

Column flow – set as '0.8 mL/min'.

Pressure pulse – set as 'no'.

Constant flow – set as 'on'.

**Column oven**

Temperature program – depends on the analysis.

Column oven coolant – set as 'off'

**Data acquisition**

Detector bunch rate – set as '1' point (80.0 Hz).

Noise monitor length – set as '16' bunched points (0.2 sec).

Detector full scale – set as '1000v' (for GC 3800, set middle detector full scale, *i.e.* FID detector, as '1000v').

## II  Gas adsorption analysis

Gas adsorption analysis was conducted in this study for obtaining nitrogen adsorption isotherms to evaluate the specific surface area and the pore size distribution of the carbon supports and catalysts. Measurements of isotherms at 77 K on samples were performed on a Micrometrics Accelerated Surface Area and Porosimetry (ASAP) 2010 analyser. Nitrogen was used as probing gas due to: (*i*) molecular size of nitrogen is well established, (*ii*) it is inert and (*iii*) nitrogen is available in high purity at a reasonable cost. Adsorption and desorption analysis of the sample (in a sample tube) was performed in a coolant bath of liquid nitrogen at 77 K. An equilibration time of 45 second was used for each isotherm data point during the analysis. The technique requires a clean surface, therefore, an over-night degassing step was performed at 453 K under vacuum to remove residue moisture and vapours.

*Determination of the specific surface area*

Specific surface area of catalysts is an important attribute for catalyst users to monitor the activity and stability of catalysts. Two of the most universal methods used for determining the specific surface area are single point method ($p/p^0 = 0.3$) and multipoint method ($0.05 < p/p^0 < 0.35$), which are based on the isothermal adsorption of nitrogen.[1] The multipoint Brunauer-Emmett-Teller (BET) method[2] is a widely accepted calculation for determining specific surface area. Measurements for the BET model evaluation are (*i*) relatively simple to obtain, (*ii*) widely applicable and (*iii*) results are highly reproducible. Therefore, in present study, the BET method was employed to determine specific surface area of activated carbon support and activated carbon supported metal catalysts.

Fig. a.2 is a representative isotherm of the carbon support/carbon supported metal catalysts used in this study. The data points in the range of 0.05–0.35 $p/p^o$, which is indicated in Fig. a.2, are transformed with the BET equation[1,2] (Eq. (a.1)) for calculating monolayer adsorbed gas quantity ($V_m$, m$^3$ g$^{-1}$) and BET constant ($C$, a constant that is related to the heat of adsorption).

$$\frac{p/p^0}{V_a(1 - p/p^0)} = \frac{1}{V_m \cdot C} + \frac{C-1}{V_m \cdot C} \cdot p/p^0 \tag{a.1}$$

In Eq. (a.1), $p/p^o$ is the relative pressure (–), $V_a$ is the adsorbed volume at a given $p/p^o$ (cm$^3$ g$^{-1}$).
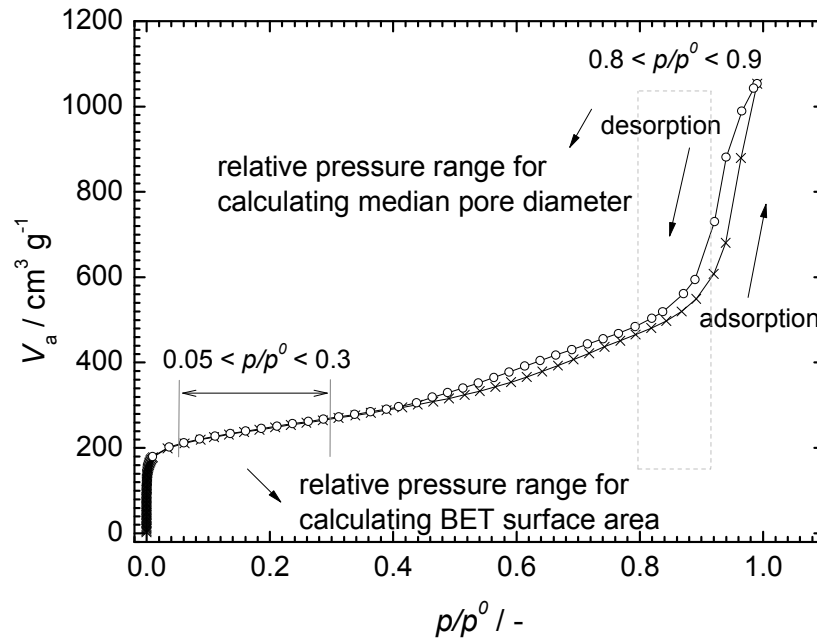
**Fig. a.2** Nitrogen adsorption isotherm of activated carbon.

A linear relationship between $\dfrac{p/p^0}{V_a(1-p/p^0)}$ and $p/p^o$ is required to obtain the quantity

of nitrogen adsorbed in the monolayer (see Fig. a.3 as a representative BET surface area plot of the carbon support/carbon supported metal catalysts used in this study). In order to obtain an intercept with positive value (to make sure the BET constant C is positive) from the linear fit, this linear part of relative pressure is restricted to a limited portion of the abovementioned range, generally between 0.05–0.20 $p/p^o$. By using Eq. (a.2) and (a.3), the slope ($A$) and intercept ($I$) of the linear fit were used to determine $V_m$ and $C$.

$$V_m = \frac{1}{A+I} \tag{a.2}$$

$$C = 1 + \frac{A}{I} \tag{a.3}$$

According to the definition of total BET surface area, Eq. (a.4), the total BET surface area of a sample can be obtained.

$$S_{BET \cdot total} = \frac{V_m \cdot N \cdot S}{v} \qquad (a.4)$$

Where $N$ is Avogadro's number $= 6.022 \times 10^{23}$ mol$^{-1}$, $S$ is adsorption cross section $= 0.162 \times 10^{-18}$ m$^2$ (for $N_2$), $v$ is molar volume of the adsorbent gas $= 0.022414$ m$^3$ mol$^{-1}$ (for $N_2$).
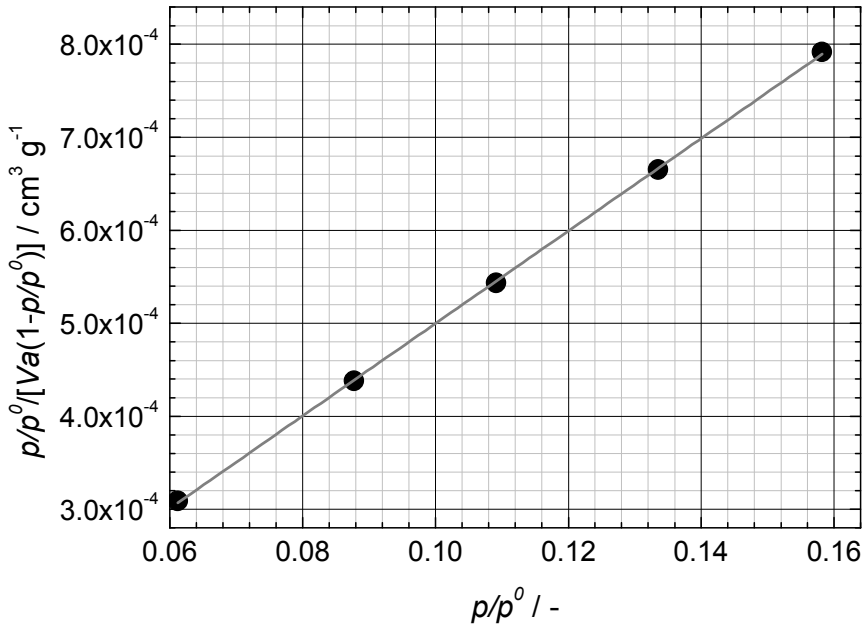


**Fig. a.3** BET surface area plot of MAST carbon.

### Determination of the average pore diameter and pore size distribution

The original Barrett-Joyner-Halenda (BJH) method was used in this study for calculating pore size (for mesopores) distributions due to its universal acceptance for determining pore structure of mesoporous materials. BJH method is based on a model of the adsorbent as a system of open-ended cylindrical pores.[3] The theory accounts for capillary condensation in the pores using the classical Kelvin equation, which in turn assumes a hemispherical liquid-vapor meniscus and a well-defined

surface tension. All the results related to BJH method such as incremental/cumulative pore volume and incremental/cumulative pore area were automatically generated by the ASAP 2010 analyser and given as report (the fraction of open-ended cylindrical pores = 1).

In the standard ASAP analysis report, the average pore diameter ($d$) of a sample was estimated on the basis of the cumulative pore volume ($V_{cu.}$) and cumulative pore area ($A_{cu.}$) according to the full adsorption/desorption relative pressure range ($0 < p/p^0 < 1$) by using Eq. (a.5).

$$d = 4V_{cu.} / A_{cu.} \qquad\qquad\qquad\qquad (a.5)$$

However, according to the BJH theory, the capillary condensation/evaporation process is only happened in the hysteresis loop closure, *i.e.* from the relatively low $p/p^0$ values used for the BET method (~0.3) towards unity. Therefore, performing the calculation for determining average pore diameters of samples by using a narrower $p/p^0$ range is essential from a practical point of view. In this study, a relative pressure range of $0.8 < p/p^0 < 0.9$ was used for calculating pore size distribution and both adsorption and desorption branch of each isotherm were analysed.

Micropore size distribution was obtained by using original Harvoth-Kawazoe method (slit-shaped pore geometry), which has been widely used for determining pore size distribution in a microporous material from a single adsorption isotherm.

## III    MS and NMR analysis

### *Mass Spectrometry (MS)*

Mass spectrometry (MS) was employed for the determination of the chemical structures of molecules such as products and by-prodcuts generated in the reactions. A microTOF (ESI–TOF) mass spectrometre from Bruker was used in this study. The

MS is controlled by OpenAccess software, with a choice of generic methods for different mass ranges and polarities. Generally it is run using an autosampler to inject the sample into a solvent stream supplied by the LC pump, without any chromatographic separation. There is also the capability for liquid chromatography to precede the mass spectrometric analysis (LC–MS). MS analysis was accomplished under assistance of Dr Anneke Lubben in the Department of Chemistry at University of Bath.

### Nuclear Magnetic Resonance (NMR)

A Bruker Nuclear Magnetic Resonance (NMR) spectrometre (300 MHz) was used to identify the chemical structures of unknown compounds. NMR spectrometre is operated in full automation and with a fully autotunable probe which allows data from a complete range of NMR-active nuclei to be acquired. Proton NMR ($^1$H NMR) analysis was most commonly carried out in this study. $^1$H NMR spectra were recorded in solution and in order to rule out the interference from solvent protons, a solvent without hydrogen *i.e.* deuterated (deuterium = $^2$H, often symbolised as D) solvents, is essentially needed for $^1$H NMR analysis. In present study, chloroform-d was used as the only solvent for preparing the samples. NMR analysis was performed in the Department of Chemistry at University of Bath.

Fig. a.4 is the $^1$H NMR spectra analysis of the byproduct identified in benzaldehyde hydrogenation. And combine with results of the MS analysis, the byproduct was revealed as shown in Scheme 3.2 in Chapter 3.
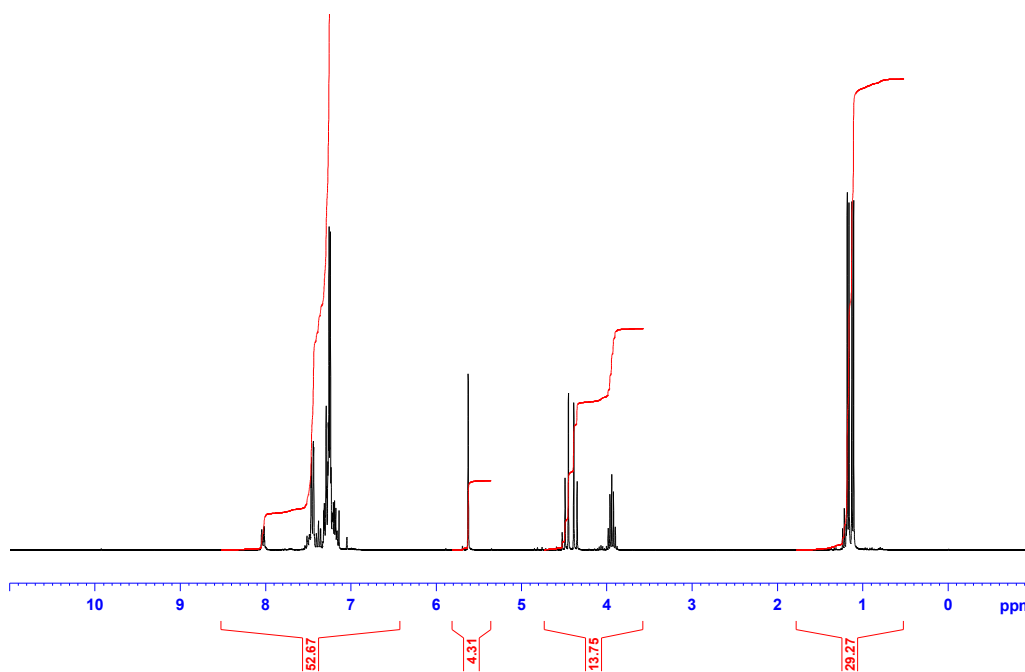
**Fig. a.4** ¹H NMR spectra of the byproduct in benzaldehyde hydrogenation.


## IV     XRD and XPS analysis of the fresh and spent Pd/C


*X-ray Diffraction (XRD) analysis*

X-ray diffraction technique (XRD) was used in this study to determine the average metal size of catalysts on the carbon support. XRD analysis was performed by Dr. Karen Wilson in the Department of Chemistry at University of York (Bruker AXS D8 Discoverer X-ray diffractometre, with Cu$K_\alpha$ radiation ($\lambda$ = 0.154 nm) and a graphite monochromator) and Mr Harry Bone in the Department of Physics at the University of Bath (Philips 4 kW X-ray generator (PW1730) with a Cu$K_\alpha$ X-ray source ($\lambda$ = 0.154 nm) and the diffractometre goniometre (PW1820) controlled via Philips (PW1877 PC-APD) software). All the scans were performed in the $2\theta$ range of 30°–55°.


Scherrer equation,[5, 6] Eq. (a.6), was used to calculate the particle diameter (*d*).


$$d = \frac{k\lambda}{\beta \cos(\theta)}$$ 
(a.6)

where *k* is the Scherrer constant (0.89 for integral breadth of spherical crystals with cubic symmetry), $\lambda$ is the x-ray wavelength, $\beta$ is the integral breadth of the peak at $2\theta$ and $\beta = (\pi/2)\cdot$FWHM (full width at half maximum) for a Gaussian shape peak), and $\theta$ is the Bragg angle.

The results of the analysis are shown as in Table a.1 and Fig. a.5 and Fig. 6.5 in Section 6.3.1.

**Table a.1** Average particle size (Pd) by XRD analysis (Scherrer equation).

| Catalyst | Preparation method | Average diameter / nm |
|----------|--------------------|-----------------------|
| Pd/C (5 wt.%) fresh | Deposition-reduction | 4.8 |
| Pd/C (5 wt.%) spent[a] | Deposition-reduction | 5.7 |
| Pd/C (5 wt.%) spent[b] | Deposition-reduction | 13.0 |
| Pd/C (3 wt.%) fresh | Incipient wetness | 5.2 |
| Pd/C (3 wt.%) spent[a] | Incipient wetness | 5.5 |

[a] used for hydrogenation and hydrodehalogenation reactions.
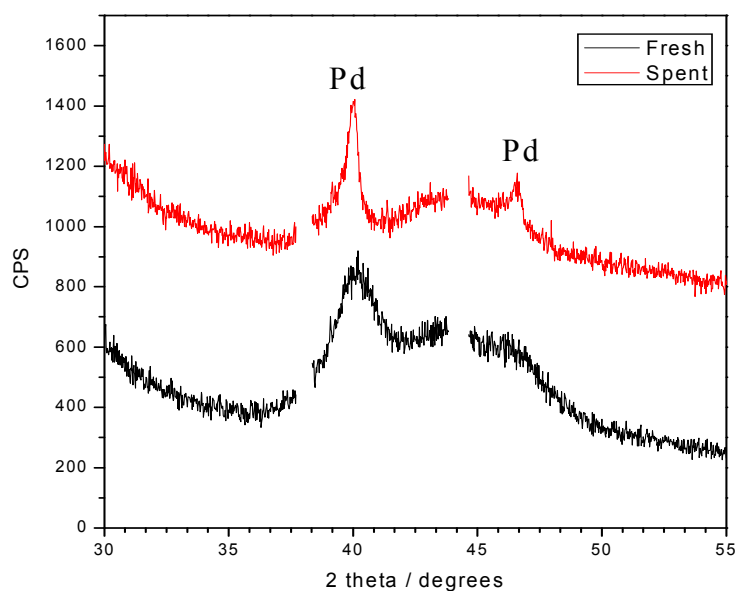[b] used for consecutive Heck reaction and hydrogenation.



**Fig. a.5** XRD pattern of Pd/C (5 wt.%) catalysts (for consecutive Heck and hydrogenation reaction) obtained using Bruker AXS D8 Discoverer X-ray diffractometre (University of York).

*X-ray Photoelectron Spectroscopy (XPS)*

X-ray photoelectron spectroscopy (XPS) was used in this study for the surface chemical analysis to determine the elemental composition of Pd/C catalysts. XPS analysis was performed by Dr. Karen Wilson at University of York using a Kratos Axis His instrument equipped with a Mg$K\alpha$ X-ray source and charge neutraliser. Spectra are acquired by using a pass energy of 20 eV with an X-ray power of 169 w. Spectra are energy-referenced using valence band and adventitious carbon, whereas quantification and deconvolution is performed using CASA-XPS version 2.3.9 software. The results of the analysis are shown as in Table a.2 and Fig. a.6.
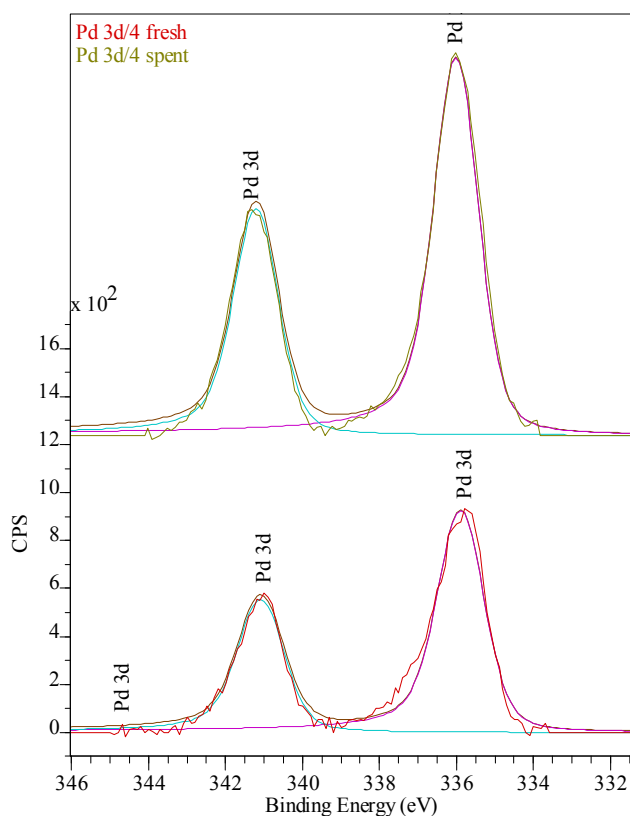


**Fig. a.6** High Resolution Spectrum for Pd(3d) signal.

**Table a.2** Elemental composition of the sample surface by XPS analysis.

| Sample | Pd / % | C / % | O / % |
|---|---|---|---|
| Pd/C (5 wt.%) fresh | 1.4 | 72.4 | 26.2 |
| Pd/C (5 wt.%) spent | 2.5 | 75.1 | 22.3 |

# V    Time constant model

*Assumptions:*

- Heat transfer only happens between the reactor main body and heat transfer fluid.
- All the physical properties of heat transfer fluids remain constant in the whole process.
- The bulk temperature of heat transfer fluids in re-circulating bath 2 remains steady for the whole process.
- After quenching, temperature of the ultimate steady state equals the bulk temperature of heat transfer fluids in re-circulating bath 2.

Experimental system for performing dynamic heat transfer experiments can be seen in Chapter 4 (Fig. 4.3).

*Description:*

- Heat transfer between reactor and heat transfer fluid 1 (high temperature one, in re-circulating bath 1) is in steady state.
- A cooler heat transfer fluid is introduced by quick switching to use re-circulating bath 2.
- The reactor is quenched by this sudden change of the temperature of the heat transfer fluid.
- The whole system achieves another heat transfer steady state at lower temperature.

*Derivation:*

Properties of the reactor:

$A$ is the area of the heat transfer interface / m$^2$

$m$ is the mass of the reactor material / kg

$c_p$ is the specific heat capacity of the reactor material / J kg$^{-1}$ K$^{-1}$

$T_w$ is the temperature of the reactor at time t / K

Properties of the heat transfer fluid 2:

$T_\infty$ is the bulk temperature / K

$h$ is the heat transfer coefficient / W m$^{-2}$ K$^{-1}$

Then the heat transfer process can be described by using Eq. (a.7):

$$hA\left(T_w - T_\infty\right) = -mc_p \frac{dT}{dt}$$  (a.7)

let $\Delta T = T_w - T_\infty$

$$hA\ \Delta T = -mc_p \frac{d\Delta T}{dt} \ \rightarrow \ \frac{d\Delta T}{dt} = -(hA/mc_p)\Delta T$$

The initial conditions are: $t = 0$, $\Delta T = T_0 - T_\infty = \Delta T_0$, where $T_0$ is the initial steady state temperature of the system which equals the temperature of heat transfer fluid in re-circulating bath 1.

$$\therefore \int_{\Delta T_0}^{\Delta T} \frac{d\Delta T}{\Delta T} = -(hA/mc_p)\int_0^t dt \ \rightarrow \ \ln\frac{\Delta T}{\Delta T_0} = -(hA/mc_p)t \ \rightarrow \ \frac{\Delta T}{\Delta T_0} = e^{-(hA/mc_p)t}$$

$$\rightarrow \Delta T = \Delta T_0\ e^{-(hA/mc_p)t} = \left(T_0 - T_\infty\right)e^{-(hA/mc_p)t} \ \rightarrow \ T_w = T_\infty + \left(T_0 - T_\infty\right)e^{-(hA/mc_p)t}$$

The dimension analysis of $hA/mc_p$: $hA/mc_p = \dfrac{\left[\dfrac{W}{m^2 K}\right]\left[m^2\right]}{\left[kg\right]\left[\dfrac{J}{kgK}\right]} = \dfrac{W}{J} = \dfrac{1}{s}$

Let $mc_p/hA = \tau$, $\tau$ is the time constant then this model (Eq. (a.8)) can be used for describing this quenching process and estimating time constant.

$$T_w = T_\infty + \left(T_0 - T_\infty\right)e^{-T/\tau}$$  (a.8)

## VI Productivity determination

*For batch reactor:*

$$P = \frac{C_{Product}}{t} \qquad (a.9)$$

Where $C_{Product}$ is the product concentration (mol L$^{-1}$), $t$ is the reaction time (h).

*For compact reactor:*

$$P = \frac{C_{Product}}{\tau} \qquad (a.10)$$

Where $C_{Product}$ is the product concentration in the outlet stream (mol L$^{-1}$), $\tau$ is the hydraulic residence time (h) and can be calculated by Eq. (a.11).

$$\tau = \frac{V_{Reaction\ channel} \cdot \varepsilon}{F_{Liquid}} \qquad (a.11)$$

Where $V_{Reaction\ channel}$ is the total volume of the reaction channels used, $\varepsilon$ is the catalyst packing voidage (–, in this case $\varepsilon = 0.4$), $F_{Liquid}$ is the volumetric flow rate of liquid phase (L h$^{-1}$).

# Reference

1. Rouquerol, F.; Rouquerol, J.; Sing, K., *Adsorption by Powders and Porous Solids: Principles, Methodology and Applications*. Academic Press: London, 1999.

2. Brunauer, S.; Emmett, P. H.; Teller, E., Adsorption of gases in multimolecular layers. *J. Am. Chem. Soc.* **1938,** 60, (2), 309–319.

3.     Barrett, E. P.; Joyner, L. G.; Halenda, P. P., The determination of pore volume and area distributions in porous substances. I. Computations from nitrogen isotherms. *J. Am. Chem. Soc.* **1951,** 73, (1), 373–380.

4.     Horvath, G.; Kawazoe, K., Method for calculation of effective pore size distribution in molecular sieve carbon. *J. Chem. Eng. Jpn* **1983,** 16, (6), 470–475.

5.     Patterson, A. L., The scherrer formular for X-ray particle size determination. *Phys. Rev. Lett.* **1939,** 56, (10), 978–982.

6.     Langford, J. L.; Wilson, A. J. C., Scherrer after 60 Years: A survey and some new results in the determination of crystallite size. *J. Appl. Cryst.* 1978, 11, (April), 102–113.